Proceedings of the National Seminar

on

MEDICINAL CHEMISTRY

ISBN: 978-93-5279-420-1

Organized by

POST GRADUATE DEPARTMENT OF CHEMISTRY

KAHM Unity Women's College, Manjeri

Narukara (PO), Malappuram (DT), Kerala-676122

www.unitywomenscollege.in

E-mail: chemistry@unitywomenscollege.in

Co-sponsored by

KERALA STATE COUNCIL FOR SCIENCE, TECHNOLOGY AND ENVIRONMENT

Sasthra Bhavan, Pattom,

Thiruvananthapuram-695 004

Editors:

Dr. Muhammed Basheer Ummathur; M. Sc., B. Ed., Ph. D.

Associate Professor & Head, PG Department of Chemistry, KAHM Unity Women's College, Manjeri, Narukara (PO), PIN 676122, Malappuram (DT), Kerala, India.

Mrs. Suhada K M; M. Sc.

Assistant Professor, PG Department of Chemistry, KAHM Unity Women's College, Manjeri, Narukara (PO), PIN 676122, Malappuram (DT), Kerala, India.

About the College

KAHM Unity Women's College was established in 1991 and is run by Muslim Educational and Cultural Association (MECA), a registered society. Started as a First Grade Aided College and affiliated to University of Calicut it is the only aided multi-faculty (Arts, Science and Commerce) Women's College in Malappuram District. The institution aims at the upliftment of women in general and the educationally backward Muslim women in particular, through modern good quality education. The college has creditable academic as well as co-curricular accomplishments. The college has been accredited by NAAC at B^{++} level (2.77) in 2019. The college offers 10 UG and 6 PG courses.

About the Department of Chemistry

Department of Chemistry was started in 1991 with Chemistry as subsidiary subject. Chemistry as main subject was started in 1993. 24 batches have successfully completed B.Sc. Chemistry Programme. The department conducted B.Sc. Industrial chemistry course in the vocational stream with the assistance of UGC during 1999-2004. Three batches completed the course. In 2013 the Department became a Post Graduate Department. 5 PG batches have successfully completed the M. Sc. Chemistry Prgramme.

Our Vision:

To develop a sense of intellectual curiosity concerning chemical theory and an appreciation of the practical role of chemistry in life.

Our Mission:

1. To give a thorough grounding in the principle of chemistry, both in theory and in practical experience.
2. To produce scientifically literate graduates and post graduates with a broad and deep knowledge of fundamental chemical principles.

₹ 500

August 2019

ISBN 978-93-5279-420-1

9 789352 794201

***Published** by **PG Department of Chemistry**, KAHM Unity Women's College, Manjeri, Narukara (PO), PIN 676122, Malappuram (DT), Kerala, India*

Layout & Type setting: Dr. Muhammed Basheer Ummathur

Printed at Right Click, Manjeri, Malappuram (DT), Kerala

ORGANIZING COMMITTEE

1. **Dr. C. Saidalavi**, *Principal.*
2. **Dr. Muhammed Basheer Ummathur**, *Associate Professor & Head, PG Department of Chemistry.*
3. **Dr. P. Jyothi**, *Assistant Professor, PG Department of Chemistry*.
4. **Dr. Deepa K**, *Assistant Professor, PG Department of Chemistry*.
5. **Mrs. Suhada K. M.** (Seminar Convenor), *Assistant Professor, PG Department of Chemistry.*
6. **Ms. Shabana K**, *Assistant Professor (Ad-hoc), PG Department of Chemistry*.
7. **Ms. Shahila Muhammed**, *Assistant Professor (Ad-hoc), PG Department of Chemistry.*
8. **Mrs. Najeera PC**, *Assistant Professor (Ad-hoc), PG Department of Chemistry*.

PREFACE

The National Seminar on Medicinal Chemistry (NSMC-2017) is being organized by the Post Graduate Department of Chemistry, KAHM Unity Women's College, Manjeri. It is co-sponsored by Kerala State Council for Science, Technology and Environment (KSCSTE), Thiruvananthapuram. The Department of Chemistry was started in 1991 and it has always maintained a good academic record.

The seminar is designed in such a way as to provide a platform for the students and teachers to discuss the role of natural and synthetic chemicals in the field of medicines. Medicinal chemistry is a discipline at the intersection of chemistry, especially synthetic organic chemistry, pharmacology and various other biological specialties, where they are involved with design, chemical synthesis and development for marketing of pharmaceutical agents.

We gratefully acknowledge the financial support from the Kerala State Council for Science, Technology and Environment (KSCSTE), Thiruvananthapuram. We sincerely appreciate the whole hearted cooperation of the principal, management members, students, non teaching staff and faculty members of various departments of our college in making this event a grand success.

NSMC-2017 Team

ISBN 978-93-5279-420-1

TECHNICAL PROGRAMME

24/07/2017 Monday

09.00 AM-09.30 AM : **Registration**

09.30 AM-10.45 AM : **Inaugural Session**

Prayer

Welcome : **Dr. Muhammed Basheer Ummathur**
Head, Department of Chemistry

Presidential address : **Dr. C. Saidalavi**
Principal

Inauguration : **Prof. P. Mohammed Shafi** *(Retd.),*
Department of Chemistry, University of Calicut

Release of Seminar Proceedings : **Prof. P. Mohammed Shafi** *(Retd.),*
Department of Chemistry, University of Calicut

Felicitation : **Jb. O. Abdul Ali**
Manager, KAHM Unity Women's College, Manjeri;
Syndicate Member, Calicut University
: **Prof. P.N. Abdurahiman**
Former Principal, KAHM Unity Women's College, Manjeri
: **Dr. C. Abdul Majeed**
Syndicate Member, Calicut University; Associate Professor and HoD of Commerce, KAHM Unity Women's College, Manjeri
: **Mr. Mohamed Ali P**
Staff Secretary; Assistant Professor of English, KAHM Unity Women's College, Manjeri
: **Mr. Mohammed Ali Kanniyan**
Senate Member, University of Calicut; NTS Representative, KAHM Unity Women's College, Manjeri

Vote of Thanks : **Mrs. Suhada K.M,** *Seminar Co-ordinator*

10.45 AM -11.00 AM Tea Break

11.00 AM-1.00 PM :**Technical Session 1**

Chair of the session :**Dr. Geetha Nambiar**
Principal, Govt. Women's College, Malappuram

Talk 1 :**Prof. P. Mohammed Shafi** *(Retd.)*
Department of Chemistry, University of Calicut

Topic : **Medicines of Plant Origin**

Vote of Thanks : **Dr. Jyothi P**
Associate Professor, Department of Chemistry, KAHM Unity Women's College, Manjeri

01.00 PM-2.00 PM : **Lunch Break**

ISBN 978-93-5279-420-1

02.00 PM-4.00 PM : **Technical Session 2**

Chair of the session : **Dr. Muhammed Basheer Ummathur**
Associate Professor, Department of Chemistry, KAHM Unity Women's College, Manjeri

Talk 2 : **Dr. Bijudas K**
Assistant Professor, NSS College, Manjeri

Topic :**Polymorphism in Medicinal Chemistry**

Vote of Thanks : **Ms. Shabana K**
Faculty Member, Department of Chemistry, KAHM Unity Women's College, Manjeri

04.00 PM 05.00 PM : **Oral Presentations**

25/07/2017 Tuesday

09.00 AM 11.00 AM : **Technical Session 3**

Chair of the session : **Mrs. Suhada K.M.**
Assistant Professsor, Department of Chemistry, KAHM Unity Women's College, Manjeri

Talk 3 : **Dr. Muhammed Basheer Ummathur**
Associate Professor, Department of Chemistry, KAHM Unity Women's College, Manjeri

Topic :**Antitumour Activity of Some Synthetic Curcuminoids and their Al(III) Complexes**

Talk 4 :**Dr. Jyothi P**
Associate Professor, Department of Chemistry, KAHM Unity Women's College, Manjeri

Topic :**Anticancer and Antimicrobial Activities of Some Synthetic Nitrogen Heterocyclics**

Talk 5 : **Dr. Deepa K**
Assistant Professor, Department of Chemistry, KAHM Unity Women's College, Manjeri

Topic :**Medicinal Properties of Some Schiff's Base Complexes**

Vote of Thanks : **Ms. Najeera**
Faculty member, Department of Chemistry, KAHM Unity Women's College, Manjeri

11.00 AM 11.15 AM : **Tea Break**

11.15 AM 1.00 PM : **Technical Session 4**

Chair of the Session : **Dr. Bijudas K**
Assistant Professor, Dept. of Chemistry, NSS College, Manjeri

Talk 6 : **Dr. S. Ponnuswami**
Associate Professor of Chemistry, Govt. Arts College (Autonomous), Coimbatore, Affiliated to Bharathiar University

Topic

ISBN 978-93-5279-420-1

	:**Design, Synthesis, Stereochemistry, Biological Activity and Molecular Docking Studies of Substituted Piperidines**
Vote of Thanks	: **Dr. Deepa K**. *Assistant Professsor, Department of Chemistry, KAHM Unity Women's College, Manjeri*
01.00 PM 02.00 PM	: **Lunch Break**
02.00 PM 03.30 PM	: **Technical Session 5**
Chair of the session	: **Dr. Muneer CP** *Assistant Professor & Head, Department of Chemistry, Govt. Arts & Science College, Calicut.*
Talk 7	: **Dr. A. Ramasubbu** *Assistant Professor of Chemistry, Govt. Arts College (Autonomous), Coimbatore, Affiliated to Bharathiar University*
Topic	:**Nanocoposites for Biomedical Applications**
Vote of Thanks	: **Mrs.Shahila Muhammed** *Faculty Member, Department of Chemistry, KAHM Unity Women's College, Manjeri*
03.30 PM 04.30 PM	:**Oral Presentation**
04.30 PM 05.00 PM	**Valedictory Session**
Welcome	: **Mrs. Suhada KM** *Assistant Professor, Department of Chemistry, KAHM Unity Women's College, Manjeri*
Presidential Address	: **Dr. C. Saidalavi**, *Principal*
Distribution of Certificates	: **Adv. U. A. Latheef** *Secretary, KAHM Unity Women's College, Manjeri*
Vote of Thanks	: **Ms. Irfana**, *Chemistry Association Secretary*

National Anthem

ISBN 978-93-5279-420-1

CONTENTS

LECTURES BY RESOURCE PERSONS

ISBN 978-93-5279-420-1

Dr. Deepa K, *Assistant Professor of Chemistry, KAHM Unity Women's College, Manjeri*

RESEARCH PAPERS

ISBN 978-93-5279-420-1

MEDICINES OF PLANT ORIGIN

Prof. P Mohammed Shafi

Professor (Retd.), Department of Chemistry, University of Calicut, Kerala-673635

E-mail: mohamedshafi989@gmail.com

Plants are the most amazing factories where a variety of chemical compounds are being manufactured. Ever since the birth of man plants have provided him with food, shelter and drugs. World Health Organisation (WHO) has estimated that approximately 65% of the world's population relies mainly on plant-derived traditional medicines for their primary health care. Even today about 25% of the medicines used in modern medicine are plant derived compounds.

In this presentation only those molecules that 'changed the world' will be discussed in detail.

Reserpine is one of the earlier plant based molecules that got incorporated into modern medicine. This alkaloid is isolated from ***Rauvolfia serpentina***, a medicinal plant used in Ayurveda for a long time for various illnesses. In modern medicine it has been used for the treatment of high blood pressure. With the availability of better drugs this compound has only a limited use at present. However ***Rauvolfia serpentinais*** is still used in Ayurvedic preparations.

ISBN 978-93-5279-420-1

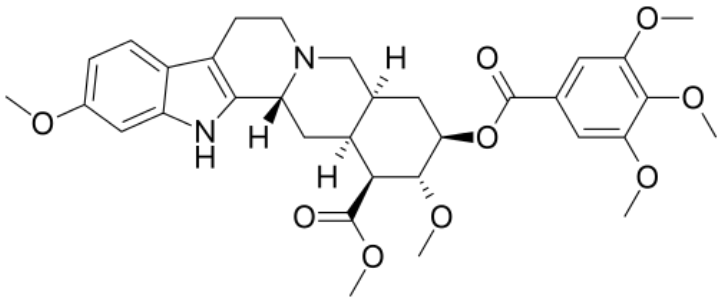

Reserpine

Leprosy was one of the most dreaded diseases of the past. With the introduction of modern medical treatments this disease is under control at present. For many centuries Indian system of medicine used the oil of the seeds of ***Hydnocarpus laurifolia*** or **Chaulmoogra** for the treatment of leprosy with partial relief. The chemical compound for the curative effect was found to be hydnocarpic acid.

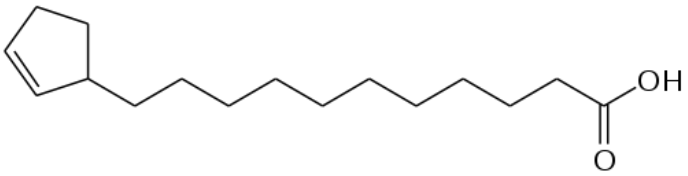

Hydnocarpic Acid

Malaria had been killing millions of people before the finding that Cinchona bark extract can cure this dreaded disease. The active ingredient with curative effect in this extract is Quinine.

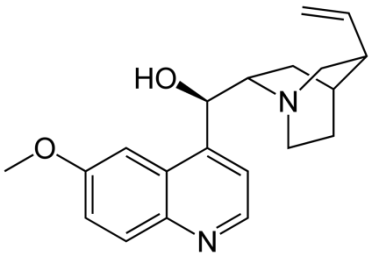

Quinine

Microbial strains causing malaria later developed resistance to quinine. During the nineteen seventies a very effective compound, Artemisinin, against malaria from a Chinese medicinal plant ***Artemisia annua*** was isolated and put into use. One of its derivatives Artesunate is more iffective than the original compound.

ISBN 978-93-5279-420-1

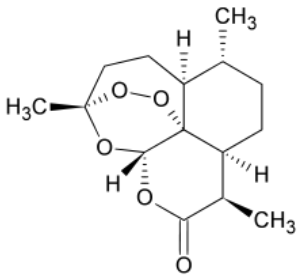

Artemisinin

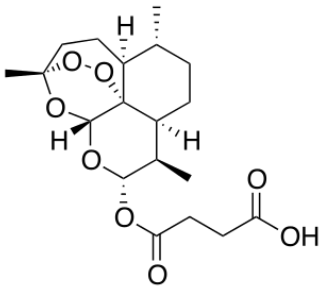

Artesunate

Some of the wonder drugs that made the treatment of heart problems are the cardiac glycosides. Examples include Digoxin from ***Digitalis lanata*** and Digitoxin from ***Digitalis purpurea***

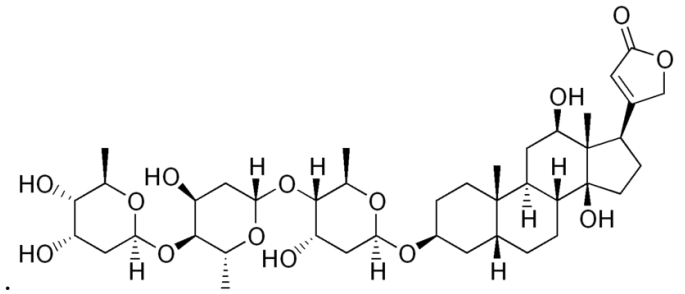

Digoxin (From *Digitalis lanata*)

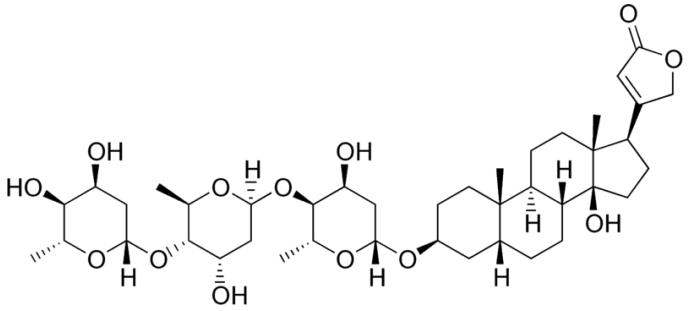

Digitoxin (From *Digitalis puruprea*)

Hippocrates, the fifth century BC Greek- physician wrote about a bitter powder extracted from willow bark that could ease aches and pains and reduce fever. The bark of willow, myrtle, American teaberry or medowsweet bark extracts contain a glycoside Salicin which on hydrolysis and oxidation gets converted to salicylic acid which can relieve pain and reduce fever. Aspirin, the acetyl derivative of salicylic acid is safer than salicylic acid itself.

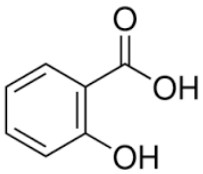

Salicylic Acid

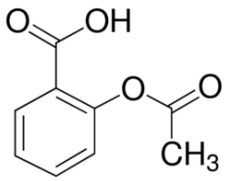

Aspirin (Acetyl salicylic acid)

In spite of its habit forming property morphine is a very effective pain reliever.

ISBN 978-93-5279-420-1

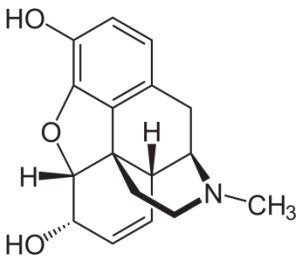

Morphine

Morphine is extracted opium plant, ***Papaver somniferum***

The vinca alkaloids Vincristine and vinblastine have made cancer treatment more effective and meaningful.

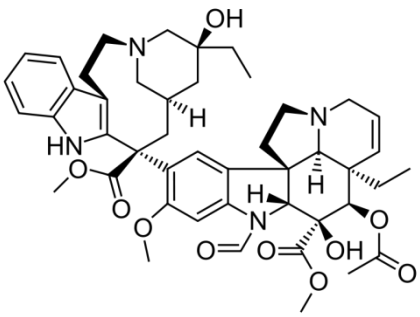

Vincristine

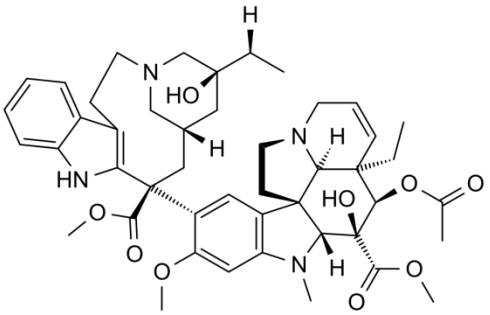

Vinblastine

Apart from some of the wonder drugs mentioned above many of the ingredients in our spices and food items also have marked curative effects.

DESIGN, SYNTHESIS, STEREO CHEMISTRY, BIOLOGICAL ACTIVITY AND MOLECULAR DOCKING STUDIES OF SUBSTITUTED PIPERIDINES

Dr. S Ponnuswamy

PG & Research Department of Chemistry, Government Arts College (Autonomous), Coimbatore – 641 018, Tamil Nadu

E-mail: kspons2001@gmail.com

Due to increase in the number of immuno compromised hosts over the past decades, the incidence of microbial infection has been increasing dramatically. In recent years, there has been much interest in the synthesis of bioactive heterocyclic compounds in the field of

ISBN 978-93-5279-420-1

medicinal chemistry due to their varied biological activity. Nitrogen heterocycles enjoy a prominent position in natural product chemistry due to their significant physiological properties which resulted in numerous medicinal applications (Figure 1). Among the heterocyclic compounds, aza-heterocycles, such as piperidines have a great importance in biological and pharmaceutical chemistry due to their presence as structural motif in numerous natural alkaloids such as solenopsin, nicotine and coniine.

The development of new synthetic methods for use in organic synthesis is one of the areas of organic chemistry that has experienced a major renaissance during the recent past. The 2, 6-diarylpiperidines and their derivatives have in recent years attracted considerable attention due to their possible bio-significance**.** The attachment of electron withdrawing groups like NO, COR, etc., at nitrogen of a 2,6-disubstituted piperidine ring has been reported by our group, as well by others, to exert major changes in the conformation of ring and orientation of the substituents. The conformational preferences of piperidine ring are largely decided by the magnitude of the resonance energy caused by the delocalization of nitrogen lone pair into the *N*-NO and *N*-C=O functions (Figure 2). The relative magnitudes of $A^{1,3}$-strain (Figure 3), torsional strain and 1,3-diaxial interaction are also the deciding factors. Further, pharmacological activity of a substance is, in general, associated with its molecular structure and stereochemistry. Traditionally, small molecules have been a reliable source for discovering novel biologically active agents. Hence the lecture will focus on the synthesis, stereochemistry, in-*vitro* and *in-vivo* biological activity and molecular docking studies on the substituted 2,6-diarylpiperidines.

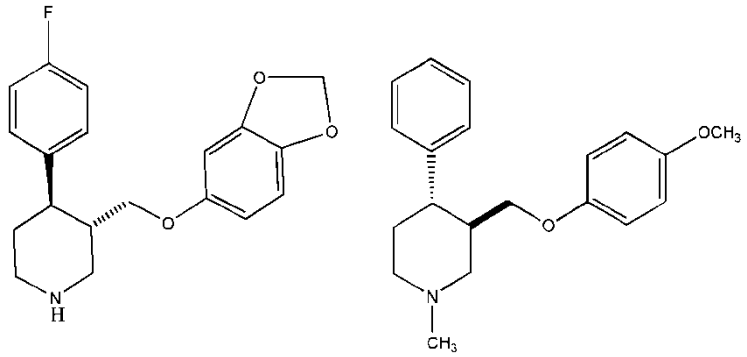

Paroxetine Femoxetine

Figure 1: Examples of biologically active piperidines

ISBN 978-93-5279-420-1

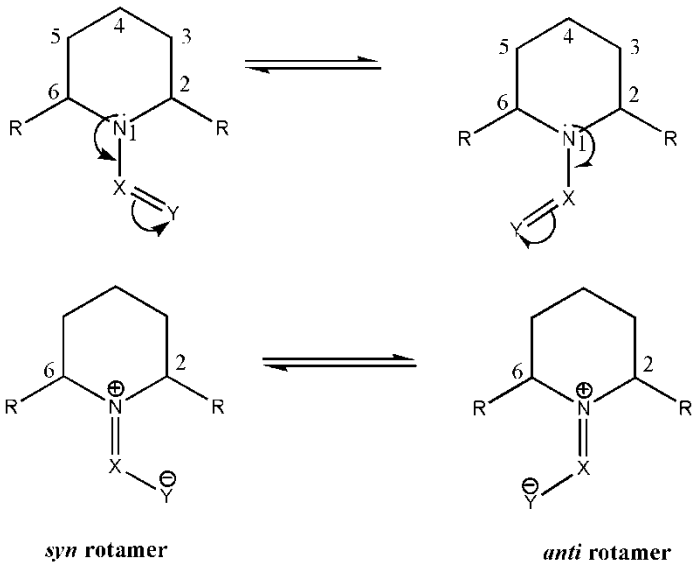

N-X=Y: NO, CHO, COMe, COPh, *etc.*, R= Aryl

Figure 2. *syn* & *anti* orientations of *N*-X=Y

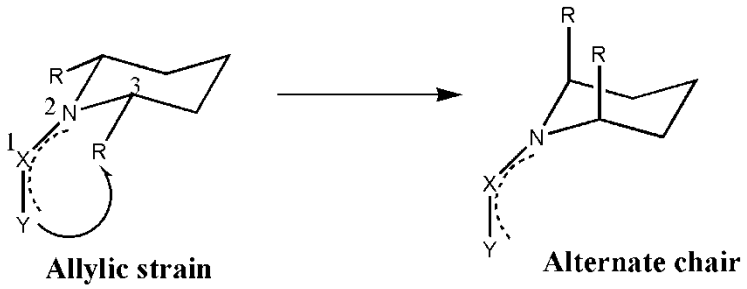

X=Y: NO, CO CH_3, R: CH_3

Figure 3. Allylic strain

References:

1. Dimmock, J. R.; Padmanilayam, M. P.; Puthucode, R. N.; Nazarali, A. J.; Motagananhalli, N. L.; Zella, G. A.; Quail, J. W.; Oloo, E. O.; Kraatz, H. B.; Prisciak, J. S.; Allen, T. M.; Santos, C. L.; Balsarini, J.; Clereg, E. D.; Manavathu, E. K. *J. Med.Chem*. **2001**, *44*, 588.
2. Perumal, R. V.; Adiraj, M.; Shanmugapandian, P. *Indian Drugs,* **2001**, *38*, 156.
3. Ravindran, T.; Jeyaraman, R.; Murray, R. W.; Singh, *M. J. Org. Chem*. **1991**, *56*, 4833.
4. Jeyaraman, R.; Senthil kumar, U. P.; Bigler. P. *J. Org. Chem*. **1995**, *60*, 7461.
5. Jeyaraman, R.; Ponnuswamy, S. *J. Org .Chem.***1997**, *62*, 7984.
6. Sakthivel, P.; Ponnuswamy, S. *J. Mol. Struct*. **2014**, *1074*, 349.

ISBN 978-93-5279-420-1

7. Akila, A.; Ponnuswamy, S.; Shreevidhyaasuressh, V.; Usha, G. *J. Mol. Struct*. **2015,** *1093*, 113.
8. Ponnuswamy, S.; Akila, A.; Krithigadevi, D. *Synth. Commun*. **2015,** *45*, 2030.
9. Sethuvasan, S.; Sugumar, P.; Maheswaran, V.; Ponnuswamy, M. N.; Ponnuswamy, S. *J. Mol. Struct*. **2016,** *1116*, 188.
10. Aridoss, G.; Parthiban, S.; Ramachandran, R.; Prakash, P.; Kabilan, S.; Jeong, Y. T. *Eur. J. Med. Chem*. **2009**, *44*, 577.
11. Ponnuswamy, S.; Kayalvizhi, R.; Jamesh, M.; Thenmozhi, M.; Ponnuswamy, M. N. *J. Mol*. *Struct*. **2016**, *1120*, 70.
12. Akila, A.; Jeganathan, P.; Ponnuswamy, S. *J. Mol*. *Struct*. **2016**, *1120*, 187.
13. Mohanraj, V.; Ponnuswamy, S. *J. Mol*. *Struct*. **2017**, *1144*, 502.

ISBN 978-93-5279-420-1

BIONANOCOMPOSITES TOWARDS BIOMEDICAL APPLICATIONS

Dr. Alagunambi Ramasubbu

PG & Research Department of Chemistry, Government Arts College (Autonomous), Coimbatore – 641 018, Tamil Nadu

E-mail: alagunambi.ramasubbu@gmail.com

Biopolymers, which are formed by any living organisms or made from biomass, are polymers that degrade by the action of micro-organisms, heat or moisture. Such Biopolymers play immense role various fields due to their advantages such as biocompatibility and degradability, flexibility, ease of handling, etc. They find immense applications Biopolymers were classified into various categories, viz., Polysaccharides (Glycogen, Starch, Cellulose, Pectin, Amono sugars, Chitin, Chitosan, Heparin (Heteropolysaccharides)), Peptides, Proteins, Nucleic Acids, DNA, Lipids, etc. The utility of Biopolymers and their nanocomposites have the potential in overcoming the limitation of conventional cancer chemotherapy that are hampered by indiscriminate distribution of drugs in the body, and multidrug resistance in cancer. Hyaluronic acid (HA), a polyanionic polysaccharide is found abundant in the extracellular matrix (ECM) and synovial fluid. Recent studies, showed that various tumors, such as epithelial, colon, and ovarian cancers, are known to over-express HA-binding receptors (CD44 and RHAMM). Consequently, these tumor cells show enhanced binding to and effective internalization of HA thereby HA acts as an effective cancer drug carrier and efficient therapeutic delivery vessel in chemotherapy with minimal or no side effects. The targeted drug delivery through enhanced therapeutic efficacy were attributed to its very high rate of accumulation around the solid tumor cells due to its anatomical and patho-physiological abnormalities of the host cancer cells/tissues, hefty vascular permeability, lack of lymphatic drainage, etc., of the polymer matrix. In a similar fashion, Owing to its favourable biological activities and anti-coagulating properties, Heparin a simple biopolymer has been employed as an anticoagulant and antithrombotic drug for more than half a century, with growing demand every day, its growing current usage is around 50 Crore doses per year prior to most major surgeries.

The impregnation of small quantities of inorganic materials viz., metal, semiconducting metal oxides and chalcogenides Quantum Dots, or SPIO, Shape Memory Alloys (SMAs), etc., into the Biopolymers resulted in the formation of novel materials with enhanced tailor made properties like enhanced stability into Biopolymer nanocomposites towards drug delivery and other applications (Scheme). They tend to modify the action of polymers; primarily the physical, mechanical and operational characteristics via ionic or co-ordination cross-linking through cohesion and adhesion to form nanocomposite materials of new architecture via synergic effects. The salient features are their higher specific surface area which leads to higher density, surface energy and a better bonding between the two phases. allowing sustained blood circulation, tissue retention, slow renal filtration, reduced / almost nil toxicity, lack of

ISBN 978-93-5279-420-1

immunogenicity, improved target specificity, etc., find promising applications in Cancer Therapy, Bio-imaging diagnostic and Therapeutic applications (Scheme).

On the other hand, our body apart from trace elements, made fully of water, bones and polymers, has a tendency to accept and accommodate and assimilate anything mimicking our body components. Hydroxyapatite that provides rigidity to bone and teeth is a major component of bone minerals and the matrix of teeth, and the systemic studies on Hydroxyapatite and its polymer nanocomposites throw light on bone tissue engineering and in orthodontic applications. Towards this preliminary works on bone tissue engineering biopolymer hydrogel encapsulated inorganic materials as scaffolds were studied. Towards this, this presentation will focus on the synthesis and characterization of various Bionanocomposites of Polysaccharides, Peptides, Proteins encapsulated with metal and metal, metal oxides, chalcogenides, SMAs, SPIOs, Hydroxyapatite, etc., in combination with standard drugs (Paclitaxel – Taxol, Daunorubicin / Doxorubicin) and their Physicochemical Characteristics, and Biological Applications towards Bone Tissue Engineering, Orthodontic Dental and Anticancer studies, etc.

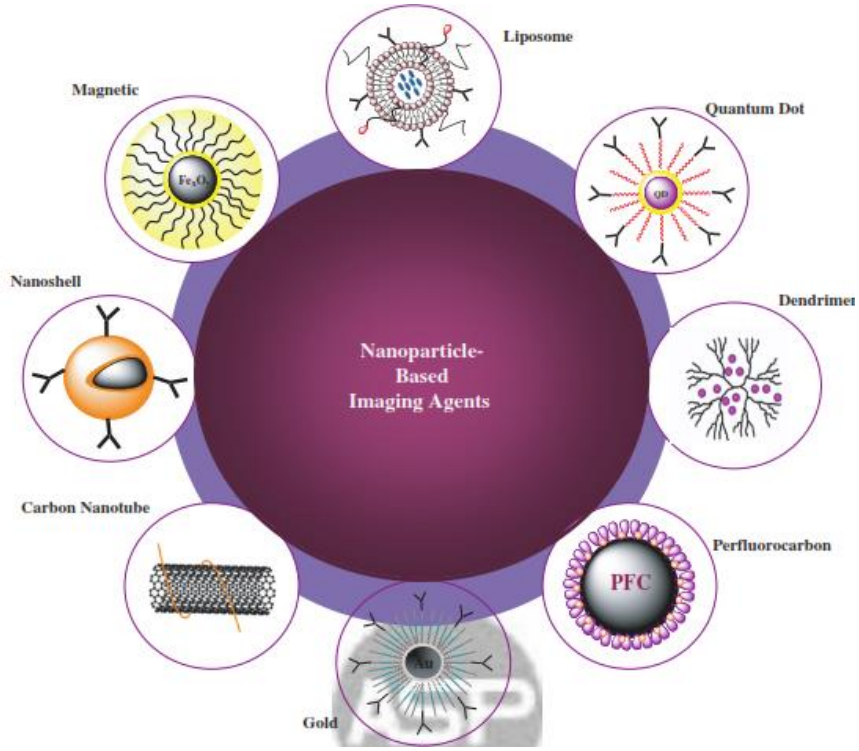

Scheme 1: Nanoparticles based Drug Delivery: Representative Nanoparticles that can target specific biological process for cellular and molecular imaging[1].

ISBN 978-93-5279-420-1

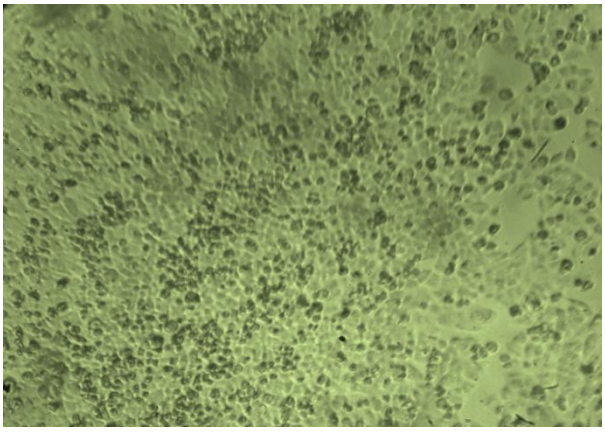

IC_{50} 100 ⌈g/mL

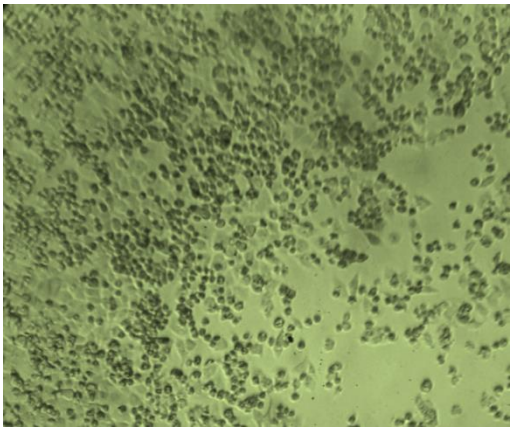

Conc. 400 ⌈g/mL

Control

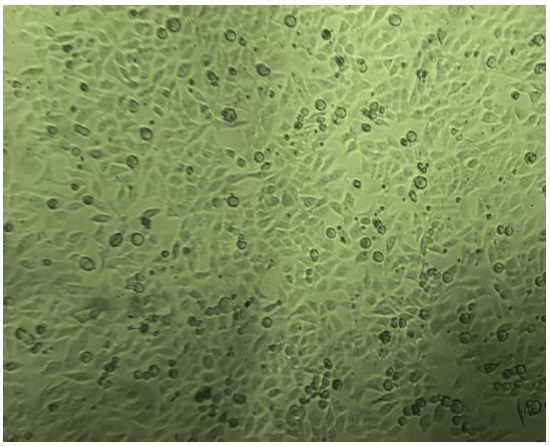

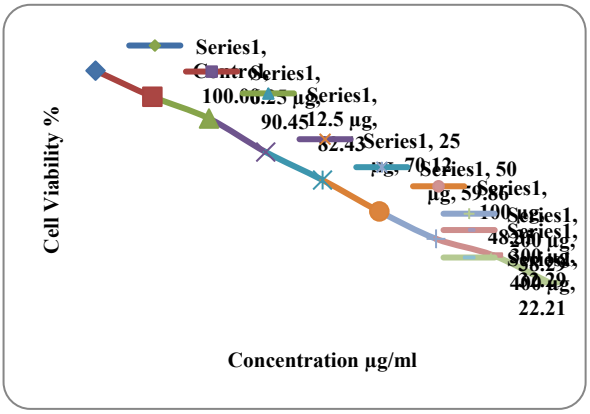

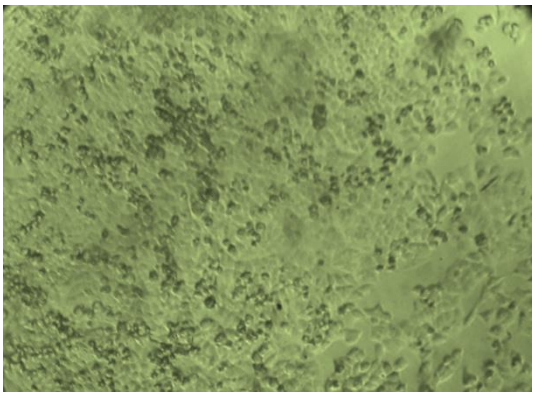

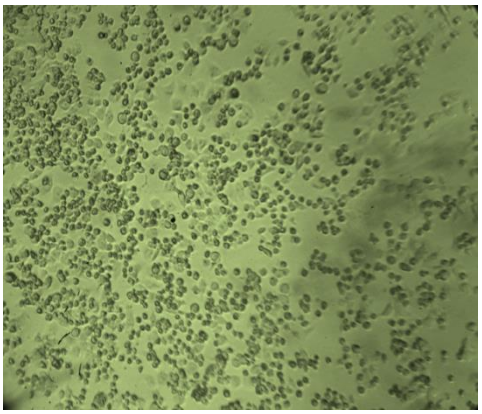

IC_{50} 100 ⌈g/mL

Conc. 400 ⌈g/mL

ISBN 978-93-5279-420-1

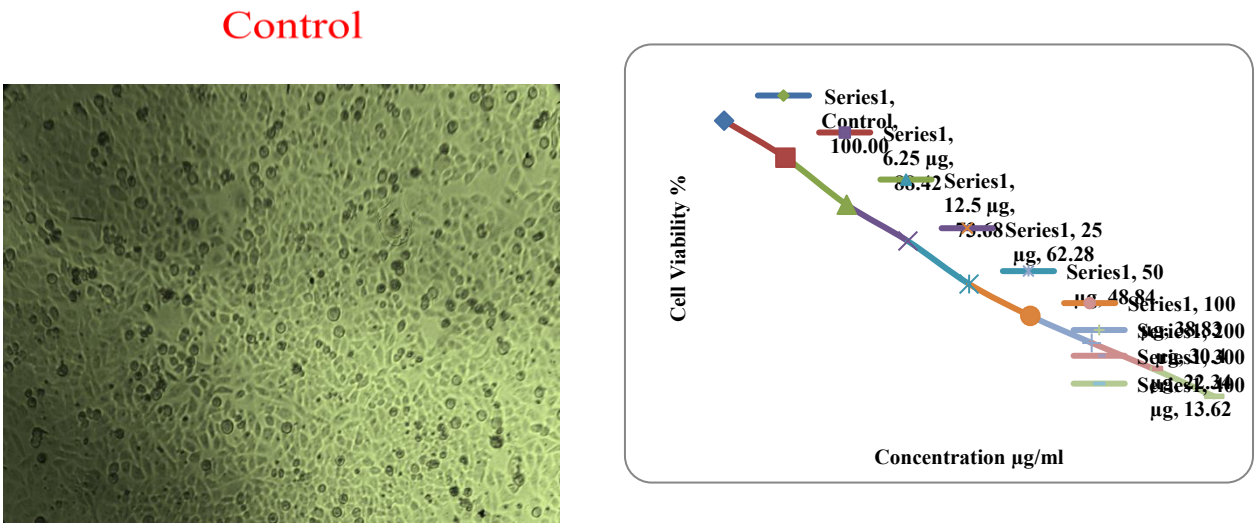

Fig. 1: *Anticancer activity of Soy Protein Isolate (Top) & PECTIN (Bottom) – NC against the Hela Cell lines*

References

1. G. Saravanakumar, K. Kim, J.H. Park, K. Rhee, I.C. Kwon, J. Biomed. Nanotechnol., 5, (2009), 20 – 35.
2. R. Saravanan, Advances in Food and Nutrition Research, Elsevier Inc., Volume 72, 2014, Chapter III, pp – 45 – 60.; http://dx.doi.org/10.1016/B978-0-12-800269-8.00003-8.

POLYMORPHISM IN MEDICINAL CHEMISTRY

Dr. Bijudas K

Department of Chemistry, N. S. S. College, Manjeri-676122, Malappuram (DT), Kerala

E-mail: bijudask@gmail.com

Polymorphism comes from the Greek word, Polus = many and morph = shape. Polymorphism is defined as the ability of a substance to exist as two or more crystalline phases that have different arrangements or conformations of the molecule in the crystal lattice. It is essentially means that in different polymorphs, the same molecule exist in different ways.

The pharmaceutical industry faces a deadly and swift saboteur. This attacker hits unexpectedly and comes under the title 'polymorphism'. A new polymorph can be catastrophic; overnight a drug manufactured for market can become less soluble and less bioavailable. Although a compound's polymorphs are chemically identical, their physical properties can be tremendously different.

A new polymorph can appear suddenly in a manufactured drug, with devastating results. Although chemically identical, the new polymorph can have very different physical properties. Polymorphism was first discovered in 1821 by the German chemist Eilhard Mitscherlich and is a widespread phenomenon in the chemical world. Polymorphs differ in

ISBN 978-93-5279-420-1

their outer form (habit) as well as their inner structure (form). For example, polymorphs of paracetamol crystals may appear as prisms or monoliths.

The first polymorph to form may be metastable and liable to convert to a different, more stable, form over time or under different conditions of re-synthesis. The most stable polymorph at room temperature may become metastable at another temperature; transitions between polymorphs may occur as the temperature is raised or lowered – a crucial consideration when shipping a pharmaceutical or food product.

It is estimated that 30–50 per cent of pharma compounds exhibit polymorphism. For eg. Paracetamol (acetaminophen) is widely used as antipyretic (fever suppressant) and analgesic (pain killer). It has been shown to exist in two polymorphic forms; one is monoclinic which is marketed whereas form II is orthorhombic which can convert to form I. Similarly polymorphism of other important drugs has been studied with the help of various analytical techniques.

In industry, the existence of polymorphs is best discovered sooner rather than later, as US pharmaceutical firm Abbott Laboratories learnt to its cost. In 1998 the company found that it could no longer make the original form of its HIV drug Ritonavir because a second polymorph had taken the place of the first during manufacture. Abbott scientists had discovered that the drug was starting to fail dissolution tests and precipitating out of capsules. Investigation showed the existence of polymorph II (needles), which was more soluble and less stable than polymorph I (rods). Form II soon spread and form I could no longer be synthesized.

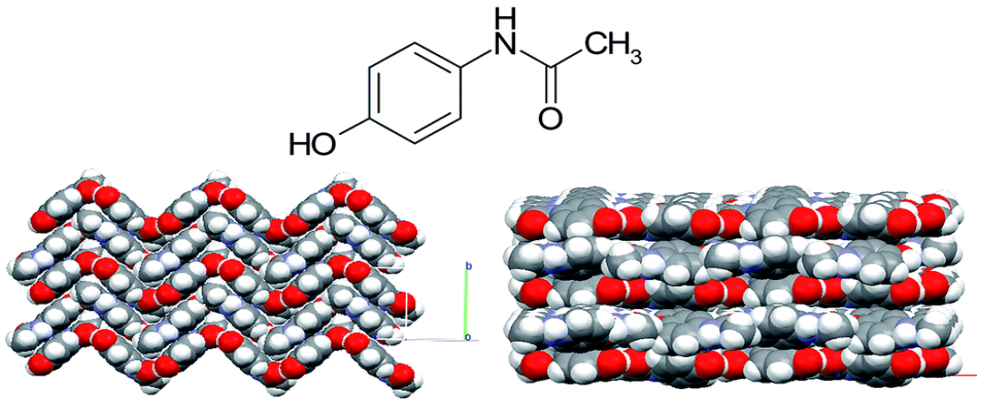

Form I (stable) Form II (metastable)

ISBN 978-93-5279-420-1

Form II Form I

References

1. Rahul Purohit & P Venugopalan. *Polymorphism: An Overview*, Resonance, September 2009.
2. J J Vittal, A Ramanan, G R Desiraju. *Crystal Engineering, A text book*, IISc Press, 2011.
3. R Hilfiker. *Polymorphism: In the pharmaceutical industry*, Wiley-VCH, Germany, 2006.
4. H G Brittain. *Polymorphism in pharmaceutical solids*, CRC Press, USA, 2009.
5. J Bernstein. *Polymorphism in molecular crystals*, International Union of Crystallography, 2002.

ANTITUMOUR ACTIVITY OF SOME SYNTHETIC CURCUMINOIDS AND THEIR Al(III) COMPLEXES

Dr. Muhammed Basheer Ummathur

PG Department of Chemistry, KAHM Unity Women's College, Manjeri-676122, Malappuram (DT), Kerala

E-mail: mbummathur@gmail.com

ISBN 978-93-5279-420-1

Curcuminoids (1,7-diaryl-1,6-heptadiene-3,5-diones), extracted from the rhizomes of the traditional Indian medicinal plant turmeric (*Curcuma longa,* Linn., *Zingiberacea* family), have been reported to possess anti-inflammatory, anti-oxidant, anti-arthritic and anti-tumour activities. Presence of phenolic group together with the conjugated β-diketone structure is responsible for their high biological activity and this led to further studies using several structurally related compounds. The medicinal importance of many plant chemicals are enhanced by complex formation with various metal ions. Metal complexation of these unsaturated 1,3-diketones lead to dramatic changes in their biochemical properties including antitumour activity. The antitumor activities of natural and synthetic curcuminoids are enhanced by complexation with some transition metal ions even though these metal ions themselves are toxic to animal body.

The curcuminiod analogues (Fig. 1) were prepared by the condensation of aromatic aldehydes with acetylacetone-boric oxide complex in ethylacetate medium in the presence of tri(*sec*-butyl)borate and *n*-butyl amine. Their Al(III) complexes (Fig. 2) were prepared from $Al(NO_3)_3.9H_2O$.

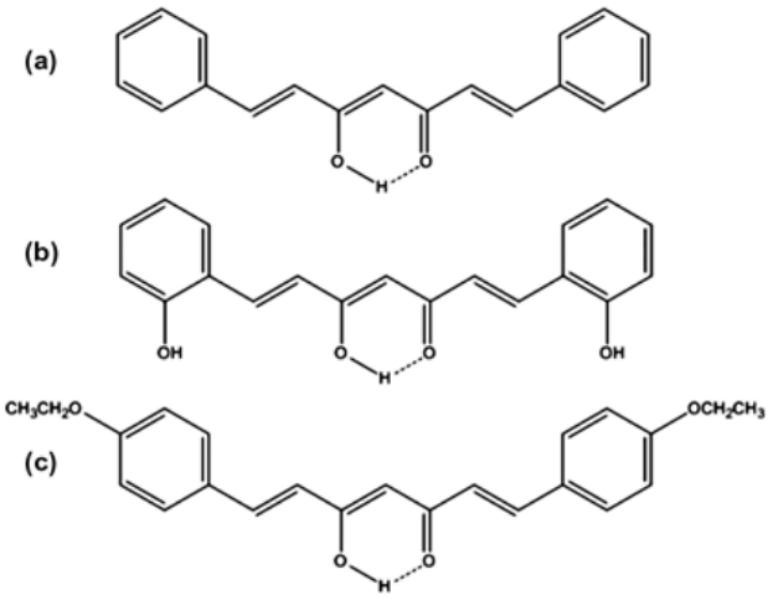

Fig. 1. Structure of curcuminoid analogues: (a) 1,7-diphenyl-1,6-heptadiene-3,5-dione (HL^1); (b) 1,7-bis(2-hydroxyphenyl)-1,6-heptadiene-3,5-dione (HL^2); (c) 1,7-bis(4-ethoxyphenyl)-1,6-heptadiene-3,5-dione (HL^3)

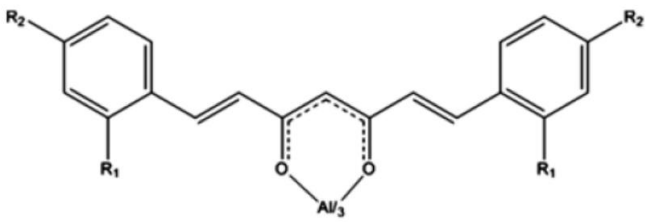

Fig. 2. Structure of the aluminium complexes of curcuminoids

	R_1	R_2

ISBN 978-93-5279-420-1

$[Al(L^1)_3]$	H	H
$[Al(L^2)_3]$	OH	H
$[Al(L^3)_3]$	H	OCH_2CH_3

Ehrlich ascites carcinoma cells were used for *in vitro* cytotoxic studies. The compounds were dissolved in minimum quantity of DMSO which does not enhance cytotoxicity. The tumour cells aspirated from the peritoneal cavity of tumour bearing mice were washed with PBS (phosphate buffered saline). The cell suspension (1 x 10^6 cells in 0.1 mL) was added to tubes containing various concentrations (1-50 ⌈g/ml) of the compounds and volume was made up to 1 ml using PBS. The mixture was incubated for 3 hours at 37^0C and the percentage of dead cells were evaluated by trypan blue dye exclusion method. The results indicate that metal chelation enhance the cytotoxicity of compounds considerably. Among the compounds subjected to short term assay the aluminium complex of HL^2, with a hydroxyl group in the phenyl ring, is found to be the most active and HL^1, which possess unsubstituted benzene ring system, shows low activity.

L929 cells were used for tissue culture studies. The cells (5 x 10^3 cells/well) were plated in tarzon's 96 well flat bottom titre plates and incubated at 37^0C in 5% CO_2 atmosphere. After 24 hours of incubation various concentrations (1-10 ⌈g/ml) of compounds were added to the wells and incubated for a further period of 48 hours. After incubation, the cells were detached by trypsinization (0.2%) and stained with crystal violet. The cytotoxicity was calculated by measuring the optical density at 570 nm after eluting the dye from the cells. The results indicate that the aluminium chelates are more cytotoxic than the respective curcuminoids. Compound HL^1 is the least active and aluminium complex of HL^2 is the most active.

Groups of Swiss albino mice (6 per group) were injected intraperitonially (ip) with Ehrlich ascites tumour cells (1 x 10^6 cells/animal). The animals were injected (ip) with test compounds (200 ⌈moles/kg body weight) suspended in gum accasia and the injections were continued for 10 days. The mortality rate of mice were noted in each group and the percentage increase in life span (% ILS) of the treated group was calculated using the formula %ILS = [100(T-C)]/C, where T is the mean survival time of treated mice and C is that of control expressed in days. All the compounds when administered intraperitonially (ip) produced significant increase (p <0.001 from normal) in the life span of mice bearing ascites tumours. Aluminium (III) complexes produced a considerable increase in life span of tumour bearing mice compared with that of curcuminoids. The percentage increase in life span (%ILS) of tumour bearing mice was found minimum for HL^1 and maximum for aluminium complex of HL^2. The results reveal that antitumour activities of curcuminoids are enhanced more by complexation with aluminium than with transition metal ions.

The effect of various compounds on solid tumour development was studied using Swiss albino mice. Groups of mice (6 per group) were injected subcutaneously with DLA cells (10^6 cells in 0.1 ml) on the right hind limbs. One group was kept as control and other groups were injected (ip) with test compounds (200 ⌈moles/Kg body weight) and the injections were continued for 10 days. Tumour diameter was measured every third day for one month and tumour volume calculated using the formula, $V = 4/3\pi r_1 r_2^2$ where r_1 and r_2 are the minor and major radii respectively. Reductions of solid tumour volume in mice by the administration of

ISBN 978-93-5279-420-1

compounds (ip) show that compared to free curcuminoids their respective aluminium (III) complexes are remarkably active in reducing tumour volume in mice.

The results clearly reveal that HL^2**,** with hydroxyl groups on the phenyl ring, shows the maximum activity towards cytotoxicity on Ehrlich ascites and cultured L929 cells, percentage increase in life span and reduction of solid tumour volume in mice. This may be due to the peculiar nature of curcuminoid analogue which can yield phenolic structure upon metabolism as well as due to the extended conjugation. Among the compounds studied HL^1, with unsubstituted benzene ring, showed least activity. Complexation with aluminium significantly increased the cytotoxic and antitumour activities of curcuminoids. The study suggests that the main group element aluminium forms stable complexes with curcuminoid analogues and significantly enhances antitumour activity of these compounds than in their transition metal complexes. This may be due to the comparatively high solubility of aluminium complexes in the body fluids than the transition metal complexes. Further studies have to be conducted to elucidate the exact mechanism of action.

References

1. S. Chitra, J. Sonia, K.B. Ajaikumar, A.B. Bharat. *Cancer Lett.*, **267**, 133 (2008).
2. J. Ravindran, G.V. Subbaraju, M.V. Ramani, B. Sung, B.B. Aggarwal. *Biochem. Pharmacol.,* **79**, 1658 (2010).
3. C.A. Mosley, D.C. Liotta, J.P. Snyder. Adv. Exp. Med. Biol., **595**, 77 (2007).
4. V.D. John, K. Krishnankutty. *Synth. React. Inorg. Met.-Org. Chem.,* **33**, 343 (2003).
5. H.J.J. Pabon. Rec. Trav. Chim., **83**, 237 (1964).
6. G. Kuttan, D.M. Vasudevan, R. Kuttan. Cancer Lett. **41**, 307 (1988).
7. J.R. Anto, K.V. Dineshbabu, K.N. Rajasekharan, R. Kuttan. Cancer Lett., **94**, 74 (1995).

ANTICANCER AND ANTIMICROBIAL ACTIVITIES OF SOME SYNTHETIC NITROGEN HETEROCYCLICS

Dr. P Jyothi

ISBN 978-93-5279-420-1

PG Department of Chemistry, KAHM Unity Women's College, Manjeri-676122, Malappuram (DT), Kerala

E-mail: jyothi@unitywomenscollege.in

The structural diversity and biological importance of nitrogen containing heterocycles have made them attractive targets for synthesis over many years. They are found in various natural products and have been identified as products of chemical and biological importance. Nitrogen heterocyclics have been widely studied and used in the synthesis of numerous alkaloids. Their importance as precursors to many biologically active compounds has focused a tremendous amount of attention on developing methods to functionalize these systems. The synthesis of nitrogen heterocyclics and their derivatives occupy an important place in the realm of natural and synthetic organic chemistry due to their therapeutic and pharmacological properties. They have emerged as integral backbones of over seven thousand existing drugs. In addition to these important biological applications, nitrogen heterocyclics are ideal scaffolds for making libraries of drug like compounds, and to generate libraries of inhibitors of HIV-1 protease.

Heterocyclic compounds are very widely distributed in nature and are essential to life. They play a vital role in the metabolism of all living cells. The pyrimidine and purine bases of DNA, essential amino acids proline, histidine, trytpophane, the vitamin and co-enzyme precursors thiamine, riboflavin, pyridoxine, folic acids, the B_{12} and E families of vitamin, the photosynthesizing pigment chlorophylls the oxygen transporting pigment, hemoglobin and its breakdown products, the cute pigments are heterocyclic compounds. Majority of synthetic heterocycles are found widespread, used as anticancer agents, analgesics, hypnotics, pesticides, weedicides and rodenticides. There are a larger number of synthetic heterocyclics with other practical application, as dyestuffs, co-polymers, solvents, photographic sensitizers, developers, antioxidants, and vulcanization accelerators in rubber industry.

Imidazolinones, a class of heterocyclic compounds, are found to have several pharmacological activities. The benzylidene imidazolinone chemistry with its diverse biological properties like central nervous system depressant, anticonvulsant and monoamine oxidaze inhibitor has received importance in recent years. Novel 4-(aminoaryl)methylene-2-aryl-2-imidazolin-5-ones were synthesized by a tandem reaction between imidic acid ester and glycene ester in presence of a base. Computational analysis was carried out to the druggability of the new molecules. *In vitro* anticancer screening of the aminoimidazolinones and one of their trichlorides were carried out using eight cancer cell lines of various origins. The results successfully establish the synthesized aminoimidazolinone derivatives as novel compounds with pronounced anticancer activity and drug like properties.

The novel aminoimidazolines synthesized were obtained in good yield and their proposed structure was confirmed by spectral analysis. The newly synthesized molecules showed drug-like properties and their properties are similar to known drugs, used as non-steroidal anti-inflammatory, sulphonamide antibacterial and immunosuppressive drug.

The cytotoxic evaluation of aminoimidazolinone obtained from 4-cyanopyridine showed that the compound is inducing moderate toxicity in the cancer cell lines: HeLa, HCT 116 and MDA-MB-231. The trichloride and aminoimidazolinone synthesized from 2-cyanopyridine are specific to the cervical cancer cell ilne HeLa. Melanoma cell line A375 amd

ISBN 978-93-5279-420-1

breast cancer cell line MDA-MB-231. On comparing the anticancer activity of trichloride and aminoimidazolinone from 2-cyanopyridine trichloride was more potent than the aminoimidazolinone to the cancer cells lines: HeLa, A375 and MDA-MB-231.

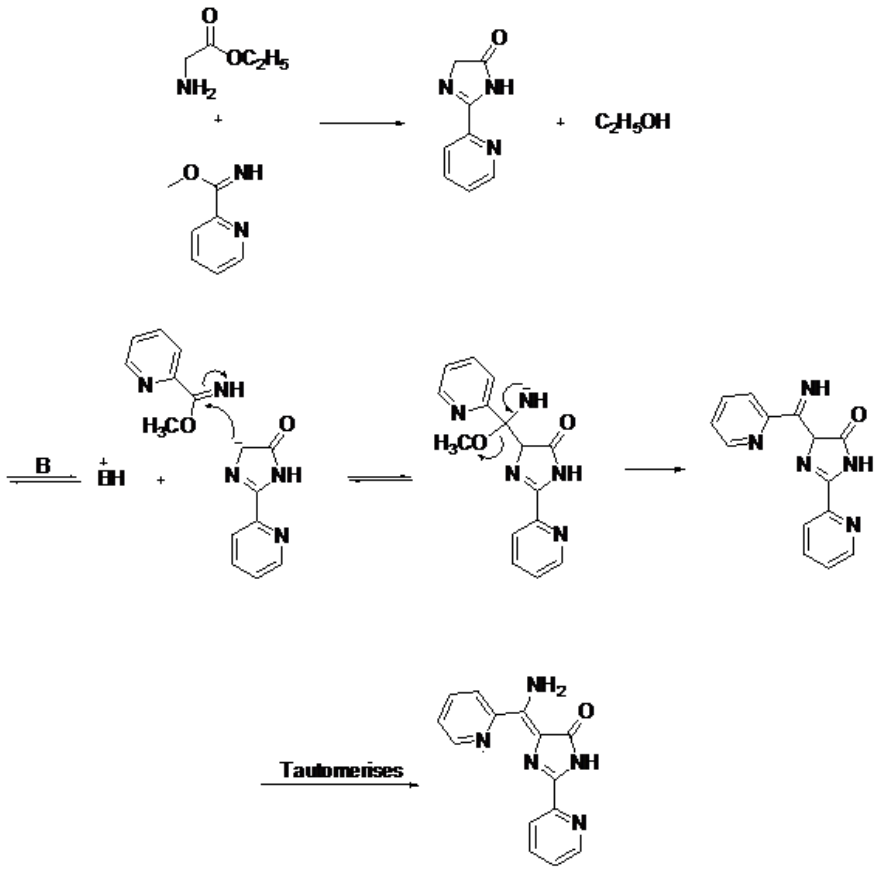

Fig. 1. Synthesis of 4-(amino-2-pyridyl)methylene-2-(2-pyridyl)-2-imidazolin-5-one

References

1. Desai NC, Bhavsar AM, Baldaniya BB. Synthesis and antimicrobial activity of 5-imidazolinone derivatives. Indian J Pharm Sci 2009, 71, 90.
2. Hossanein HH, Khalifa MM, Eli-samaloty ON, Abd El-Rahim M, Taha RA, Ismail MF. Synthesis and biological Evaluation of novel imidazolne derivatives as potential COX-2 inhibitors. Arch Pharmacol Res 2008, 31, 562.
3. Solankee A, Kapadia K, Patel, Thakor I. synthesis and antimicrobial activity of 1-phenul/substituted phenyl/benzyl/naphthyl-2-phenyl-4-(3'-phenoxybenzylidene) imidazolin-5-ones. Asian J Chem 2002, 14,699.
4. Feng Shi, Xiao-Ning Zeng, fei-Yue Wu, Shu Yan, Wei Fa Zheng, Shu Ziang Tu. Efficient microwave assisted synthesis and antioxidant activity of 4-arylidine-2-phenyl-1H-imidazol 5(4H)-ones. J Heterocyclic Chem 2012, 49, 59.

MEDICINAL PROPERTIES OF SOME SCHIFF'S BASE COMPLEXES

ISBN 978-93-5279-420-1

Dr. Deepa K

PG Department of Chemistry, KAHM Unity Women's College, Manjeri-67612, Malappuram (DT), Kerala

E-mail: deepakarat@yahoo.com

Compounds containing an azomethine group (-CH=N-), known as Schiff bases are formed by the condensation of a primary amine with a carbonyl compound. Schiff bases of aliphatic aldehydes are relatively unstable and are readily polymerizable while those of aromatic aldehydes, having an effective conjugation system, are more stable. These compounds and their metal complexes are very important as catalysts in various biological systems, polymers, dyes and medicinal and pharmaceutical fields. Schiff bases appear to be an important intermediate in a number of enzymatic reactions involving interaction of an enzyme with an amino or a carbonyl group of the substrate. One of the most important types of catalytic mechanism is the biochemical process which involves the condensation of a primary amine in an enzyme usually that of a lysine residue, with a carbonyl group of the substrate to form an imine, or Schiff base. Several azomethines were reported to possess remarkable antibacterial, antifungal, anticancer and diuretic activities. The activity is usually increased by complexation. Therefore understanding the properties of both ligands and metal can lead to the synthesis of highly active compounds. The influence of certain metals on the biological activity of these compounds and their intrinsic chemical interest as multidentate ligands has prompted a considerable increase in the study of their coordination behaviour. Development of a new chemotherapeutic Schiff bases and their metal complexes is now attracting the attention of medicinal chemists.

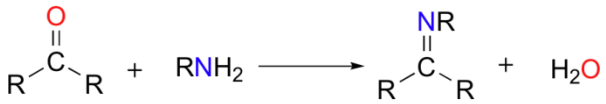

Schiff base (imine)

Metal complexes of Schiff base derived from 2-thiophenecarboxaldehyde and 2-aminobenzoic acid have been recommended and/ or established a new line for search to new antitumor particularly when one knows that many workers studied the possible antitumor action of many synthetic and semi synthetic compounds.

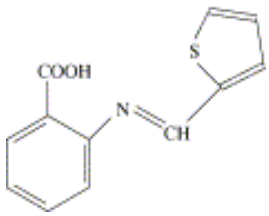

Schiff base derived from indoline-2, 3-dione and 2-aminobenzoic acid and its tin complex showed antibacterial activity against *Staphylococcus aureus*. The results compared with standard drug (Imipinem) have indicated that compounds were active, but activity was lesser than the standard drug. This activity might be due to the presence of a hydroxyl and phenyl group.

ISBN 978-93-5279-420-1

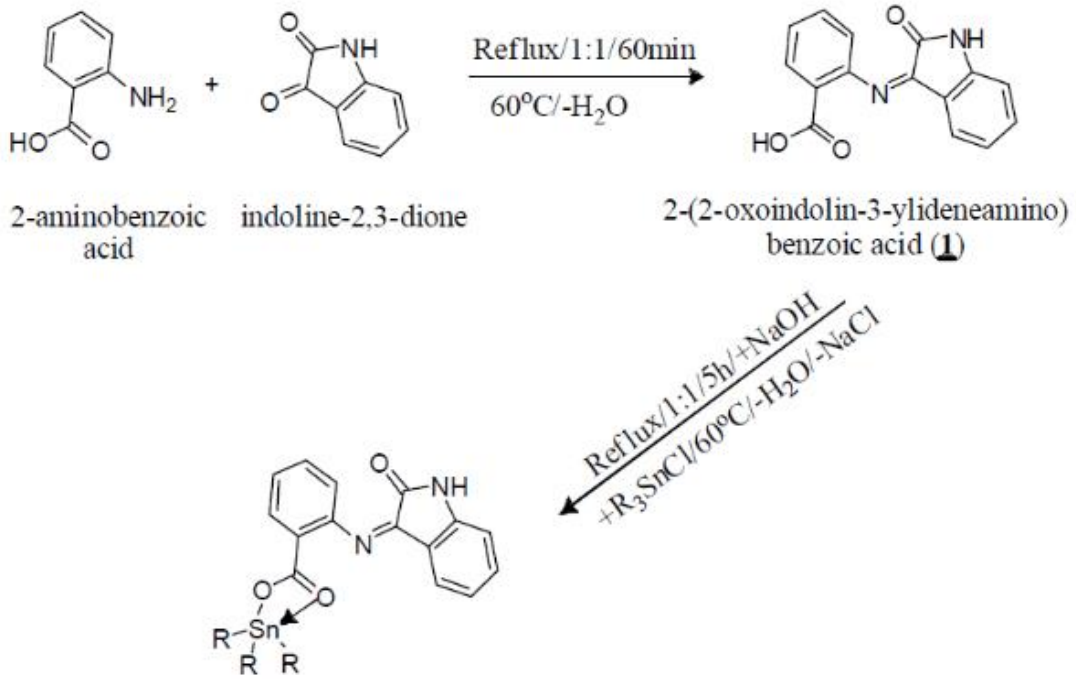

Schiff bases and metal complexes of 4–aminoantipyrine are also known for their great variety of applications in the area of catalysis and biological activity ranging from antitumour, fungicide, bactericide, antiinflammatory and antiviral activities. Reports on drugs showed increased activity when administered as metal complexes rather than as organic compounds. Investigation on the interaction of DNA with small molecules is also important in the design of new types of pharmaceutical molecules. Some kinds of metal complexes interact with DNA that could induce breakage of DNA strands. In light of research, it have been concluded that the precise nature of the Schiff base ligands is of remarkable importance in the interaction of the complex with the DNA molecule.

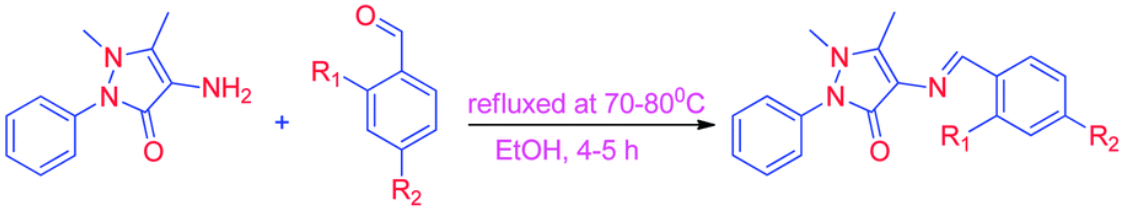

Where, $R_1 = H$, $R_2 = H$: AAPB
$R_1 = OH$, $R_2 = H$: AAPS
$R_1 = H$, $R_2 = Cl$: AAPC
$R_1 = H$, $R_2 = OCH_3$: AAPM

ISBN 978-93-5279-420-1

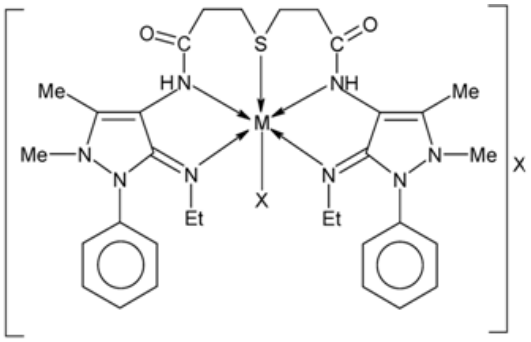

References

1. T.Barboiu, M.Luca, C.Pop, E.Brewster, M.E. Dinculescu. Eur. J. Med. Chem., 31, (1996) 597.
2. E.Ispir, S.Toroglu, A.Kayraldiz, Transition Met. Chem 33 (2008) 953.
3. Keypour, M.Rezaeivala, L.Valencia, P.Perez-Lourido, H.Raza Khavasi. Polyhedron 28(2009) 3755.
4. Salvat, L.Antonnacci, R.H.Fortunato, E.Y.Suarez, H.M.Godoy, J. App. Microbiol, 32 (2001) 293.
5. Hodnett E.M, Wu A.W., French F.A., Eur. J. Med. Chem. Chem. Ther. 13(1987) 577.
6. Hodnett EM, Mooney PD, Antitumor Activities of Schiff Bases, J Med Chem, 13(4) (1970) 786.
7. Hodnett EM, Dunn WJ, Cobalt Derivatives of Schiff Bases of Aliphatic Amines as Antitumor Agents, J Med Chem, 15(3) (1972) 339.
8. Raman N, Raja SJ, Joseph J, Raja JD, Synthesis, Spectral Characterization and DNA Cleavage Study of Heterocyclic Schiff base Metal Complexes, J Chilean Chem Soci, 52 (2007) 1138.

ISBN 978-93-5279-420-1

PHYTOTOXIC EFFECT OF HEAVY METAL IONS ON THE ROOT NODULE FORMATION AND PLANT GROWTH OF *Vigna unguiculata*

Muhammed Basheer Ummathur[1*], Ramees Jebin Paravakkal[1] and Usman Areerath[2]

[1]*PG Department of Chemistry, KAHM Unity Women's College, Manjeri-676122, Kerala*

[2]*PG Department of Botany, KAHM Unity Women's College, Manjeri-676122, Kerala*

[*]*E-mail: mbummathur@gmail.com*

Abstract: Effect of five heavy metal ions; cadmium, cobalt, lead, manganese and copper were investigated on leguminous plant species cowpea (*Vigna unguiculata*). The plant growth characters are seriously affected by a concentration of 0.3, 0.6 and 0.9 ppm of Cd(II), Pb(II), Co (II) and Cu(II); but the concentration of manganese favor the plant growth characters. The root and shoot growth of the cowpea plant is decreased by various concentration of heavy metal ions. The plant could not germinate in the soil containing 0.9 ppm concentration of Cd(II) and Pb(II). The formation of root nodules was also severely affected by the presence of heavy metal ions in the soil. The different heavy metals used in this study were found to vary in their phytotoxic effects with Cd being the most toxic and Mn the least toxic. Soils contaminated by heavy metals probably lead to substantial lose in dry matter and seed yield of cowpea plant.

KeyWords: *Vigna unguiculata;* Cowpea plants; Heavy metal ions; Root growth; Shoot growth; Root nodule formation.

Introduction

Contamination of agricultural soil by heavy metal ions has become a critical environmental concern due to their potential adverse ecological effects[1,2]. Such toxic elements are considered as soil pollutants due to their widespread occurrence, and their acute and chronic toxic effect on plants grown of such soils[3].

Heavy metals with adverse health effects in human metabolism (including lead, cadmium, and mercury) present obvious concerns due to their persistence in the environment and documented potential for serious health consequences[4]. Acute heavy metal intoxications

ISBN 978-93-5279-420-1

may damage central nervous function, the cardiovascular and gastrointestinal (GI) systems, lungs, kidneys, liver, endocrine glands, and bones. Chronic heavy metal exposure has been implicated in several degenerative diseases of these systems and may increase the risk of some cancers[5].

Once the soil is destructed by heavy metals, metals found naturally within the soil or accumulated as a result of anthropogenic activities, it becomes uninhabitable for microbial communities or unsuitable for crop production[6]. On the other hand, *Rhizobia* among soil bacteria has been the organism of great interest for agronomist in general and legume growers in particular primarily due to their ability to provide nitrogen to plants. Considering the benefits of *Rhizobia* in nitrogen economy and the role of legumes in animal and human health, attention in recent times has been paid onto understanding how metals could affect the very survival of *Rhizobia* either present as free-living organism or when they are in intimate relationship with legumes. Heavy metals are inhibitory to *rhizosphere*, microorganisms, and processes mediated by them, like nitrogen-fixing ability of *Rhizobia* are lost when they are in symbiotic association with the legume host growing in metal-enriched[7].

Present investigation aims to analyze the effect of cadmium, cobalt, lead, manganese and copper on plant growth characters (root length and shoot length), crop productivity (fresh weight and dry weight) and nodulation parameters (total numbers of root nodules per plant cambered to control) of legume plant cowpea (*Vigna unguiculata*).

Materials and Methods

The soil in which the experiments have been conducted was a sandy clay loam and had received no exogenous input of metals. The soil was sieved and homogenized and the test heavy metals were added as the solutions. Effect of five heavy metal ions; cadmium, cobalt, lead, manganese and copper were investigated on leguminous plants species cowpea (*Vigna unguiculata*). Effects of these metals were studied on 0.3, 0.6, and 0.9 ppm concentrations. For the test of host plant productivity, after 45 days the plants were uprooted and the number of nodules per plant, root length, shoot length, fresh and dry weight were recorded in different concentration of heavy metal treatment.

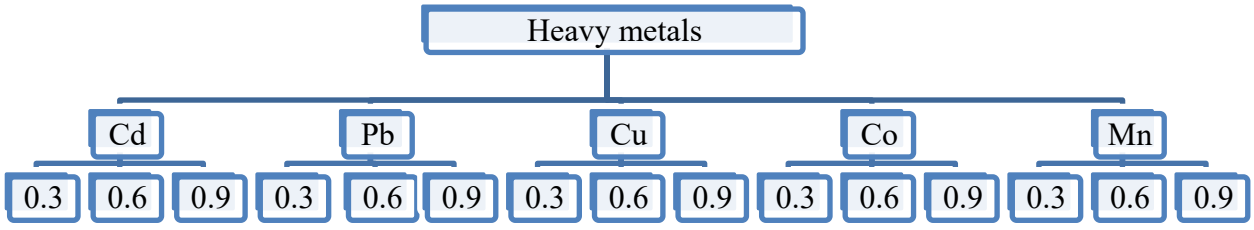

ISBN 978-93-5279-420-1

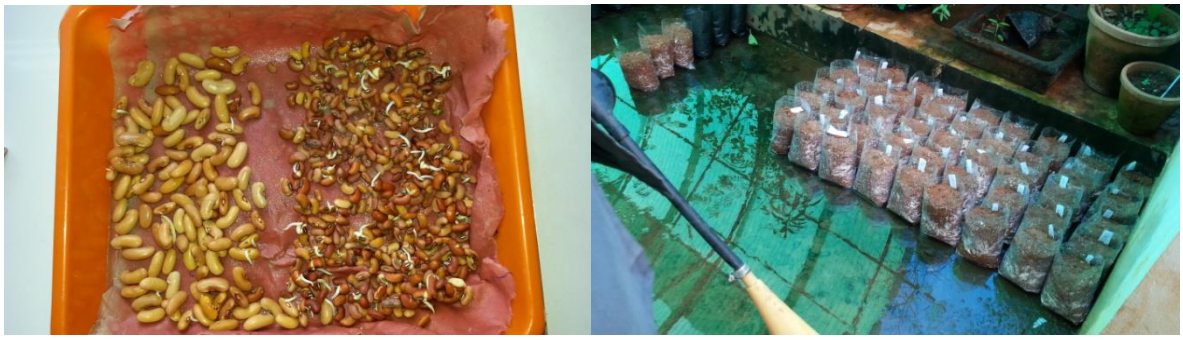

Seed germination and preparation for sowing of seeds

Results and Discussion

Effect of heavy metals on root growth

The data corresponding to the root growth of the cowpea (*Vigna unguiculata)* and the dose of the heavy metal are reported in Table.1. In all doses (0.3, 0.6 and 0.9 ppm) Cd, Pb, Cu and Co decreased the root growth except for Mn as compared to the root growth of the control. The maximum effect is reported on cadmium. At 0.9 ppm concentrations no germination was reported in Cd. At 0.9 ppm concentrations of Pb, Cu and Co the length of root were 0, 18.5 and 16.4 cm respectively.

Effect of heavy metals on shoot growth

The effect of heavy metals on shoot growth of the cowpea (*Vigna unguiculata)* and the dose of the heavy metal ions are reported in Table.1. In all doses (0.3, 0.6 and 0.9 ppm) Cd, Pb, Cu and Co decreased the shoot growth except Mn as compared to the shoot growth of the control. In manganese maximum shoot growth was reported (116.5 cm). At 0.9 ppm concentrations no germination was reported in Cd. At 0.9 concentration of Pb, Cu and Co the length of root were 0, 12.5 and 9 cm respectively.

Effect of heavy metals on formation and development of root nodules

The result showed that the presence of heavy metal ions severely affect the root nodule formation of leguminous plants leading to the decrease in their nitrogen fixing capacity (Table 1). In the various doses of heavy metal ions (0.3, 0.6 and 0.9 ppm), Cd, Pb, Cu and Co show decreased number of root nodules as compared to control plants except manganese. At 0.9 and 0.6 ppm concentrations of Cd, no nodules were formed (Table 1). These results indicate that the presence heavy metal ions in large concentration severely affect the root nodules and nitrogen fixing capacity of leguminous plants.

Table 1. ***Effect of Different Heavy Metal ionss on Plant Growth Characters and Root Nodule Formation***

Heavy metal	*Concentration (ppm)*	*Shoot Length (cm)*	*Root Length (cm)*	*Total (cm)*	*Root Nodules (No. per plant)*	*Fresh Weight (g)*	*Dry Weight (g)*
Cd(II)	0.3	32.6	19.2	51.9	13.3	3.8	0.8

ISBN 978-93-5279-420-1

	0.6	0	0	0	0	0	0
	0.9	0	0	0	0	0	0
Pb(II)	0.3	39.5	22.6	62.2	14.3	4.6	1.5
	0.6	32.1	18.7	51.0	14	3.7	0.9
	0.9	0	0	0	0	0	0
Cu(II)	0.3	84.5	30.5	115.1	27	6.3	1.5
	0.6	78.7	26.3	105.1	36	5.6	1.4
	0.9	12.5	18.5	31	13	2.9	0.3
Co(II)	0.3	65.2	27.5	92.8	20	5.4	1.5
	0.6	45.4	23.0	68.4	26	4.0	0.8
	0.9	9.0	16.4	22.4	0	0.9	0.5
Mn(II)	0.3	100.3	37.1	137.4	35	8.1	1.4
	0.6	108.1	52.2	160.3	40.3	9.03	1.7
	0.9	116.5	57.6	174.1	51.6	10.3	1.7
Control		123.0	34.3	157.4	38.9	9.5	2.5

Each value is an average of five replicates

Effect of heavy metals on productivity of plants

The data corresponding to fresh and dry weight of the cowpea (*Vigna unguiculata)* and the dose of the heavy metal ions (Table 1) show that in all doses (0.3, 0.6 and 0.9 ppm) Cd, Pb, Cu and Co decreased the fresh and dry weight except for Mn as compared the control. The maximum effect is reported with cadmium and all other heavy metal ions also affect the productivity of plants.

Effect of Cd on plant growth & root nodule formation

0.3 0.6 0.9 Control

Effect of Cobalt on plant growth & root nodule formation

0.3 0.6 0.9 Control

Effect of Cu on plant growth & root nodule formation

Effect of Pb on plant growth & root nodule formation

ISBN 978-93-5279-420-1

0.3	0.6	0.9	Control	0.3	0.6	0.9	Control

Effect of manganese on plant growth & root nodule formation

0.3	0.6	0.9	Control

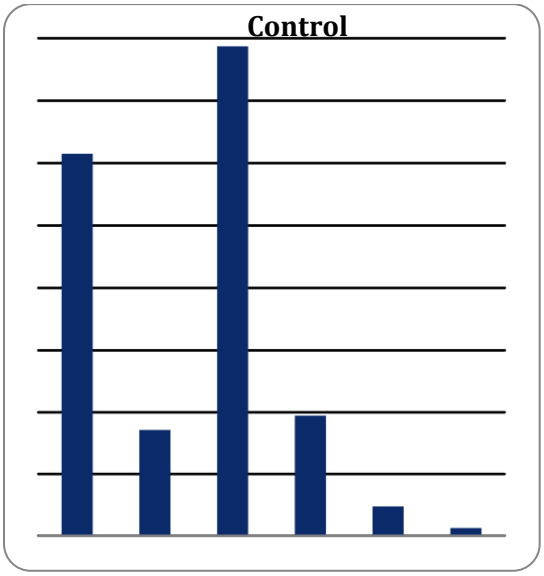

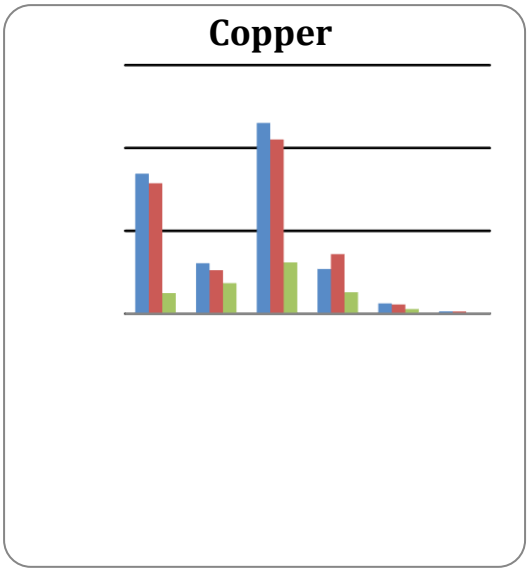

ISBN 978-93-5279-420-1

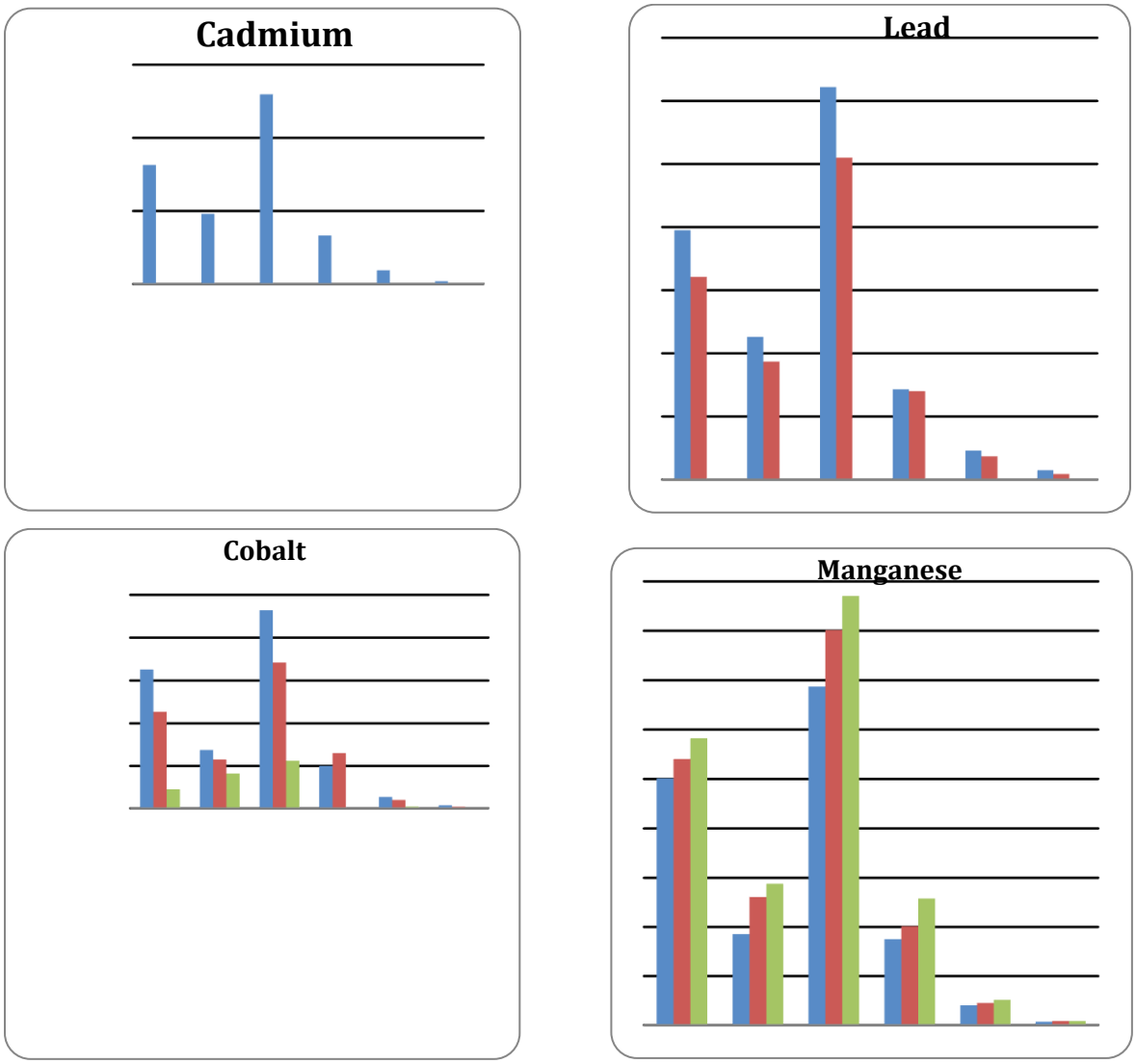

Fig. 1. *Phytotoxic effect of heavy metal ions on the root nodule formation and plant growth*

Conclusion

The plant growth characters of cowpea (*Vigna unguiculata)* are seriously decreased by a concentration of 0.3, 0.6 and 0.9 ppm of Cd, Pb, Co and Cu but the same concentration of manganese favors the plant growth characters. The root and shoot growth of the cowpea plant is decreased by various concentration of heavy metal ions. The plants did not show any capabilities to germinate in the soil containing 0.9 ppm concentration of Cd and Pb ions. The formation of root nodules was also severely affected by the presence of heavy metals in the soil. The ions also affect the nitrogen fixing capacity of leguminous plants like cowpea. It is indicated that at the time of sowing of seed, the soil testing shall be done and the quality of soil must be identified to help for better crop production.

References

ISBN 978-93-5279-420-1

1. Wo´jcik, M. and Tukiendorf, A. (2004); Phytochelatin synthesis and cadmium localization in wild type of *Arabidopsis thaliana*. *J. Plant Growth Regul.,* 44: 71–80.
2. Mohanpuria, P., Rana, K.N. and Yadav, S.K (2008); Biosynthesis of nanoparticles: technological concepts and future applications. *J. Nanoparticle Research*, 10: 507-517.
3. Sharma, P. and Dubey, R.S. (2005); Lead toxicity in plants. *Braz J. Plant Physiol*, 17: 35–52.
4. Pohl, H.R., Roney, N. and Abadin, H.G. (2011); Metal ions affecting the neurological system. *Met. Ions. Life Sci*., 8: 247-62.
5. Peraza, M.A., Ayala-Fierro, F., Barber, D.S., Casarez, E. and Rael, L.T. (1998); Effects of micronutrients on metal toxicity. *Environ Health Perspect.,* 106 Suppl 1: 203-16.
6. Sumner, M.E. and Noble A.D. (2003); Soil acidification: the world story. In: Rengel Z, ed. Handbook of soil acidity, New York, USA: Marcel Dekker, 1–28.
7. Broos, K., Uyttebroek, M., Mertens, J. and Smolders, E. (2004); A survey of symbiotic nitrogen fixation by white clover grown on metal contaminated soils. *Soil Biol Biochem*., 36:633–640.

BACTERICIDAL EFFECTS OF TRANSITION METAL OXIDE NANOPARTICLES: A COMPARATIVE STUDY

Bindu U* and Jeena V R

Department of Chemistry, N.S.S. College, Pandalam, Pathanamthitta (DT), Kerala

**E-mail: bindu.unni15@gmail.com*

Abstract: Increase in drug resistance among pathogenic bacteria has made the search for new antimicrobials inevitable. The unique physiochemical properties of the nanoparticles combined with the growth inhibitory capacity against microbes has led to the increase in the research on

ISBN 978-93-5279-420-1

nanoparticles and their potential application as antimicrobials. In this work, transition metal oxide nanoparticles of Cu, Zn, and Ti were prepared through aqueous route. Formation of monoclinic, hexagonal wurtzite and anatase phases of CuO, ZnO, and TiO_2 was confirmed by XRD analysis. We tested the anti-microbial activities of these metal oxide nanoparticles in an aqueous culture medium against both Gram positive as well as Gram negative bacteria. CuO NPs showed strong growth inhibition against all the organisms. ZnO NPs also exhibited significant activity, whereas TiO_2 NPs showed little antibacterial activity. The above observations suggest the potential application of metal oxide NPs to disinfect airborne pathogens.

Introduction

Metal oxide nanoparticles have a unique place among nanomaterials due to their characteristic electronic and optical properties making them extremely useful in applications ranging from optoelectronics to biomedical research.[1-5] Recently, resistance to commercially available antimicrobial agents by pathogenic bacteria and fungi is increasing at a threatening rate. Treatment of bacterial infection is being increasingly complicated because of the ability of the pathogens to develop resistance against a broad spectrum of existing antibiotics. Bacteria like *Staphylococci, Klebsiella pneumoniae and Pseudomonas spp*. are becoming more and more common. To circumvent this, novel methods or novel strategies are required. The successful approach is the use of natural antimicrobials, combination or synergistic therapy and more recently use of metal nanoparticles[6-10].

The bactericidal effect of metal nanoparticles has been attributed to their small size, and high surface to volume ratio, which allow them to interact closely with microbial membranes. Metal oxide nanoparticless of Cu[11-14] and Zn[15-19] are found to be antimicrobial agents because of their effectiveness on resistant strains of microbial pathogens, low toxicity, and resistance to heat. To realize the potential of transition metal oxide nanoparticles to act as antibacterial agents, we synthesized CuO, TiO_2, and ZnO nanoparticles through aqueous route. The antibacterial activitiy was studied against one Gram-positive bacteria (*Staphylococcus aureus*) and one Gram-negative bacteria (*Escherichia coli*).

Experimental

Materials and methods: Titaniumbutoxide (97%, Merck), and ethyl acetate (SigmaAldrich) for the preparation of TiO_2 nanoparticles were used as purchased. ZnO and CuO nanoparticle are prepared from Zinc acetate ((SISCO, extra pure) and copper sulphate (SISCO, extra pure). Reagent solutions were prepared in doubly distilled water.

In a typical procedure, 250ml Zinc acetate solution taken in a 250 mL reaction vessel and NaOH solution is added drop wise till the pH reached 12. The mixture is stirred continuously till a white precipitate of ZnO is formed. It is kept overnight at room temperature. The precipitate is washed with water, followed by ethanol, and calcined at 400^0C for 4 hours in a muffle furnace. The preparation of CuO nanoparticles is carried out in a similar manner. About 250ml copper sulphate solution is taken in a 250mL reaction vessel and NH_4OH solution is added drop wise in excess. The mixture is stirred continuously till a blue precipitate of $Ca(OH)_2$ is formed. It is kept overnight at room temperature. The precipitate is washed with water, followed by ethanol, and calcined at 400^0C for 5 hours in a muffle furnace.

ISBN 978-93-5279-420-1

For the preparation of TiO_2 nanoparticles, about 12.8ml $Ti(OBu)_4$ is taken in a reaction vessel and dispersed in 38.4 ml ethyl acetate with constant stirring for 5 minutes. 12.8ml of distilled water is added to this reaction mixture with stirring for 1hr to hydrolyses $Ti(OBu)_4$. A white slurry of TiO_2 was formed instantaneously and it was kept overnight at RT for drying followed by calcination at 400°C. The photographic images of the samples are presented in Figure1. The wide angle powder X-Ray Diffraction results of the catalyst samples are collected using Rigaku Miniflex 600 diffractometer.cu (k-alpha-0.15404nm) and are also given in Figure 1(inset).

Antibacterial Activity: Antibacterial activities of the prepared nanoparticles samples are carried out by Disc Diffusion method

Results and Discussion

Powder samples of CuO, TiO_2, and ZnO are characterized using XRD analysis. The diffraction patterns are shown in Fig. 1. All diffraction peaks of sample correspond to the characteristic monoclinic, anatase, and hexagonal wurtzite structures of CuO, TiO_2, and ZnO respectively. Absence of any additional peaks shows the single phase sample formation. Average particle size of these nanoparticles calculated using Scherrer equation is 16.0, 23.0, and 19 nm respectively.

The objective of the present study was to analyze the growth-inhibitory effect of ZnO, CuO, and TiO_2 on the microorganisms, *Escherichia coli* and *Staphylococcus aureus*. CuO nanoparticles showed remarkable antibacterial activity against both the strains. The inhibition zones are rather significant and are comparable to those usually given by strong antibiotics.Studies have also shown positive results for the ZnO nanoparticles. Interestingly, we did not observe any notable antibacterial activity for the TiO_2 nanoparticles. A comparison of the zones of inhibition for the tested nanoparticle against the studied gram-positive and gram-negative bacteria is given in the Fig. 2 and the results are summerized in Table 1.

The inhibition zone is observed to be a maximum in the case of the gram-positive bacterium studied, *Staphylococcus aureus* (zone diameter = 12 mm in the case of CuO and 8nmin thecase of ZnO). The gram-negative bacteria also responded well to both CuO and ZnO, although to a lesser degree. The observed difference may be attributed to their structural differences. It is well established that in gram-negative bacteria, the cell wall consists of a few layers of peptidoglycan (a polymer consisting of sugars and amino acids), which provides the wall shape and structural strength, whereas in gram-positive bacteria the cell wall is not protected as much.

ISBN 978-93-5279-420-1

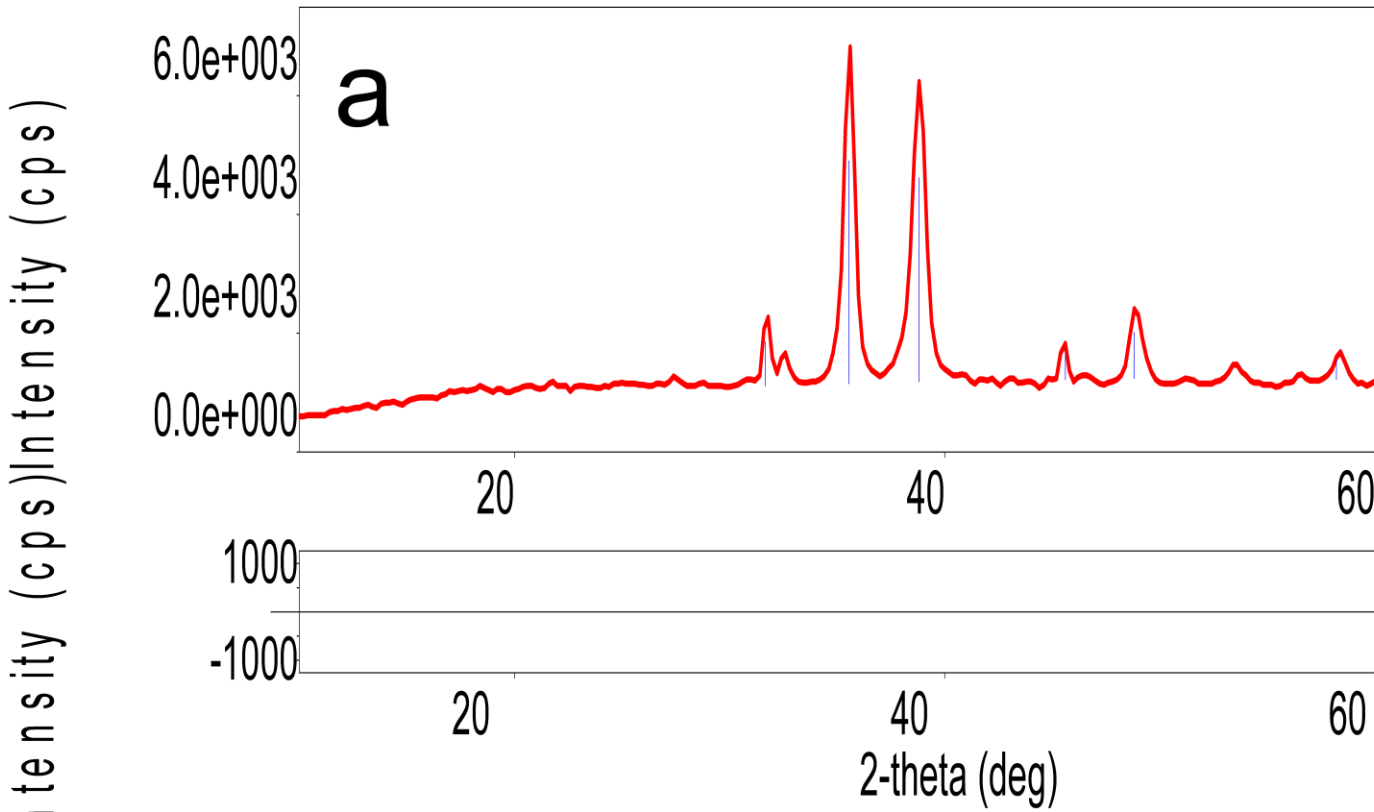
a
6.0e+003
4.0e+003
2.0e+003
0.0e+000
Intensity (cps)Intensity (cps)
20
40
60
1000
-1000
20
40
60
2-theta (deg)

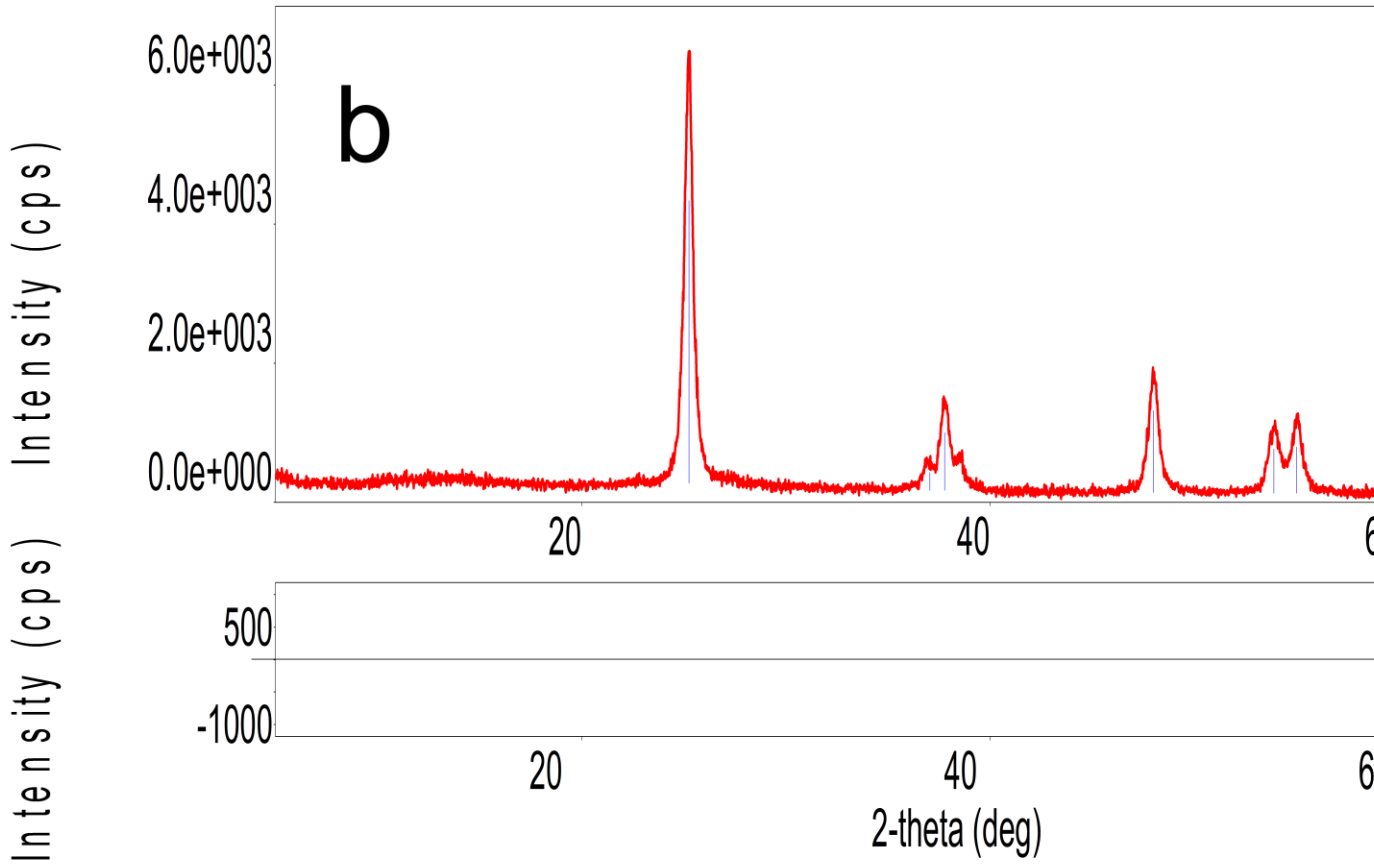
b
6.0e+003
4.0e+003
2.0e+003
0.0e+000
Intensity (cps)
20
40
500
-1000
Intensity (cps)
20
40
2-theta (deg)

Fig. 1: Wide angle X-ray diffraction patterns of the nanoparticles prepared: (1)CuO; (2)TiO_2;(3)ZnO. Photographic images of the particles are also shown in inset.

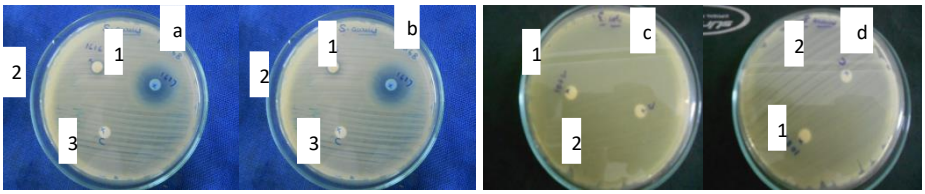

Fig. 2. a and b: Photographic images of CuO and ZnO nanoparticles against (a) *Staphylococcus aureus;* (b) *Escherichia coli.* (1) CuO; (2) ZnO; (3) Control; **c and d.** (1) Photographic image of TiO_2 against (c) *Staphylococcusaureus* and against *(d) Escherichia coli.*(1) TiO_2;(2) Control

Table 1. ***Zones of Inhibition exhibited by ZnO, CuO, and TiO_2 nanoparticles***

Sl No	*Bacteria*	*Zones of Inhibition*	*CuO*	*TiO_2*	*ZnO*
1	*Escherichia coli*	Dia (mm)	10mm	NZ	7mm
2	*Staphylococcus aureus*	Dia (mm)	12mm	NZ	8mm

A histogram showing the diameter of the inhibition zones for the nano systems against various bacterial strains is shown in Fig. 3.

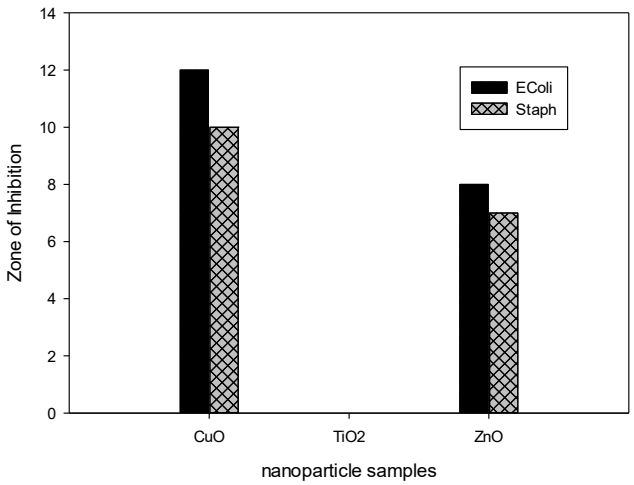

Fig. 3. Zones of inhibition (diameter, in mm) shown by CuO,TiO_2,ZnO against different bacterial strains

Conclusions

In summary, we have demonstrated that CuO exhibited best bactericidal ability against two tested bacteria than TiO2 and ZnO. Nano ZnO showed considerable activity against both the strains. However, TiO_2 samples did not exhibit any notable activity against any of the

ISBN 978-93-5279-420-1

bacterial strains used which may be due to some kind of deactivation on the surface of these particles. Thus, it is concluded that CuO and ZnO nanoparticles can be used as potent, eco-friendly, antibacterial medicine in several cases, where conventional antibiotics fail due to the resistance earned by the bacteria against such drugs. These results also indicate that different bacteria species exhibit various toxicological responses to various nanoparticles.

References

1. Bradley FN. Chapter 2. In: Bradley FN, editor. *Materials for Magnetic Functions*. New York, NY: Hayden; 1976.
2. Mitsuyu T, Yamazaki O, Ohji K, Wasa K. Piezoelectric thin films of zinc oxide for saw devices. *Ferroelectrics*. 1982;42(1):233–240.
3. O'Regan B, Gratzel M. A low-cost, high-efficiency solar cell based on dye-sensitized colloidal TiO2 films. *Nature*. 1991;353(6346):737–740.
4. Ravishankar RV, Jamuna BA. Nanoparticles and their potential application as antimicrobials, science against microbial pathogens. *Commun. Curr. Res. Technol. Adv*. 2011; 1: 197–209.
5. Adams LK, Lyon DY, Alvarez PJJ. Comparative eco-toxicity of nanoscale TiO2, SiO2, and ZnO water suspensions. *Water Research* 2006; 40: 3527-3532.
6. Gabbay J, Borkow G, Mishal J, Magen E, Zatcoff R, Shemer-Avni Y. Copper oxide impregnatedtextiles with potent biocidal activities. *Journal of Industrial Textile* 2006; 35: 323-335.
7. Gojova A, Guo B, Kota RS, Rutledge JC, Kennedy IM, Barakat AI. Induction of inflammation in vascular endothelial cells by metal oxide nanoparticles: effect of particle composition. *Environmental Health Perspectives* 2007; 115: 403-409.
8. Sawai J. Quantitative evaluation of antibacterial activities of metallic oxide powders (ZnO, MgO, CaO) by conductimetric assay. J. Microbiol. Methods 2003; 54: 177–182.
9. Li Y., P. Leung, L. Yao, Q.W. Song & E. Newton. Antimicrobial effect of surgical masks coated with nanoparticles. *J. Hosp. Infect*. 2006; 62: 58–63.
10. Makhluf S, Dror R, Nitzan Y, Abramovich Y, Jelinek R ,Gedanken, A microwave-assisted synthesis of nanocrystalline MgO and its use as Bacteriocide. *Adv. Funct.Mater*. 2005;15: 1708–1715.
11. Jeyaraman R, Kadarkaraithangam, J, Arumugam, M, Govindasamy R, Abdul, A. Synthesis and antimicrobial activity of copper nanoparticles. *Mater. Lett*. 2011; 71: 114–116.
12. Emami-Karvani Z, Chehrazi P. Antibacterial activity of ZnO nanoparticle on grampositive and gram-negative bacteria. *Afr. J. Microbiol. Res*. 2011; 5: 1368–1373.
13. Azam A, Ahmed AS, Oves M, Khan MS, Memic A. Size-dependent antimicrobial properties of CuO nanoparticles against Gram-positive and -negative bacterial strains. *Int. J. Nanomed*. 2012; 7: 3527–3535.
14. Yamamoto O, Sawai J, Sasamoto T. Change in antibacterial characteristic with doping of ZnO in MgO-ZnO solid solution. Int *J Inorg Mater*. 2000; 2: 451–454.

ISBN 978-93-5279-420-1

15. Jones N, Ray B, Koodali RT, Manna AC. Antibacterial activity of ZnO nanoparticles suspensions on a broad spectrum of microorganisms. *FEMS Microbiol Lett*. 2008; 279: 71–76.
16. Ohira T, Yamamoto O, Iida Y, Nakagawa Z. Antibacterial activity of ZnO powder with crystallographic orientation. *J Mater Sci Mater Med*. 2008; 19:1407–1412.
17. Padmavathy N, Vijayaraghavan R. Enhanced bioactivity of ZnO nanoparticles – an antibacterial study. *Sci Technol Adv Mater*. 2008; 9: 035004.
18. Emami-Karvani Z, Chehrazi P. Antibacterial activity of ZnO nanoparticle on grampositive and gram-negative bacteria. *Afr. J. Microbiol. Res*. 2011; 5: 1368–1373.

IN VITRO STUDY ON α –AMYLASE INHIBITORY ACTIVITY AND PHYTOCHEMICAL SCREENING OF *Sarcostemma acidum*

Akhila K K[1*] and Sindhu Ramachandran[2]

DGM MES Mampad College, Mampad, Malappuram (DT), Kerala

Department of Chemistry, N. S. S. College, Manjeri, Malappuram (DT), Kerala

[*]*E-mail: akhilabalakrishnan4@gmail.com*

Abstract: Pancreatic α-amylase inhibitors offer an effective strategy to lower the levels of post prandial hyperglycemia via control of starch breakdown. Methanolic extract of *Sarcostemma acidum* showed inhibition against α-amylase. The medicinal plant was subjected to sequential solvent extraction, phytochemical analysis, compound identification and tested for α-amylase inhibition. Phytochemical analysis revealed the presence of Flavonoids, phenols, Reducing sugar, sterols, Anthraquinone as probable inhibitory compounds

Introduction

Somlata (*Sarcostemma acidum*) belonging to the family *Asclepiadacea* is grown in India, Europe and US is an underutilized crop. The herb is highly used by the rural and tribal people in curing various disorders like asthma, swelling, fever and cold, dyspepsia, inflamematory infection and gastric problem etc. It is found in dry rocky places in Bihar, Bengal, Konkan, Deccan, Tamil Nadu, Maharashtra, Madhya Pradesh and Kerala. The use of medicinal plants as raw materials in the production of new drugs is ever increasing because of their potentials in combating the problem of drug resistance in micro-organisms. Demand for medicinal plants is increasing in both developing and developed countries. Research on medicinal plants is one of the leading areas of research globally.A fraction of this plant extract has been reported to have larvicidal potential against larvae of the laboratory reared mosquito species, , antiallergic and anti-inflammatory activities. It also inhibited the contractions induced by acetylcholine and histamine on isolated guinea pig ileum, and produced broncho-spasmolytic activity. It is traditionally used to reduce vitiations of pitta in the treatment of pyschosis, depression and fatigue. According o folklore the whole part of the plant is used in

 ISBN 978-93-5279-420-1

the treatment of asthama, Juice given to children to get relief from cold, latex dropped in eyes in case of cataract for remedy.

Materials and Methods

The plant material used for this investigation was collected from Perinthalmanna, Malappuram, Kerala.

Preparation of plant extract: Fresh plant was crushed and treated with sufficient amount of pure methanol for six hours in a soxhlet extractor. The extract was filtered through a cotton plug followed by Whatman No. 1 filter paper. The filtrate was then evaporated under reduced pressure to give a dark green viscous mass and stored at 4 °C until use.

Phytochemical screening: The crude methanol extract of Sarcostemma acidum underwent phytochemical screening to detect presence of potential phytochemical constituents like alkaloid, flavonoid, saponin, tannin, carbohydrate, glycoside, glucoside, fat and fixed oil, steroid and terpenoid.

***In vitro* α-amylase inhibitory activity:** This study was performed by a modified starch iodine protocol. In short, 1 mL of plant extract or standard of different concentration was taken in pre-labeled test tubes. A volume of 20 µL of α-amylase was added to each test tube and incubated for 10 min at 37 °C. After the incubation 200 µL of 1% starch solution was added to each test tube and the mixture was re-incubated for 1 h at 37 °C. Then 200 µL of 1% iodine solution was added to each test tube and after that, 10 mL distilled water was added. Absorbance of the mixture was taken at 565 nm. Sample, substrate and α-amylase blank were undertaken under the same conditions. Each experiment was done in triplicate. IC_{50} value was calculated by using regression analysis.

% α-amylase inhibition= [1-(SA-SBB)-SMB/AAB]X100

SA=Sample absorbance, SMB=Sample blank, SBB=Substrate blank, AAB=α-Amylase blank.

Results and Discussion

Class of Compounds	*Tests Performed*	*Results*
Carbohydrates	Molish's test	+
	Fehlings test	+
Phenols	Phosphomolybdic test	+++
Flavanoids	Shinoida test	+++
	Lead acetate test	+++
Tannins	Braemers test	--
Sterols	Salkowski's test	+++
Alkaloids	Draggendrof,s test	-

ISBN 978-93-5279-420-1

Glycosides	Legal's test Brontrangers's test	+ +
Saponins	Foam test	--
Anthraquinones	Brontrangers's test	++
Aminoacid test	Ninhydrin test	--
Fixed oils and fats		--

+++ : High amount, ++ : Moderate quantity + Traces -- Absence

α-Amylase inhibitory activity: α-Amylase is one of the main enzymes in human body that is responsible for the breakdown of starch to more simple sugars. α-Amylases hydrolyze complex polysaccharides to produce oligosaccharides and disaccharides which are then hydrolyzed by α-glycosidase to monosaccharide which are absorbed through the small intestines into the hepatic portal vein and increase postprandial glucose levels. Amylase inhibitors are also known as starch blockers because they prevent dietary starch from being absorbed by the body and thereby lower postprandial glucose levels. Slowing the digestion and breakdown of starch may have beneficial effects on insulin resistance and glycemic index control in people with diabetes. In our investigation we found that methanolic fruit extract moderately inhibited α-amylase. From phytochemical screening we can see that presence of saponin, steroid and terpenoid which may be responsible for this therapeutic activity. Natural polyphenols have been reported to inhibit the activity of carbohydrate hydrolyzing enzymes like α-amylase, α-glucosidase. Terpenoids represent a promising source for biologically active natural compounds which have potential for research and development of new substances with pharmacologic activity. α-Amylase inhibitory activity was related only for oleanane, ursane and lupane type terpenoids. In a previous study saponins have also been found to be a probable α-amylase inhibitor.

***In vitro* α-amylase inhibitory activity:** Methanol extract showed IC_{50} value 33mg/mL Methanol extract significantly inhibited α-amylase activity in a dose dependent manner. Therefore we can conclude that this extract have moderate α-amylase inhibitory activity.

Conclusions

Presence of flavanoid, steroid and terpenoid were identified in the extract. The results showed that methanol extract had moderate α-amylase inhibitory activity [IC_{50} value33 mg/mL]. These findings suggest that the plant may be a source for the development of new oral hypoglycemic agent.

References

1. Gupta S. and Kohli S., Physicochemical analysis and anatomical studies of aerial part of Sarcostemma acidum W. & Arn., Nutracost, Mario Donati, Italy., May/June 2011,17-21.
2. Gupta S., Kohli S. International Journal of Pharmacy and Life Sciences, 2010, 1(3), 170-173.

ISBN 978-93-5279-420-1

3. K.G.Lalitha and M.G. Sethuraman, Phytochemical and pharmacological evaluation of the flowers of Sarcostemma brevistigma wight, Oriental Pharmacy and Experimental Medicine, 9 (3) (2009) 00-00.
4. Khare D. P., Tiwari S.S, Khare A. and Khare M.P. (1980). "Structure of brevobiose". Elsevier Scientific Publishing Company, 79, 279-286.
5. Khare D. P., Khare A. and Khare M.P. (1980). "Structure of sarcobiose". Elsevier Scientific Publishing Company, 81, 275-283.
6. Khare D. P., Khare A. and Khare M.P. (1980). "Structure of tigmobiose". Elsevier Scientific Publishing Company, 79, 287-292.
7. Rahuman A.A., Bagavan C., Kamaraj E., Zahir A.A Parasitol Res, 2009, 104, 1365-1372.
8. Harbone J.B., Methods of Plant Analysis Chapter II In: Phytochemical methods: A guide to modern techniques of plant analysis Toppan Company Ltd, Japan., 1973, (1), pp 4 – 5.
9. Nizam Uddin,* Md. Rakib Hasan, Md. Monir Hossain, Arjyabrata Sarker, A.H.M. Nazmul Hasan, A.F.M. Mahmudul Islam, Mohd. Motaher H. Chowdhury, and Md. Sohel Rana , *In vitro α-amylase inhibitory activity and in vivo hypoglycemic effect of methanol extract of Citrus macroptera Montr*. Fruit, Asian Pac J Trop Biomed. Jun 2014; 4(6): 473–479.
10. Review α-Amylase inhibitors: a review of raw material and isolated compounds from plant source.[J Pharm Pharm Sci. 2012]
11. alpha-Amylase inhibitory activity of some Malaysian plants used to treat diabetes; with particular reference to Phyllanthus amarus.[J Ethnopharmacol. 2006]
12. Saponins isolated from the root of Panax notoginseng showed significant anti-diabetic effects in KK-Ay mice.[Am J Chin Med. 2008]
13. Antidiabetic effect of total saponins from Entada phaseoloides (L.) Merr. in type 2 diabetic rats.[J Ethnopharmacol. 2012]

ISBN 978-93-5279-420-1

PHYSICO-CHEMICAL CHARACTERISATION OF ALBENDAZOLE POLYMORPHS

Bashpa P* and Bijudas K

Department of Chemistry, N. S. S. College, Manjeri, Malappuram, Kerala, 676122

**E-mail: bashpabiju@gmail.com*

Abstract: Albendazole is a medication used for the treatment of a variety of parasitic worm infestations. It shows polymorphism and two polymorphic forms of albendazole were characterized. These are named as Form I and Form II. Commercial albendazole tablets manufactured and marked by various pharmaceutical companies were collected, powdered and after proper clean up procedure their melting points were determined to identify its polymorphic form. This was further confirmed by infra red spectral analysis. It was found that all the commercial drug samples under study belong to the polymorphic form I.

Key words: Albendazole; Polymorphism; melting point; infra red spectrum.

ISBN 978-93-5279-420-1

Introduction

Albendazole is a medication used for the treatment of a variety of parasitic worm infestations. It is useful for giardiasis, trichuriasis, filariasis, neurocysticercosis, hydatid disease, pinworm disease, and ascariasis, among others and is taken by mouth. Albendazole is a broad-spectrum antihelminthic agent of the benzimidazole type. Albendazole was developed in 1975 and is on the World Health Organization's list of essential medicines, the most effective and safe medicines needed in a healthsystem. Albendazole having chemical name methyl-[6-(propylthio)-lH- benzoimidazol-2-yl]carbamate is a member of the benzimidazole compounds.

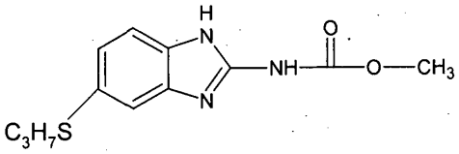

Albendazole shows polymorphism and exists in two forms. Form I with melting point 220 ^{0}C is used commercially as drug while the stable form II has a melting point 160 ^{0}C. There are lots of reports on the studies of polymorphism shown by albendazole tablets[1-7]. The extensive use of albendazole and the polymorphic properties shown by it prompted to carry out this work.

Experimental

Commercial albendazole tablets manufactured and marked by various pharmaceutical companies have been collected from medical shops in and around Manjeri and listed below.

1. Bendex 400 (Cipla Limited, Mumbai)
2. Albendol 400 (Micro Labs Limited, Bangalore)
3. Zentel 400 (Glaxosmithkline Pharmaceuticals Limited, Mumbai)
4. Albendazole 400 (Cadila Healthcare Limited, Ahmedabad)

The collected drug samples were finely powdered and proper clean up procedure was carried out as in literature[8-9]. The dried samples were recrystallised and the melting point was determined by using a digital melting point apparatus. The obtained results were compared with the authentic values reported in literature.

The infra red spectrum of drug samples was recorded by Jasco FT-IR double beam spectrophotometer. The obtained infra red spectrum was analysed and peaks due to various functional groups were identified for structural elucidation. Moreover the obtained spectrum was compared with the reported one in the literature.

Results and Discussion

The polymorphic study of commercial albendazole tablets was carried out by determining its melting point. The melting point determination is done in triplicate and all results are tabulated in Table 1.

ISBN 978-93-5279-420-1

Table 1. ***Melting points of various commercial albendazole tablets***

Sl No:	*Trade name*	*Manufactured by*	*Melting point (^0C)*
1.	**Bendex 400**	Cipla Limited, Mumbai	218± 2
2.	**Albendol 400**	Micro Labs Limited, Bangalore	218± 2
3.	**Zentel 400**	Glaxosmithkline Pharmaceuticals Limited, Mumbai	216± 2
4.	**Albendazole 400**	Cadila Healthcare Limited, Ahmedabad	216± 2

All the albendazole tablets under investigation have melting point in the range 216 - 220 ^{0}C. This shows that all drug molecules belong to polymorphic form I. Polymorphic form I is commonly used for commercial preparation and is reported elsewhere[10-11].

The IR spectrum was recorded from KBr pellets using Jasco FT-IR 4100 spectrophotometer (Japan) and is shown in Figure 1.

The peak at 2750 cm $^{-1}$ belongs to N-H stretching, peak at 1740 cm $^{-1}$ shows the C=O stretching. A sharp peak at 3050 cm^{-1} indicates the presence of C-H stretching and a medium C=C peak at 1600 cm^{-1}. Presence of all these peaks leads to the conclusion that the analyte is albendazole which was further proved on comparison the IR spectrum available in literature[12-14].

All the albendazole tablets under investigation have melting point in the range 216-220 ^{0}C. This shows that all drug molecules belong to polymorphic form I. This can be further proved by various advanced analytical techniques like XRD, SEM, TEM *etc*.

ISBN 978-93-5279-420-1

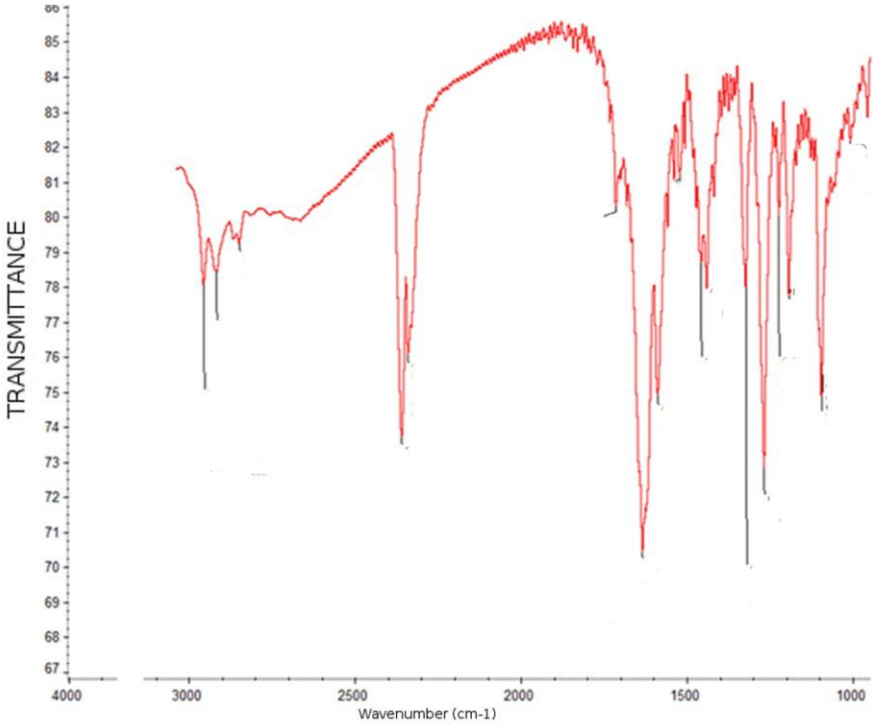

Fig. 1. IR spectrum of albendazole (Zental)

Conclusions

Albendazole is a common drug used for the treatment of a variety of parasitic worm infestations. Various commercial albendazole drug samples were collected and their polymorphic structure is determined by melting point determination. These results clearly confirm that all the albendazole drugs under study belong to Form I polymorph. These drug samples were further analysed by infra red spectral analysis and can further be done by advanced techniques like NMR, XRD, SEM, TEM *etc*.

References

1. Llinas A, Goodman M J. *Drug Discovery Today,* 13, **2008**, 5&6.
2. Bond A D, Boese R, Desiraju G R. *Angewante Chemie Int. Edn*., 46, **2007**, 618.
3. Pranzo B M, Cruickshank D, Coruzzi M, Caira M R, Bettini R. *J. Pharm. Sci.* 99(9), **2010,** 3731.
4. Lixandrao K, Ferreira F. *Acta Cryst.* A70, **2014,** C1808.
5. Belew S, Getachew M, Suleman S. et al. *Plos One.* 10, **2015**, 4057.
6. Sanos O M M, Reis M E D, Jacon J T, Lino M E S, Simoes J S, Doriguetto A C. *Braz. J. Pharm. Sci.* 50, **2014,** 1-24.
7. Spong B R, Price C P, Jayasankar A, Matzger A J, Hornedo N R. *Adv. Drug Deliv. Rev.* 56(3), **2004**, 241.

ISBN 978-93-5279-420-1

8. Perrin D D. Armarego WL, Perrin DR. *Purification of Organic Compounds*, Oxford, Pergamon Press, **1966.**
9. Vogel A I. *Text book of practical organic chemistry*, Longman, London, **1967.**
10. Chattah A K, Zhang R, Mroue K H, Pfund L Y, Longhi M R, Ramamoorthy A, Garnero C. *Mol. Pharmaceutics*. 12(3), **2015**, 731.
11. Thakur A, Thipparaboina R, Kumar D, Gouthami K S, Shastri N R. *Cryst. Engg. Comm.,* 18, **2016**, 1489.
12. Silva V H D. Goncalves J L, Vasconcelos V C, Pimental M F, Periera C F. *J. Pharm. Biomed. Anal.,* 115(10), **2015,** 587.
13. Brittain H G. *J. Pharm. Sci.,* 101(2), **2012**, 464.
14. Marcos L M, Lamprou D A, McBurney R T, Halbert G W. *Int. J. Pharm.,* 499, **2016,** 175.

ISBN 978-93-5279-420-1

INFLUENCE OF NANOCLAY AND GRAFT COPOLYMER ON THERMO-MECHANICAL PERFORMANCE OF FIBER REINFORCED POLY (LACTIC ACID) BIOCOMPOSITES

Sajna V P[1, 2, 3*], Smita Mohanty[1, 2] and Sanjay K Nayak[1, 2]

[1]*Advanced Research School for Technology & Product Simulation, Central Institute of Plastics Engineering and Technology, Chennai-600 032, Tamil Nadu*

[2]*Laboratory for Advanced Research in Polymeric Materials, Central Institute of Plastics Engineering and Technology, Bhubaneswar, Orissa-751024*

[3]*Pocker Sahib Memorial Orphanage College, Tirurangadi, Malappuram (Dt), Kerala*

[*]*E-mail: sajnavp88@gmail.com*

Abstract: The poly(lactic acid) (PLA) biocomposite reinforced with silane treated banana fibers (SiB) were prepared using melt blending technique. To improve the thermal and mechanical performance, Cloisite 30B (C30B) nanoclay as well as a graft copolymer (GC) obtained by grafting glycidyl methacrylate (GMA) onto PLA were incorporated within the biocomposite. FTIR and ^{1}HNMR characterization confirmed the successful synthesis of GC. The influences of C30B and GC on the mechanical properties of PLA/SiB biocomposites were investigated using flexural and impact tests. The mechanical result showed that the GC compatibilized PLA/SiB/C30B (PLA/SiB/C30B/GC) bionanocomposite significantly improved the flexural and impact strength as compared with uncompatibilized bionanocomposites (PLA/SiB/C30B). Differential Scanning Calorimetry (DSC) thermograms showed improvement in thermal properties as a significance of C30B whereas GC improved the melting behaviour of composites. Further, Dynamic Mechanical Analysis (DMA) results revealed an increment in storage modulus and α-relaxation temperature as a function of C30B, while incase of PLA/SiB/C30B/GC bionanocomposites a slight reduction was found to be in storage modulus due to the plasticizing effect of GC.

Keywords: Compatibilization, nanoclays, nanocomposites, biopolymers, fillers

Introduction

In recent years, renewable resource based polymer composites have fascinated a great deal of attention in polymer industry and research, because of its favourable properties and increasing environmental regulation [1-2]. Among renewable resource based polymer, poly (lactic acid) (PLA) has been studied broadly because it satisfies the environmental impact criteria required for replacement of conventional petroleum based product. PLA is manufactured from starch rich renewable resource (corn/potato) by fermentation method and it is fully biodegradable to carbon monoxide and water by hydrolysis [1, 3]. The major factors

ISBN 978-93-5279-420-1

holding back PLA are its high cost and brittleness. Reinforcing PLA with lignocellulosic fiber is one of the solutions for cost reduction [4].

The use of lignocellulosic fiber in composites has increased due to its availability, biodegradability, less cost, light weight, negligible health hazard and comparable mechanical strength and stiffness [5]. However fabrication of hydrophobic PLA and polar fiber results non-uniform dispersion of fiber within the PLA matrix, which impairs interfacial bonding. Many researchers have paid particular awareness to improve the interfacial adhesion between fiber and matrix [6-9]. Hydrophilic character of natural fibers is the main cause of incompatibility. Moisture absorption through capillary action by free hydroxyl group in cellulose results swelling of fiber [10]. Impregnated fiber in composites starts debonding with matrix and cause formation of voids, which generate weak interface and hence diminution in mechanical properties [11]. Different chemical structure of polymer matrix and fiber is another major reason for poor compatibility. Chemical modification of fiber with silane is the most common way to reduce the hydrophilic tendency by disruption of hydrogen bonding as well as change in the chemical structure of fiber surface to achieve better interfacial bonding [12-13].

Another setback of lignocellulosic fiber reinforced PLA composites is the limited processing temperature since the natural fiber undergoes degradation above 200ºC. Due to natural resources and ability to improve the thermal barrier as well as mechanical properties, nanoclay has attracted the attention of researchers [14]. Nowadays, nanoclays are considered to be vital fundamentals in various industrial sectors [15]. Many researchers have studied on polymer nanocomposites and reported that nanoparticle can offer enhancement to mechanical as well as thermal properties in an effective way [16-20]. The gas permeability of nanoclay can inhibit the formation and escape of volatile by-product and hence improve the thermal properties.

More recently, several alternatives such as plasticizer, graft copolymer, coupling agent, compatibilizer and soft polymer which can attach to the polymer backbone have been used with PLA to limit the brittleness, which is another negative aspect of this polymer [21-24]. Many studies have been made to use maleic anhydride-grafted polymer as a compatibilizer for polymer composites [25]. Further many researches focused on use of glycidyl methacrylate-grafted-polymer as a coupling agent to improve interfacial bonding of lignocellulosic fiber reinforced PLA composites [26-28]. Ya-nan et.al [29] has studied the compatibilizing effect of PLA-graft-glycidyl methacrylate on performance of PLA/bamboo flour biocomposites and Chin-San et.al [30] investigated the influence of PLA-graft-maleic anhydride on properties of PLA/Ganoderma lucidum fiber composites. In both the studies, the composites with graft copolymer exhibited, superior mechanical and thermal properties. In this work, we prepared 70/30 wt% of PLA/SiB biocomposite with 3 wt% of Cloisite30B (C30B) nanoclay and 15 wt% graft copolymer (GC) by melt blending. The influence of nanoclay and GC as a compatibilizer on the mechanical, dynamic-mechanical and thermal properties were studied and reported.

Experimental

Materials

PLA (4042 D) was obtained from Nature Works LLC, USA. Banana fibers (density 1.35 g/cc) were kindly supplied by Chandra Prakash & Co, India. 3-Aminopropyltriethoxysilane (APS) was procured from Aroma Chemical Agencies, India.

ISBN 978-93-5279-420-1

Methyltallow bis (2-hydrxyethyl) ammonium modified nanoclay (Cloisite 30B) was purchased from Southern Clay Product Inc, USA. Glycidyl methacrylate (GMA), benzoyl peroxide (BPO), xylene, methanol and ethanol were supplied by TCI chemicals, India.

Methods

Fiber modification: APS (0.6 %) was mixed with ethanol/water (6:4) mixture and stirred for about15 minutes. Subsequently the banana fibers were dipped into the solution for 1 hour. Finally, the fibers were washed with distilled water and dried in air for 1 day followed by in vacuum oven at 80ºC for 12 hours. The dried silane treated banana fibers (SiB) were chopped into 2–3mm length for composite preparation.

Synthesis of graft copolymer: 80 wt% PLA and 20 wt% GMA mixed with BPO were melt blended using an internal mixer (Haake PolyLab-Rheomix600, Germany) at 165ºC temperature with rotor speed 80 rpm for 12 minutes. The obtained melt mix was crushed into granules and dissolved completely in xylene at 130ºC for 1 hour using an oil bath. Then an excess of methanol was added and left aside at room temperature. The pure graft copolymer was separated by precipitation. The precipitate was washed with methanol and finally, the precipitates were dried at 65ºC for 24 hours.

Preparation of composites: PLA, GC and SiB were predried at 60ºC for 4 h, whereas the nanoclays were pre-dried at 80ºC for 8 hours. Batch mixer (Haake PolyLab-Rheomix600, Germany) was used for the melt blending of the PLA matrix with 30 wt% fibers at 180ºC processing temperature with screw speed of 60 rpm for 10 minutes mixing time. The melt mixes obtained were cooled to room temperature, granulated and conditioned at 60ºC. These pellets were subsequently injected within a mini twin-screw compounder (DSM 15mL xplore, Netherlands) at 175ºC maintained for three zones with a screw speed of 60 rpm. Melt collected from the compounder was moulded to samples by mini injection jet at a mould temperature of 40ºC and melt temperature 170ºC. The PLA/SiB/C30B bionanocomposites and PLA/SiB/C30B/GC compatibilized bionanocomposites were also prepared using the above process wherein PLA/SiB (70/30) biocomposites along with 3 wt % of nanoclay and 15 wt% GC were taken. The modifications of fiber and volume fraction of fiber as well as nanoclay have been selected based on our previous findings [31].

Characterization

FTIR Spectroscopy: FTIR spectra of the fibers, PLA and GC were recorded from 400 to 4000 cm^{-1} with 4 cm^{-1} resolution using Thermo Nicolet 6700 FTIR spectrometer, Thermofisher, USA.

^{1}HNMR Spectroscopy: The ^{1}HNMR spectrum of the PLA and GC was carried out by FT-NMR –Bruker-Avance (400MHz). CDCl3 and tetra methyl silane (TMS) were used as solvent and the internal standard respectively for ^{1}HNMR characterization.

Mechanical Testing: Flexural properties of composites (dimension 127x12.7x3mm) were performed using Universal Testing Machine (Instron, UK) in accordance with ASTM D 790 at a crosshead speed of 1.33 mm/min. The unnotched impact strength of specimens made from all composites was tested using dimension of 63.5x12.7x3mm in an Impactometer (Tinius Olsen, USA) according to ASTM D 256.

ISBN 978-93-5279-420-1

Scanning Electron Microscopy (SEM): The morphology of the impact fractured surfaces of the composites sputter coated with gold/palladium mixture was observed using scanning electron SEM (EVO MA 15, Carl Zeiss, SMT Ltd, Germany) analysis.

Differential Scanning Calorimetry (DSC) Analysis: DSC (Q20, TA instruments USA) was used to evaluate the thermal transitions of composites (5-10mg) at temperature from 30ºC to 200ºC at a heating rate of 10ºC/min. The glass transition temperature (Tg), melting temperature(Tm) and crystallization temperature (Tcc) were noted. The degree of crystallinity (χ_{max}) of all sample are calculated as follows; where Ƒ is the weight fraction of PLA, ΔH_m and ΔH_m^0 are the melting enthalpy of composites and 100% crystalline PLA (93 J/g).

$$\chi_{max} = \frac{\Delta H_m}{\mathit{F}\Delta H_m^0} \times 100 \qquad (1)$$

Dynamic Mechanical Analysis (DMA): DMA of composites with dimension 63.5 x 12.7 x 3mm was tested at temperature range 30-120ºC with 1Hz frequency at heating rate of 10ºC/min in dual cantilever mode using DMA Q 800 M/s TA Instruments, USA. The storage modulus and damping factor (tanδ) of the materials were examined as a function of temperature.

Results and Discussion

Fiber characterization

The FTIR spectra of untreated (UTB) and silane treated (SiB) banana fiber is enumerated in Fig. 1. The characteristic peaks at 1620 and 3328 cm^{-1} are related to bending vibration of absorbed water molecule and stretching vibration of hydroxyl groups in the fiber constituents of which were prominently observed in UTB. However, the intensity of these peaks is decreased significantly, after silane treatment. It can be attributed to less hydrophilic nature of SiB over UTB by the reaction of silanol. Silane compounds have the conceivable ability to reduce the amount of free hydroxyl group of fiber. During silane treatment, silanol react with these free hydroxyl group and form stable bonding with fiber. This results in a decrease in moisture absorption by the free hydroxyl group. Similarly, as compared with UTB, SiB shows the decrease in intensity of peaks at 1726 cm^{-1}, corresponding to the –C=O stretching vibration of carboxyl group in pectin and ester group in hemicellulose, revealing the partial removal of hemicellulose. In addition to these, the additional peaks at 1079 and 899 cm^{-1} are attributed to symmetric and asymmetric stretching vibration of –Si-O-Si- or –Si-O-C- and -Si-O-H group respectively, confirming the condensation reaction of silanol with fiber.

ISBN 978-93-5279-420-1

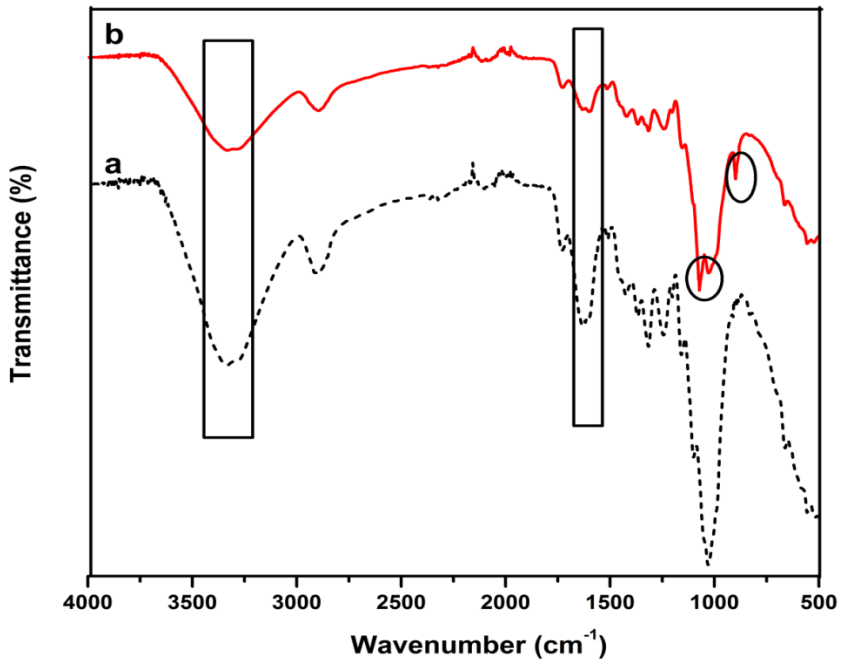

Fig.1. FTIR spectra of (a) UTB and (b) SiB

Graft copolymer characterization

Fig. 2 depicts the FTIR spectra of PLA, GMA and GC. The characteristic peaks of PLA appear at 2952 and 1743 cm^{-1} and are attributed to the C-H and –C=O stretching vibration respectively. Similarly, the peaks at 1720, 1637 and 911 cm^{-1} are associated to –C=O stretching, -C=C- stretching and stretching vibration of epoxy group respectively in GMA. However, the grafting of GMA into PLA caused the disappearance of characteristic stretching vibration of -C=C-, which indicates that C=C bond was involved in grafting reaction. Moreover, the additional peak at 912-914 cm^{-1} observed in GC, which was associated to epoxy group which also confirms the grafting of GMA into PLA. The free radical obtained from initiator, BPO by homolytic scission abstract hydrogen from PLA converting it to PLA macroradical. Moreover, this macroradical initiate the coupling reaction with GMA.

ISBN 978-93-5279-420-1

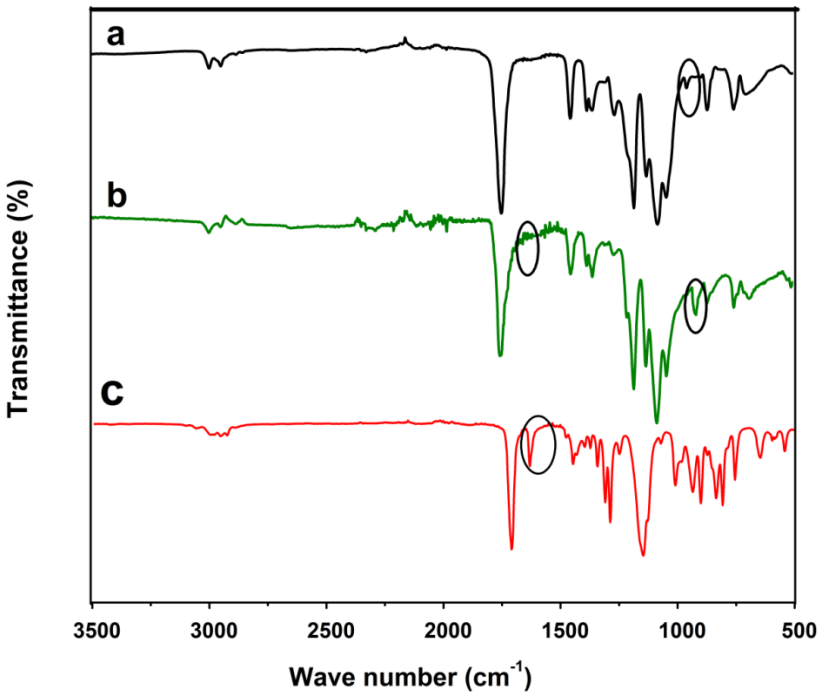

Fig. 2. FTIR spectra of (a) PLA, (b) GC and (c) GMA

In order to confirm the grafting of GMA onto PLA, their ^{1}HNMR spectra were studied. Fig. 3 represents the ^{1}HNMR spectra of PLA and GC. It can be observed that, the characteristic peaks at δ=1.57 and 5.1 ppm correspond to methane proton and methyl proton of –O-C**H** (C**H**$_3$)-(C=O) –which are common in both PLA and GC. However, multiple peaks between 1-4.3 ppm were observed in ^{1}HNMR spectrum of GC. These additional peaks could be associated to proton of –CH, -CH_2, -CH_3 groups of GMA. In other hand, the peaks observed in GC at δ=2.6 and 2.8 ppm were assigned to proton of –CH_2 group, while at δ=3.2 ppm, corresponds to –CH group of epoxy of GMA. Thus the ^{1}HNMR peaks further, evidenced that the synthesis of GC was successful.

ISBN 978-93-5279-420-1

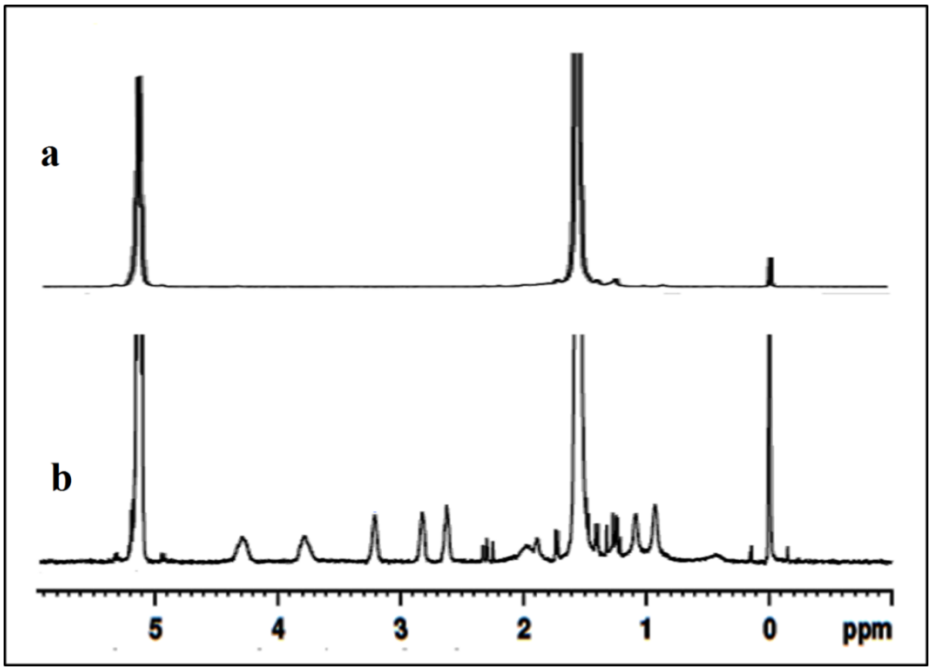

Fig. 3. [1]HNMR of (a) PLA and (b) GC

Mechanical properties of composites

The flexural and impact properties of composites were systematically studied and summarized in Table 1. The flexural property analysis of PLA resulted that, the flexural strength and modulus were 94 MPa and 3818 MPa respectively, while the impact strength was approximately 207 J/m. It is observed that PLA has superior strength but lacks in ductility. However, SiB reinforced PLA biocomposites show significant improvement in flexural strength and modulus with respect to PLA. This behaviour is probably due to the stiffening effect of fiber and the addition of SiB increases the compatibility with PLA. Moreover, it increases the brittleness of composites, which is evident from the decrease in impact strength to 151 J/m. The flexural strength and modulus of C30B nanoclay incorporated biocomposites increased by 5.3% and 10.6%, while the strength and modulus of PLA/SiB biocomposite are 103 MPa and 6986 MPa respectively. This can be attributed to the stiffness brought about by high modulus nanoclay as well as fiber and better compatibility of fiber and PLA matrix in the presence of nanoclay. However, a further reduction in impact strength of PLA/SiB/C30B bionanocomposites was observed due to the effect of nanoclay, which minimize the polymer chain mobility and hence flexibility.

Table 1. ***Flexural and impact properties of composites***

Composites	*Flexural properties*		*Impact strength (J/m)*
	Strength(MPa)	*Modulus (MPa)*	
PLA	94±1	3818±16	207±5.3
PLA/SiB	103±1	6986±11	151±1.5
PLA/SiB/C30B	108±3	7725±36	121±3.5
PLA/SiB/C30B/GC	126±1	7614±19	212±4.9

ISBN 978-93-5279-420-1

Hence, in order to improve the ductility, GC has been used as a reactive compatibilizer to PLA/SiB/C30B bionanocomposites. The addition of GC increased the flexural strength significantly while PLA/SiB/C30B/GC compatibilized bionanocomposites resulting reaction in flexural modulus. The PLA/SiB/C30B/GC compatibilized bionanocomposites showed flexural strength and modulus of 126 MPa and 7614 MPa, respectively. The compatibilization effect by GC may be responsible for the high flexural strength. During melt mixing GC produces a cross linked network with PLA, fiber as well as nanoclays, which is greatly facilitate to promote better interface. However, stiffening effect of fiber and nanoclays is reduced due to plasticizing effect of GMA as well as self aggregation effect of PLA in GC, which in turn cause for marginal reduction in flexural modulus. At the same time, it was interesting to note that the composite shows improvement in impact strength up to 212 J/m, which is attributable to the presence of GC as a plasticizing agent, by providing effective resistance to crack propagation during fracture.

Morphology of composites

Fig.4 represents the SEM micrographs of PLA and its biocomposites with C30B nanoclay and GC. In Figure 4(b), the interfacial interaction between PLA matrix and SiB is good, which indicates the effectiveness of silane to act as a coupling agent in biocomposites while Fig. 4(a)

ISBN 978-93-5279-420-1

confirms the brittle nature of PLA. However, in Fig. 4(b), some of the

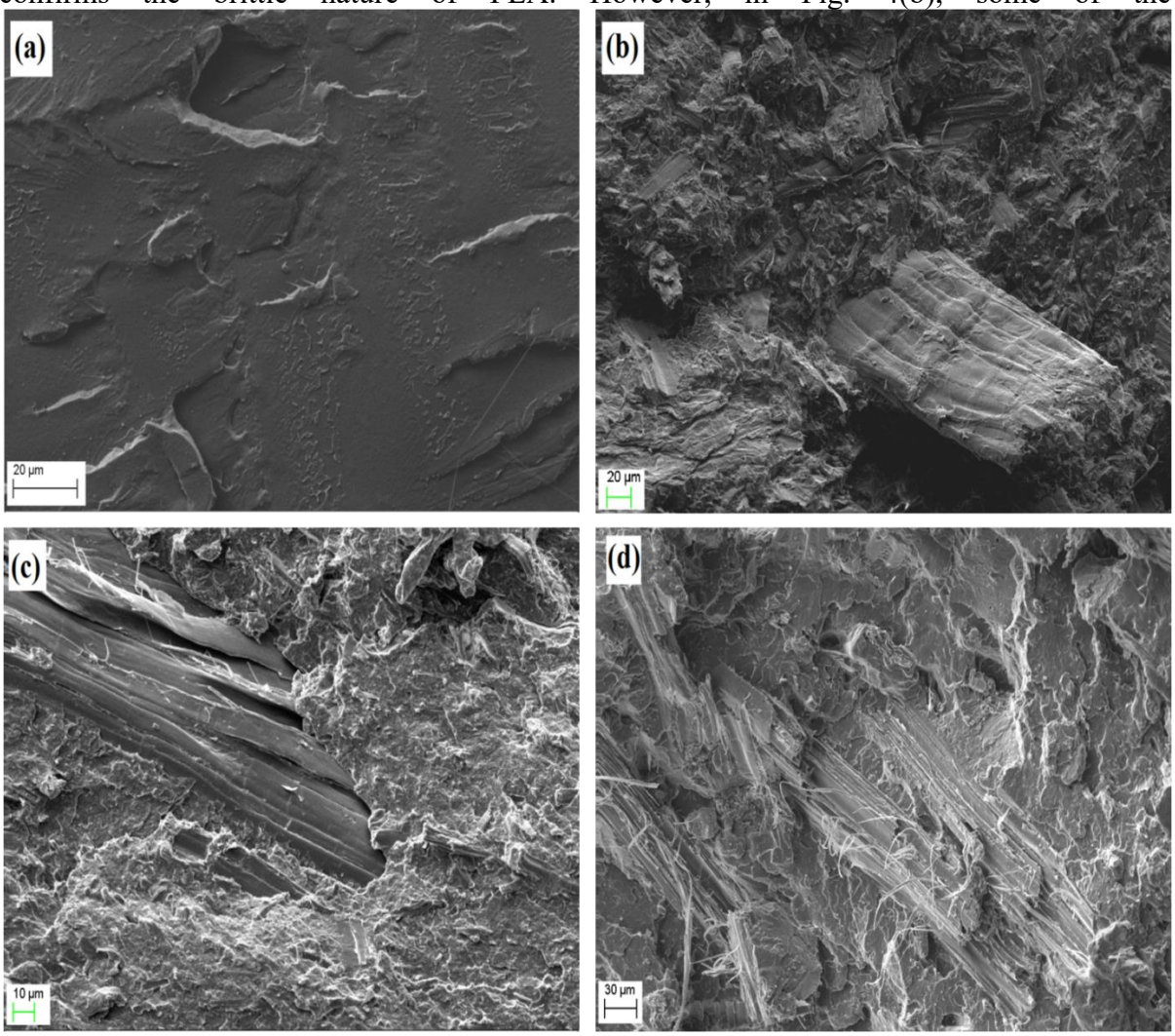

Fig. 4. SEM micrographs of (a) PLA, (b) PLA/SiB, (c) PLA/SiB/C30B and (d) PLA/SiB/C30B/GC

dispersed fibers have been pulled out of the matrix with clean surface or without matrix on surface during impact fracture, indicating weakness of silane coupling agent to produce completely strongly bonded, void free composites. Furthermore, with the addition of C30B nanoclay (Fig. 4(c)), the fiber pullout mechanism disappears and shows improved interface owing to the effect of C30B nanoclay. The intercalated and exfoliated C30B nanoclay are uniformly dispersed in composites, which is the main reason behind the reduction of microvoids and hence increasing the interfacial adhesion significantly. Inorder to show the compatibilizing effect of GC, the SEM micrographs of bionanocomposite compatibilized with GC is depicted in Fig. 4(d). Interestingly, fracture surface of PLA/SiB/C30B/GC compatibilized bionanocomposites showed distinct difference as compared with that of PLA/SiB/C30B bionanocomposites. The plasticizing effect due to the presence of GMA in GC reduces the brittle tendency of PLA and its biocomposites.

DSC analysis of composites

ISBN 978-93-5279-420-1

Crystallization behaviour, which is influenced by the arrangement of amorphous/ crystalline phase and consequently thermal properties have been studied by DSC. Incorporation of fillers, reinforcement as well as compatibilizing effect could change the above mentioned behavior of PLA. The thermal behaviour of PLA/SiB biocomposites with both C30B nanoclay and GC was investigated by DSC in the temperature range of 30-200ºC at 10ºC/min. The DSC thermograms depicted in Fig. 5 have been used to estimate the glass transition temperature (T_g), cold crystallisation temperature (T_{cc}), melting temperature (T_m) and degree of crystallinity (χ) of PLA, PLA/SiB biocomposites as well as compatibilized and uncompatibilized bionanocomposites from the first heating cycle. The first endo thermic peak gives the T_g value of composites, while first exothermic peak denotes the T_{cc} and the T_m determines from the second endothermic peak. The resulting parameters are registered in Table 2. The mechanical properties of PLA, PLA/SiB biocomposites and PLA/SiB/C30B bionanocomposites were well correlated with the obtained DSC parameters, while DSC parameters of PLA/SiB/C30B/GC compatibilized bionanocomposite are in opposite agreement with its mechanical properties. GC compatibilization did not significantly alter the T_g and T_m of composites, however, T_{cc} and degree of crystallinity of composites were reduced.

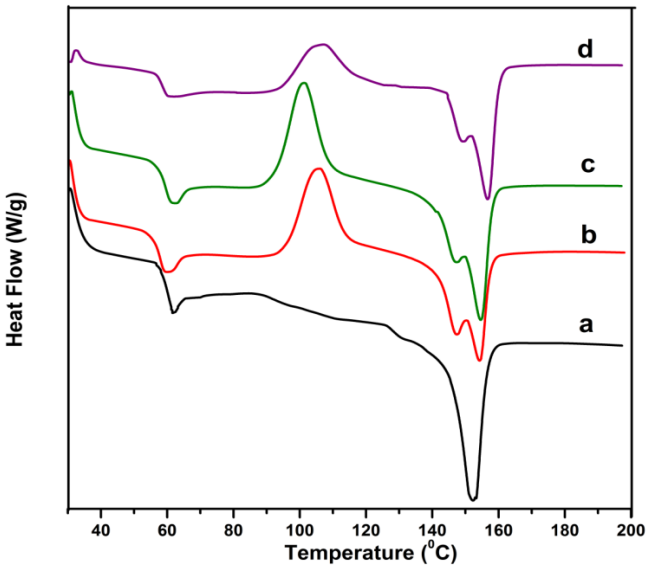

Fig. 5. DSC curves of (a) PLA, (b) PLA/SiB, (c) PLA/SiB/C30B and (d) PLA/SiB/C30B/GC

Fig. 5 shows an endothermic transition on the DSC curves of PLA at 59.45ºC, which is recognized as the T_g, corresponding to relaxation of polymer chain segments on heating. However, the incorporation of SiB causes negligible decrease of Tg in PLA biocomposite, which provides evidence for increase of mobility of PLA chain as a function of added fiber. However, nanoclay reinforcement of PLA/SiB biocomposite resulted improvement in T_g (59.34ºC) as compared with PLA/SiB. It suggests that, there is decrease in mobility of polymer chain and free volume between fiber and matrix after incorporation of nanoclay. Fully exfoliated C30B nanoclay is able to disperse uniformly within the composite, which limited the polymer chain mobility. Moreover, the better adhesion along with plasticization effect occurred in GC compatibilized PLA/SiB/C30B bionanocomposites, resulted marginal drops in Tg. It results very less reduction in Tg to 59.05ºC.This result is oppositely correlated with the tensile strength observed in previous sections.

ISBN 978-93-5279-420-1

The cold crystallization peak, an exothermic peak obtained during heating, which is revealed the reorganization of amorphous phase to crystalline due mobility and flexibility upon increasing temperature. However, PLA is not able to form crystalline structure at a rate of 10ºC/min, which describes the fact that at a heating rate of 10ºC/min was not sufficient to generate crystallization peak, since it is a semicrystalline material. Poor crystallisation is one of the demerits of PLA. As compared with PLA, a cold crystallisation (T_{cc}) peak is observed for PLA/SiB biocomposites at 105.42ºC. It can be attributed that crystallization ability of PLA was boosted by SiB as a nucleating agent in composites [32]. In general, the low T_{cc} value obtained during heating cycle and high value for cooling cycle indicates fast crystallization [33]. On other hand, T_{cc} of PLA/SiB/C30B bionanocomposites was observed at 101.81ºC, which is less than that of PLA/SiB. It might be due to nucleating capacity of nanoclay, which can reduce the activation energy for crystallization. Addition of C30B tends to decrease the mobility and force for faster crystallization. Nevertheless GC increased the crystallization peak to 106.43ºC, revealing the plasticizing effect of GC despite the slow crystalline character of PLA in GC. In addition to, the crystallinity calculated for all samples are in good agreements to the T_{cc} results. The introduction of fillers affected crystallinity of PLA. More clearly the crystallinity increased from 36.6 % for PLA to 41.5 % for PLA/SiB biocomposites, due to crystalline nature of cellulose. After C30B addition, the crystallinity significantly improved to 45.9 %. However, GC compatibilization led to depression of the crystallinity of composites. This trend was in good agreement with the crystallization temperature observed for composites.

Table 2. ***DSC analysis of PLA and its composites***

Composites	T_g(ºC)	T_{cc}(ºC)	T_m(ºC)		χ_{max}(%)
			T_{m1}	T_{m2}	
PLA	59.45			152.81	6.56
PLA/SiB	58.02	105.42	147.12	153.83	1.47
PLA/SiB/C30B	59.34	101.81	147.63	155.35	5.92
PLA/SiB/C30B/GC	59.05	106.43	149.19	156.92	7.46

T_g: glass transition temperature, T_{cc}: cold crystallisation temperature, T_m: melting temperature and χ_{max}: maximum crystallinity

As observed in figure, a double endothermic peak was detected for all composite, whereas PLA results only one melting peak at 152.81ºC. PLA/SiB biocomposite possessed double melting points at 147.12and 153.83ºC, whereas the primary melting point at 147.12ºC and secondary melting peak at 153.83ºC are corresponds to the melt crystallisation and remelting of PLA in PLA/SiB biocomposites. This indicates that, the heterogeneous nucleation as a function of fiber addition. On other hand it can be due to the presence of more than one crystal structure in composites as compared with PLA. Hence, the less perfect crystal melts first and reorganizes into crystals which remelt at high temperature. Further, incorporation of C30B to the tune of 3 wt% does show appreciable increase in melting temperature, which is probably due to the formation of genuine interface in PLA/SiB/C30B bionanocomposites. However, in case of PLA/SiB/C30B/GC compatibilized bionanocomposites, the melting temperatures were observed at 149.19 and 156.92ºC. The higher melting temperatures were observed from the DSC thermogram of PLA/SiB/C30B/GC compatibilized

ISBN 978-93-5279-420-1

bionanocomposites, which is probably ascribed to the confinement of compatibilization of GC within the bionanocomposites.

Dynamic mechanical analysis

Dynamic mechanical analysis has been used to investigate the viscoelastic properties of composites. Fig. 6 (a) illustrates, the storage modulus curves of composites as a function of temperature. The storage modulus of all composites are higher than those of PLA and above 60ºC, the modulus of all composites decreased with increasing temperature, which is due to the softening of composites upon heating [33].

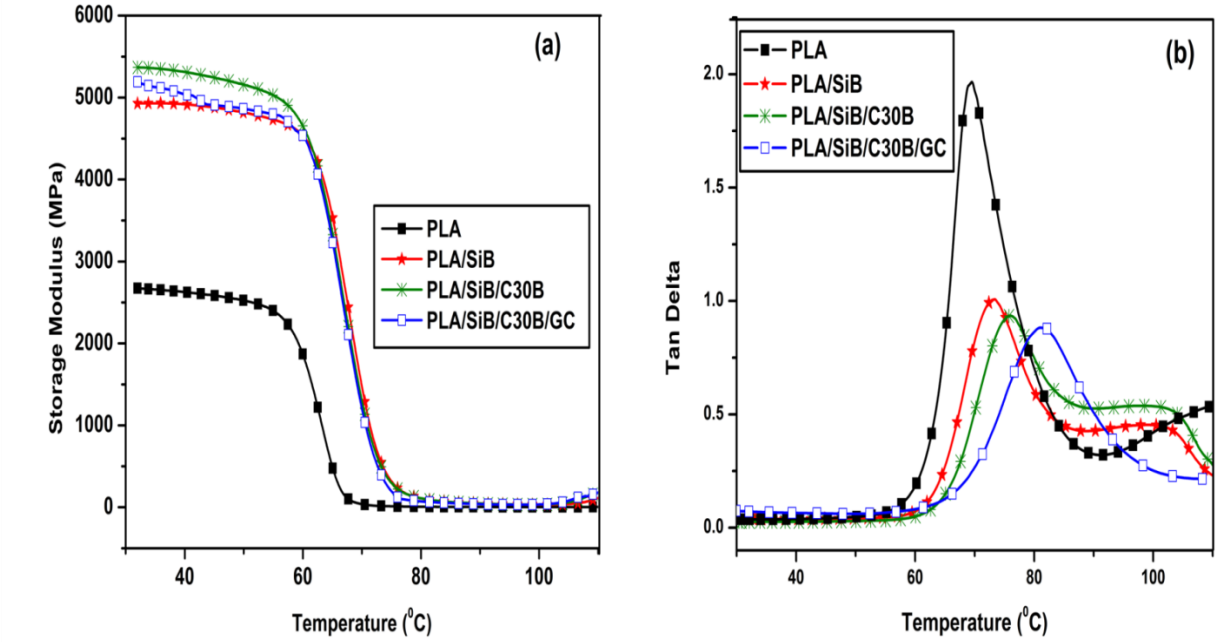

Fig. 6(a). Storage modulus and (b) Tan delta curves of PLA and its composites

The storage modulus of PLA was 2671 MPa at 30ºC, while were 4928 and 5367 MPa for PLA/SiB biocomposite and PLA/SiB/C30B bionanocomposites, respectively. This result indicates that both SiB and C30B nanoclay improved the stiffness of PLA matrix. More importantly, it was also noted that the PLA/SiB/C30B bionanocomposites have higher modulus that those of PLA/SiB/C30B/GC compatibilized bionanocomposite (5191 MPa). The reduction trend in storage modulus of PLA/SiB/C30B/GC compatibilized bionanocomposite is similar with the change noticed in flexural modulus. The lower storage modulus may be associated with the plasticizing effect of GC, and it suppresses the modulus imparted by fiber and nanoclay. In other words, the higher modulus observed for PLA/SiB/C30B bionanocomposite due to enhanced interfacial adhesion was offset by flexibilizing effect of GC in PLA/SiB/C30B/GC. This is also believed to be the cause of minute reduction in Tg of composites. Moreover, the storage modulus of composite except PLA again start to increase at temperature ranging from 100-110ºC, which is the typical effect of cold crystallisation observed in composites as described previously in DSC results.

ISBN 978-93-5279-420-1

Tan δ (damping factor), which is related to dissipation energy, of all samples are illustrated in Figure 6(b). The magnitude of tan δ peaks of all composites was lower than the PLA matrix. It has also been described that C30B nanoclay is well adhered to the PLA/SiB biocomposite, hence the mobility of polymer chain is reduced, resulting in less intensity. At the same time, PLA/SiB/C30B/GC composites also exhibit improved tan δ. Moreover, tan δ curves shows relaxation around 60-80ºC, which corresponds to α-relaxation temperature of composites. The α-relaxation temperature at 69.04ºC for PLA shifted to 72.99ºC by addition of SiB. Further addition of C30B results higher relaxation temperature at 75.91ºC, which is associated with the decreased PLA chain mobility. Further, GC compatibilized composites also shifted the tan δ peak to higher temperature (81.24ºC). This may be due to the effective crosslinking of GC in bionanocomposites which decreases the mobility of polymer chain segment. The obtained result is in good agreement with flexural data, but opposite in trend to that noticed from DSC.

Conclusions

In this study, the biocomposite, PLA/SiB were prepared with nanoclay as well as graft copolymer by melt blending. Graft copolymer was synthesized from PLA and GMA using BPO as an initiator which acted as a compatibilizing agent in bionanocomposites. FTIR spectra have been used to elucidate the chemical structures of SiB and GC and the graft copolymerization was further confirmed by ^{1}HNMR. The effect of C30B and GC on the mechanical, thermal and dynamic-mechanical behaviour of PLA/SiB biocomposite has been investigated. Mechanical studies indicated that incorporation of C30B nanoclay increased the flexural strength and modulus and failed to reduce the brittleness of PLA. Further, addition of GC improved the ductility of PLA, while retaining the flexural strength. However, PLA/SiB/C30B/GC compatibilized bionanocomposites are resulted reduction in flexural modulus. DSC thermograms revealed that C30B nanoclay decrease the PLA chain mobility and hence resulted improved T_g and T_m. whereas due to dual role of GC as a compatibilizer and plasticizer, there was reduction in Tg and improvement in T_m. The storage modulus and relaxation temperature connected to tan δ obtained from DMA confirmed the above results.

References

1. D. B. Dittenber and H. V. S. Ganga.Rao, Compos: Part A **43**, 1419 (2012).
2. M. Avella, G. B.Gaceva, A. Buzarovska, M. E. Errico, G. Gentile and A. Grozdanov. J. Appl. Polym. Sci. **108**, 3542 (2008).
3. H. P. S. A. Khalil, A. H. Bhat and A. F. I. Yusra. Carbohydr. Polym. **87**, 963 (2012).
4. M. Zhou, J. Yan, Y. Li, C. Geng, C. He, K. Wang and Q. Fu. RSC Adv. **3**, 26418 (2013).
5. M. J. John and S. Thomas. Carbohydr. Polym. **71**, 343 (2008).
6. F. Shukor, A. Hassan, M. S. Islam, M. Mokhtar and M. Hasan. Mater. Des. **54**, 425 (2014).
7. M. S. Huda, L. T. Drzal, A. K. Mohanty and M/ Misra. Compos. Sci. Technol. **68**, 424 (2008).

ISBN 978-93-5279-420-1

8. K. Oksman, M. Skrifvars and J. F. Selin, Compos. Sci. Technol. **63**, 1317 (2003).
9. G. Faludi, G. Dora, K. Renner, J. Moczo and B. Pukanszky, Carbohydr. Polym. **92**, 1767 (2013).
10. V. Paul, K. Kenny and G. G. Redhi, Compos.: Part A **68**, 90 (2015).
11. M. M. Kabir, H. Wang, K. T. Lau and F. Cardona, Compos.: Part B **43**, 2883 (2012).
12. O. Faruk, A. K Bledzki, H. P. Fink and M. Sain, Prog. Polym. Sci. **37**, 1552 (2012).
13. T. Yu, J. Ren, S. Li, H. Yuan and Y. Li, Compos.: Part A **41**, 499 (2010).
14. M. A. Mosiewicki and M. I. Arangure, Eur. Polym. J. **49**, 1243 (2013).
15. R. Kumarm, M. K. Yakabu and R. D. Anandjiwala, Compos.: Part A, (2010).
16. K. Chrissafis and D. Bikiaris, Thermochim. Acta **523**, 1 (2011).
17. K. Majeed, M. Jawaid, A. A. Bakar, H. P. S. Khalil, A. A. Salema and I. Inuwa, Mater. Des. **46**, 391 (2013).
18. T, D. Hapuarachchi and T. Peijs, Compos.: Part A **41**, 954 (2010).
19. N. Putu, G. Suardana, M. S. Ku and J. K. Lim, Mater. Des. **32,** 1990 (2011).
20. A. Javadi, Y. Srithep, J. Lee, S. Pilla, C. Clemons, S. Gong and L. Turng, Compos: Part A **41**, 982 (2010).
21. I. S. M. A. Tawakkal, M. J. Cran and S. W. Bigger, Ind. Crop. Prod. **61**, 74 (2014).
22. S, H. Lee and S. Wang, Compos: Part A **37**, 80 (2006).
23. S. Lin, W., Guo, C. Chen, J. Ma and B. Wang, Mater. Des. **36,** 604 (2012).
24. T. Yu and Y. Li, Compos: Part A **58**, 24 (2014).
25. W. R. Jiang, R. Y. Bao, W. Yang, Z. Y. Liu, B. H. Xie and M. B. Yang, Mater. Des. **59**, 524 (2014).
26. A. Petchsuk, W. Submark and P. Opaprakasit, Polym. J. **45**, 406 (2012).
27. P. Juntuek, C. Ruksakulpiwat, P. Chumsamrong and Y. Ruksakulpiwat, J. Appl. Polym. Sci. **125**, 745 (2012).
28. J. Liu, H. Jiang and L. Chen, J. Polym. Environ. **20**, 810 (2012).
29. Y. Wang, Y. Weng and L. Wang, Poly. Test. **36**, 119 (2014).
30. C. S. Wu, Compos. Sci. Technol. **102**, 1 (2014).
31. V. P. Sajna, S. Mohanty, S. K. Nayak, J. Reinf. Plast. Compos. **33**, 1717 (2014).
32. T. Xu, Z. Tang and J. Zhu, J. Appl. Polym. Sci., (2012).
33. Y. Du, T. Wu, N. Yan, M. T. Kortschot and R. Farnood, Compos.: Part B **56**, 717 (2014).

SYNTHESIS, CHARACTERIZATION AND ANTIFUNGAL STUDIES OF 2-[2-IMINO-N-PHENYLBUTANAMIDO]BENZOIC ACID AND ITS Co (II), Ni (II), Cu (II) AND Zn (II) COMPLEXES

ISBN 978-93-5279-420-1

Rema V. T and Susannah Seth*

PG and Research Department of Chemistry, Malabar Christian College,

Kozhikode- 673001, Kerala

**E-mail: susannahseth@yahoo.co.in*

Abstract: In the present workthe synthesis, characterization and antifungal activities of a Schiff base derived from anthranilic acid and acetoacetanilide and its Co (II), Ni (II), Cu (II) and Zn (II) complexes are discussed. The synthesized compounds were characterized by elemental analyses, magnetic susceptibility measurements, IR, HNMR and mass spectra. The complexes were found to be penta coordinate with the general formula [ML (H_2O) (CH_3COO)], where M is the metal and L is the mono anion of the ligand. These compounds were also screened against *A. niger* to assess the antifungal activity. Anthranilic acid since it contains both carboxyl as well as amino group is similar to amino acids. The work is intended to extend to amino acids and develop medicines which are less toxic.

Introduction

Developments in Coordination chemistry, over the years have led to the synthesis of an important class of bases known as Schiff bases. Coordination compounds including Schiff base ligands play a pivotal role in industry(Hamon J and Saillard J 2010), technology (Matsunaga S and Shibasaki M2014), and biological processes (Kostova I and Saso L 2013). The condensation products of primary amines with carbonyl compounds are often referred to as Schiff bases. These are compounds containing azomethine group (>C=N) and have the general structure R-N=C-R' where R and R' are aryl, alkyl, cycloalkyl or heterocyclic groups which may be variously substituted. Often they are referred to as anils, imines or azomethines.A Schiff base can nitrogen analog of an aldehyde or ketone in which the C=O group is replaced by C=N-R group. It is usually formed by condensation of an aldehyde or ketone with a primary amine according to the following scheme:

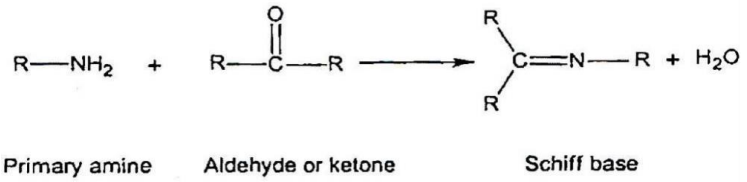

Scheme 1. Formation of Schiff base

R may be hydrogen, alkyl or aryl group. Schiff bases that contain aryl substituents are more stable and more readily synthesized, while those which contain alkyl groups are relatively unstable. The formation of chelates gives extra stability to the complexes especially when the ring is five or six membered. Hence the presence of a functional group with replaceable hydrogen atom near to >C=N will be additional factor of stability. The investigators in the area of Schiff base ligands are concentrating on their biological activity as potent inhibitors and ability in variable bonding.While the C=N linkage is essential for biological activity, there has

ISBN 978-93-5279-420-1

been increasing emphasis on the screening of new and more effective antimicrobial drugs with low toxicity (Trujillo A, *et al* 2013). Various Schiff bases have been found to posses pharmacological activities such as antitubercular, anticancer (Cheng J *et al*2014), antitumor, antibacterial **(**Karmakar I, Mandal S, Mitra A 2015), fungicidal etc. Considering these properties of Schiff bases, in the present work the antifungal activities of Schiff bases derived from anthranilic acid and acetoacetanilide and its Co (II), Ni (II), Cu (II) and Zn (II) complexes are studied.

Materials and Methods

All the metal salts used were E. Merk, analar grade, and were used as such. For the synthesis of Co (II), Ni (II), Cu (II) and Zn (II) complexes, corresponding metal acetates were used.The ligand was synthesized by mixing 0.68g (0.005mol) of anthranilic acid in methanol with 0.88g(0.005mol) of acetoacetanilide in methanol and stirring for 20 minutes. The precipitate formed was washed with benzene, filtered and dried under IR lamp. Yield was noted. Metal complexes were synthesized by adding aqueous methanolic solution of the metal salt to a boiling solution of the ligand in 1:1 ratio and refluxing the resulting solution for 1h. The precipitated complexes were filtered, washed with water and methanol and dried. Metal Complexes were analyzed by independent pyrolysis to determine the metal content. 0.1g of the complexes was accurately weighed and converted them into their oxide by thermal decomposition.Carbon, Hydrogen and Nitrogen percentages were obtained by microanalysis from CDRI, Lucknow. Magnetic susceptibility measurements were done from Calicut University by using a MagwaySharewood MSB employing $Hg[Co(NCS)_4]$as calibrant. Diamagnetic corrections were made using Pascal constants and corresponding effective magnetic moments were calculated.Mass, IR and ^1H NMR spectra were obtained from SAIF, CDRI-Lucknow. Molar conductance of the Schiff base ligand and their metal complexes were determined in methanol at room temperature by using a conductometer at 20 μS. Fungal strain used in the present study is *Aspergillus Niger*in Potato agar medium. A 2000ppm solution of Amphotericin B in ethanol was used as control drug.The growth of the fungiwas observedafter 24 hours and the inhibition zone diameter was measured. A triplicate was also conducted.

Results and Discussion

The elemental percentages of C, H and N reported by microanalysis showed close agreement with the molecular formula $C_{17}H_{16}N_2O_3$ for the ligand.The metal complexes on thermal decomposition yield their oxides.ie, Co (II) and Cu (II) gives black colored oxides ($Co_2O_3$and CuO), Ni (II) gives brown colored oxide (NiO) and Zn (II) gives white oxide (ZnO). The elemental percentage and other physical data of the ligand and its complexes are included in the Table 1. The elements of the first transition series form complexes with magnetic moment values in close agreement with Bose-Stoner spin only formula, $\mu=[n(n+2)]^{1/2}$ BM, where n is the number of unpaired electrons in the system. The Co (II), Cu (II) and Ni (II) complexes are found to be paramagnetic in nature, where as the Zn (II) complex is diamagnetic as expected. The magnetic moment values of complexes indicated high spin geometry. Thus the magnetic moment values obtained for these complexes were within the range expected for the proposed geometry.The molar conductance of the Schiff base in methanolic and its complexes in DMSO solutions suggested that all the complexes were non-electrolytes in the roomtemperature.

The IR spectra of the ligand shows almost all bands expected for Schiff base. The strong absorption in the 1603.58 cm^{-1} region is assigned as the azomethine group present in theSchiff base. Other bands and corresponding vibrations are given in the Table 2.

ISBN 978-93-5279-420-1

Table1.***Physico-chemical data of the synthesized compounds***

Compound	*Yield %*	*Colour*	*Elemental analysis Calculated(found)*				*Magnetic moment(μ_{eff}) BM*	*Conductancex 20µs*
			C	*H*	*N*	*M*		
Ligand	71.54	Light brown	68.92 (68.02)	5.41 (5.01)	9.46 (9.20)	-	D	9.1
Co complex	55.69	Light pink	52.91 (51.95)	6.49 (6.12)	6.49 (6.05)	13.67 (13.50)	5.1937	19.6
Ni complex	81.26	Light green	52.94 (52.12)	6.50 (6.04)	6.50 (6.16)	13.63 (13.36)	3.5387	4.7
Cu complex	64.29	Green	52.35 (51.88)	4.59 (4.23)	6.43 (6.12)	14.59 (14.38)	2.1114	19.5
Zn complex	45.73	White	52.13 (51.56)	4.57 (4.12)	6.40 (6.08)	14.95 (15.26)	D	8.1

Table 2.***Important IR spectral bands of the ligand***

Wave number (υ in cm^{-1})	*Assigment*
1603.58	-C=N-
1668	>C=O
3369	O-H of COOH
3019	N-H of amide
1496	C-C in aromatics
1320	C-O of COOH
667.42	-CH aromatics
1410.75	-CH of CH_3
762.09	-CH rock of CH_3
1218.31	-CN of amide
1325.88	-CH of CH_2

The ^{1}HNMR spectrum of the ligand showed all the peaks expected**.**The ^{1}HNMR spectrum of the complex is given in table3. The disappearance of OH peak of COOH group indicates thecoordination of the group to the metal. Additional peaks at 1.544 and 1.430indicate the coordination of water and acetate to the metal atom respectively. In the mass spectra of ligand, the base peak is found to be at 137.94m/e corresponds to molecular weight of anthranilic acid.The M+1 peak was at 297.02 m/e.

Table 3.***Chemical shift of the ligand and the Zinc complex***

Ligand		***Zn(II) Complex***	
Chemical shift	*Assignment*	*Chemical shift*	*Assignment*
2.301	-NC-CH_2-CO-	1.544	H_2O
9.179	Ar-COOH	1.430	CH_3 of acetate
7.086-7.944 m	Ar-H Benzenoid	6.909-7.606 m	Ar-H Benzenoid
6.672	Ar-NH-CO- Amide	6.661	Ar-NH-CO- Amide
1.717	CH_3-CN-	1.687	CH_3-CN-

ISBN 978-93-5279-420-1

Peak corresponding to acetoacetanilide moiety was obtained at 178.06.In the mass spectra of Cu complex (Fig.1), the base peak is found to be at 297.05 m/e. Molecular weight of a structure involving one molecule each of the ligand, water, acetate and Cu atom is found to be 435.88. But M+2 peak is obtained at 437.96 instead of the corresponding M^+ ion peak. This indicates penta coordination around the metal atom, since molecular ion peaks corresponds to other coordinations were absent in the spectra.

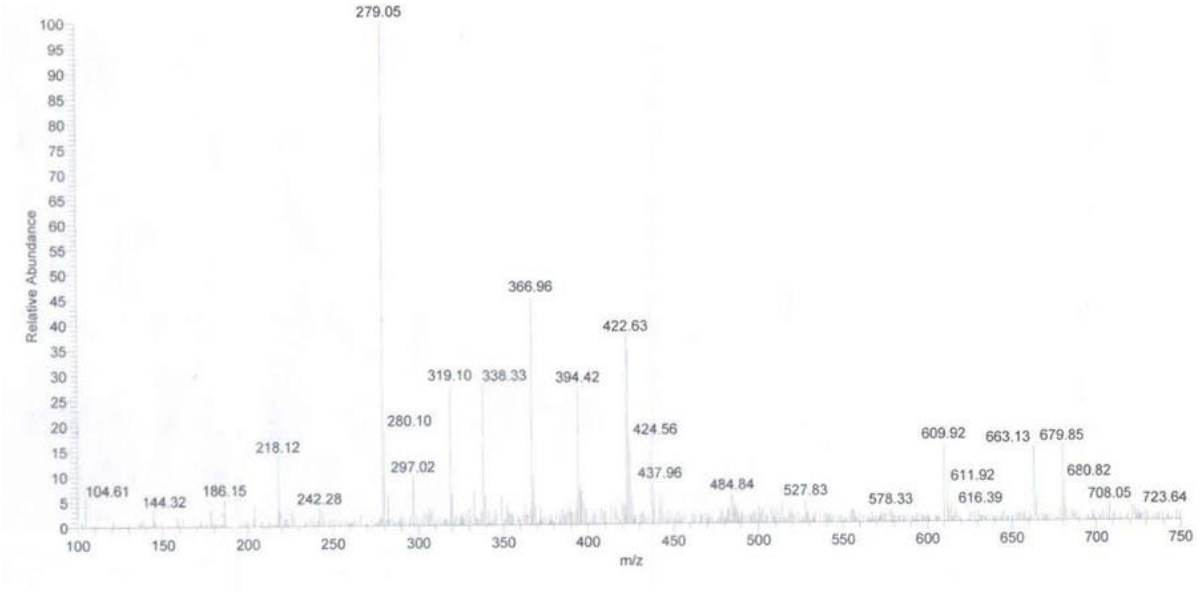

Fig.1. *Mass spectrum of copper complex*

The ligand forms stable complexes with Co(II), Ni(II), Cu(II) and Zn(II). All complexes are colored solids. The close agreement between the calculated and observed metal percentages and also evidences from the spectral studies shows that the general formula of the complexes to be [ML(H_2O)(CH_3COO)], where M is the metal and L is the mono anion of the ligand.The fungal studies detailed in table4 indicate that the Schiff base and Cu complex are very active against the fungus *Aspergillus Niger* while Co, Ni and Zn are less active against them. The photograph of the fungal activity after 24 h is depicted as Fig.2. Methanol as well as DMSO which are used as the solvents shows moderate activity.

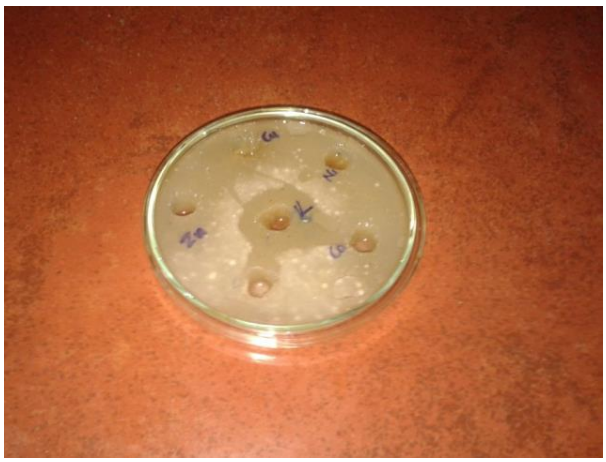

ISBN 978-93-5279-420-1

Fig.2. *Image showing the inhibition zone of ligand and its complexes*

Table 4.***Antifungal activity measurements of the compounds***

Compound	*Diameter of inhibition zone (mm)*		
	1	*2*	*3*
Amphotericin B	30	30	30
Methanol	15	15	15
DMSO	25	25	25
Schiff base	30	29	29
Co complex	24	25	24
Ni complex	20	20	21
Cu complex	27	28	27
Zn complex	24	23	23

Conclusions

The structure of the ligand has been confirmed by the physico-chemical methods. The ligand and complexes were characterized by spectral technique, molar conductance and magnetic measurements. All the evidences shows that the ligand acts as tridentate neutral ligand coordinated through N of azomethine (-CH=N-) and also by the oxygen's of CO and COOH group. A penta coordinate Geometry has been assigned for all the four complexes.Antifungal activity of the Schiff base and its complexes developed were checked and found that the Schiff base and Cu (II) complex are very active against the fungus *Aspergillus Niger* and Co(II), Ni (II) and Zn(II) complexes shows moderate activity.On the basis of the available data, the following structures (Fig. 3 and Fig. 4) are assigned for the ligand and complexes.

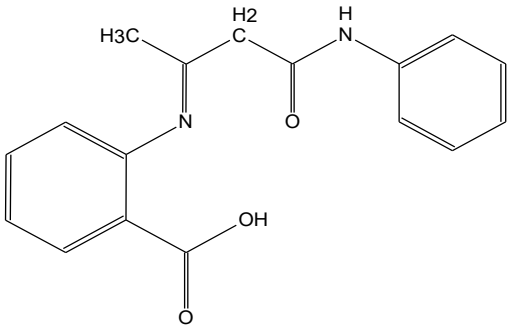

Fig.3. *Structure of the ligand2-[2-imino-N-phenylbutanamido]benzoic acid*

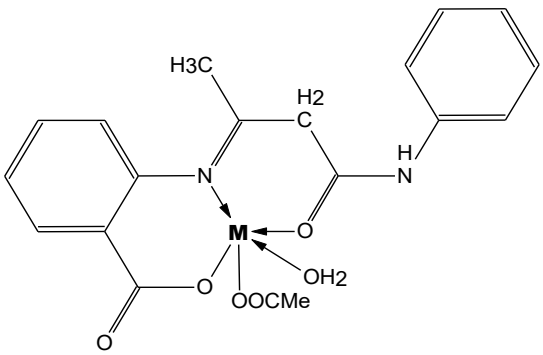

Fig.4. *Tentative structure of the metal complexes; M= Co, Ni, Cu, Zn*

ISBN 978-93-5279-420-1

References

1. **Cheng J**, Ma X, Zhang Y, Liu J, Zhou X and Xiang H (2014), Optical ChemosensorsBased on Transmetalation of Salen-Based Schiff Base Complexes, Inorg.Chem., 53 (6):3210.
2. **Hamon J** and Saillard J (2010), Synthesis, Spectral, Structural, Second-Order Nonlinear Optical Properties and Theoretical Studies On New Organometallic Donor-Acceptor Substituted Nickel(II) and Copper(II) Unsymmetrical Schiff-Base Complexes Inorg. Chem.49: 2750.
3. **Karmakar I**, Mandal S, Mitra A (2015), Potential Antimicrobial Properties of Two New Synthetic Metal Complexes Containing a Tetradentate Schiff Base, International Journal of advanced Research 3, 8: 1230.
4. **KostovaI** and SasoL (2013), Advances in Research of Schiff-Base Metal Complexes as PotentAntioxidants, Current Medicinal Chemistry, 20:4609.
5. **Matsunaga S** and Shibasaki M (2014), Recent advances in cooperative bimetallic asymmetriccatalysis: dinuclear Schiff base complexesChem. Commun.,50: 1044.
6. **Trujillo A**, Fuentealba M, Carrillo D, Manzur C, Ledoux-Rak I, Qin W , Long S , Panunzio M and Biondi S (2013), Schiff Bases: A Short Survey on an Evergreen Chemistry Tool, Molecules, 18: 12264.

ISBN 978-93-5279-420-1

STUDY ON AROMAS TRANSFER THROUGH EVA-CELLULOSE BLEND POLYMER

Smitha M

Department of Chemistry, N.S.S College, Manjeri, Malappuram, Kerala-676122

E-mail: m.smitha.saj@gmail.com

Abstract: Numerous applications of polymers like packaging of foods and beverages, protective coating and membrane separation process are critically dependent on the rate at which various molecular species permeate. So the study of transport phenomena through polymeric membrane is very important in recent days to achieve significant improvement in this area . In this project The diffusive migration in the vapour phases of three volatile organic compounds (VOC's: benzene, toluene, and xylene) through the samples of different cellulose-EVA-Cellulose blend polymers (1%,5%,10%) were compared based on both sorption and diffusion tests. The effects of structure and morphology of the blend membranes on the permeability were investigated. The permeability was found to decrease with increase in the percentage of cellulose content which has been attributed to the semicrystalline nature of cellulose. The permeation process has been observed to be controlled mainly by the molecular mass of the penetrants.

Introduction

Diffusion and permeation in polymeric materials is of fundamental importance in many applications and is the subject of considerable scientific interest. The applications of polymeric films as protective coating in membrane separation process, in food packaging etc depend on its permeation properties [1, 2, 3]. Many aromatic vapours exist in food, medicine, cosmetic and diverse daily chemicals such as flavor snack food, flavor, perfume, soap, shampoo and so on. Dissipating or adding of aromatic vapor will affect the quality and marketing of products directly. Polymers, during their life time are exposed to a variety of hostile chemical environments. The use of polymer membranes as liners and storage tanks for hazardous liquids is increasing [4, 5]. So the knowledge of the performance of polymers in the environment of hazardous solvents, vapours and temperature is essential for their successful applications. Vapour permeation is one of the most prospective routes used in industries related to membrane technology. It is both widely employed to separate azeotropes and in the dehydration of solvents/alcohols [6]. It is considered as an attractive alternative to per vapouration in which the component to be separated from a liquid feed mixture has to be vapourized through a membrane [7]. In addition, the vapour permeation method promises greater simplicity in technical design and significant opportunities for energy savings [8–9]. So, an understanding of the transport phenomena of the polymers and their interaction with different penetrants plays

ISBN 978-93-5279-420-1

a vital role in the various applications in chemical and food industries [10, 11]. Conversely, the vapor permeation technique is a good tool for the thermodynamic characterization of polymer blends. Analysis of equilibrium sorption of a vapour by the solid polymer blend can provide useful information regarding the polymer-polymer interactions.

The vapour permeation through different polymeric films has been studied by several researchers [12–15]. On the basis of the permeation data of benzene and cyclohexane vapours by poly (urethane urea) (PUU), Wolinska-Grabczyk et al. [16] predicted the pervaporation performance of PUU-based membranes for the separation of benzene/cyclohexane mixtures. Vapor transport also offers one of the unique ability to study the structure property relationships in polymers. The sorption characteristic of water and ethanol vapors in poly (vinylalcohol) (PVA) membranes of different crystallinity was investigated by Perrin et al. [17]. They reported that higher the crystallinity of the membranes, the lower the values of limiting diffusion coefficient and plasticization coefficient.

The goal of this study was to examine the solvent vapour permeation properties of EVA-cellulose blend membranes using different organic solvents. The organic solvents used for study were benzene, toluene and xylene Particular attention has been given to the effects of blend ratio and nature of penetrants on the permeation behavior and the correlation of the results with the morphology of the matrices.

Materials and Methods

Materials: The polymeric materials used for study were the samples of different EVA-cellulose blend polymers, viz., 1%, 5%,10% and the solvents used were benzene, toluene and xylene.

Vapor Permeation study: The vapour permeability was determined at room temperature by measuring the weight loss from small vials containing organic solvents such as benzene, toluene and xylene, which were closed tightly by using the blend membranes. The experiments were triplicates in most cases and the deviation was within ± 0.001 to 0.003 mole percentage. The results of the vapor permeation experiments were expressed by plotting the amount of vapor permeated, Mt, versus time, t. [18]

Blend Morphology: The blend samples for scanning electron microscopy (SEM) were prepared by cryogenically fracturing them in liquid nitrogen. These samples were sputter coated with gold and SEM examinations were performed on a Cambridge Instrument (S360).

Results and Discussion

Effect of filler

Fig.1 shows that the amount of vapour permeated through 1% and 4% cellulose loaded to EVA system. It has been observed from the figure that 1% EVA-cellulose membrane showed higher permeability than 4% EVA-cellulose system. The higher permeability in the former membrane may be due to more volume of matrix. Adding cellulose to EVA phase improves barrier property. The incorporated cellulose in the matrix fills in the normally pores structure of the EVA membrane. Thus, the gases passing through the matrix must travel a tortus path created by the added cellulose particle hence the permeability of the vapour decreases.

ISBN 978-93-5279-420-1

Effect of Amount of filler

Fig.2 shows the amount of vapour permeated through composite membrane with varying amount of cellulose. 5% and 10% loaded cellulose shows almost comparable permeabilities. It can be seen that the 10% loaded cellulose system has very low rate of permeability due to dispersion of the filler in the matrix. This study shows the importance of blending natural polymers like cellulose to synthetic polymers (EVA) which decreases the permeability of the membrane. This property of the membrane is useful to make biopolymers and can be applied in food packages which will preserve aroma and flavor naturally.

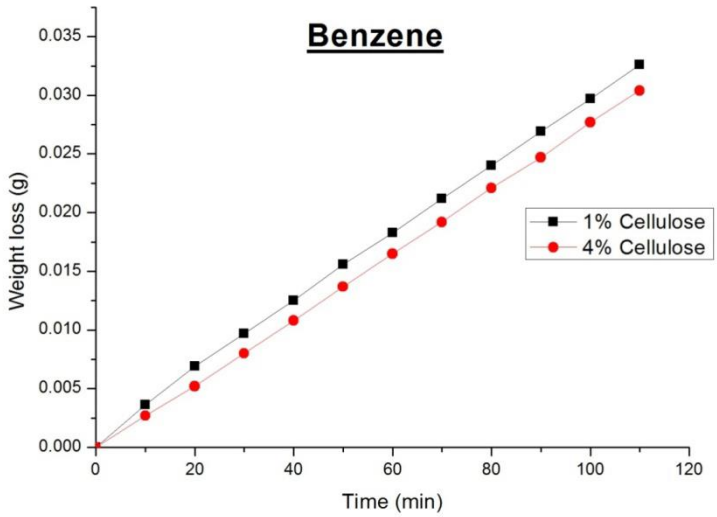

Fig. 1. *The amount of vapour permeated through 1% and 4% cellulose loaded to EVA system*

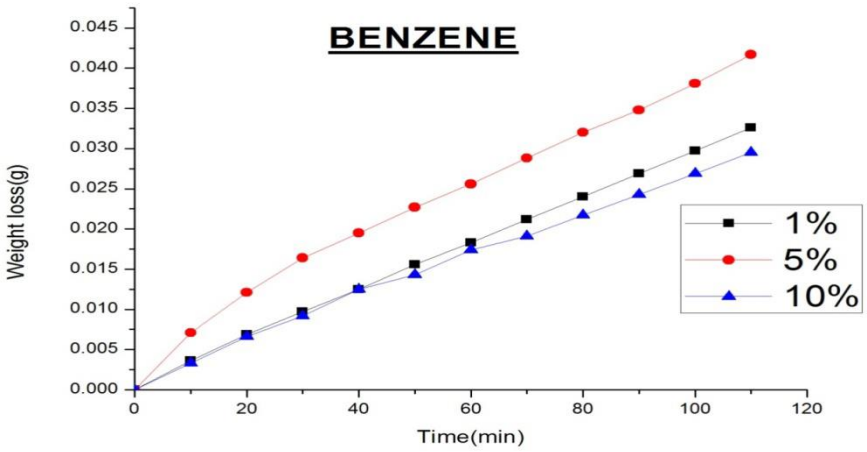

Fig.2. *The amount of vapour permeated through composite membrane with varying amount of cellulose*

Effect of Solvents

ISBN 978-93-5279-420-1

Fig.3 shows the rate of permeation in different solvents. From the figure it is obvious that the three different organic solvents showed different permeability which was time dependent. Benzene has low molecular size, which can pass through the free volume of the membrane easier than the larger molecules (toluene, xylene). So the rate of permeation is more through benzene. The order of permeation according to penetrant size for given membrane has been found to be benzene > toluene > xylene

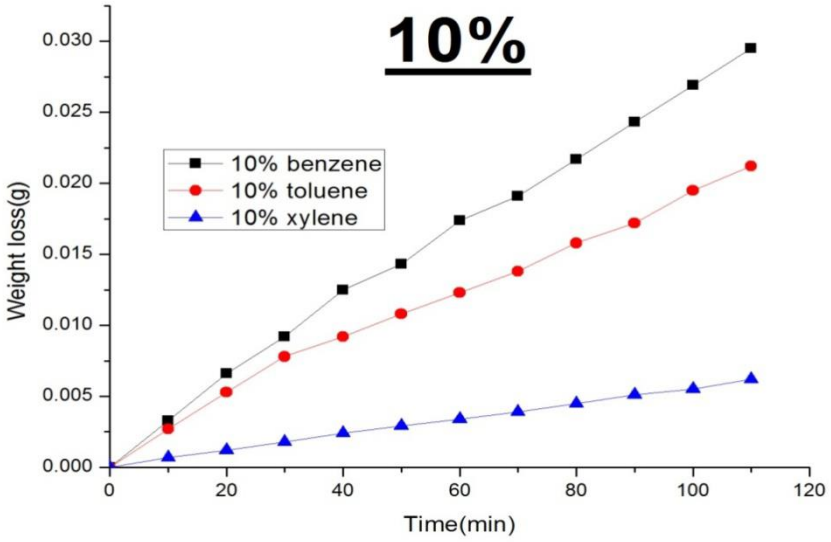

Fig. 3. *The rate of permeation in different solvents, benzene, toluene and xylene*

Comparative morphological study of filler loaded in different systems

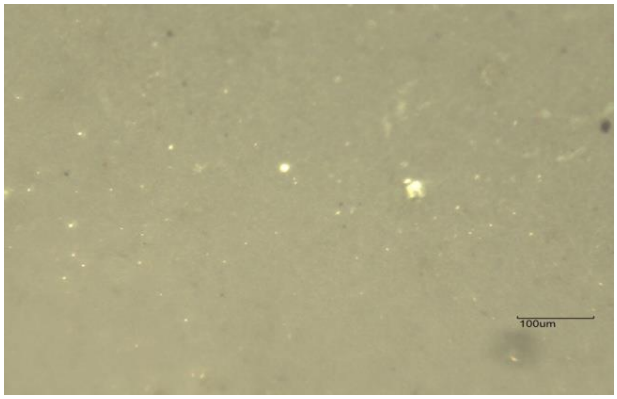

Fig. 4. *SEM of pure EVA*

ISBN 978-93-5279-420-1

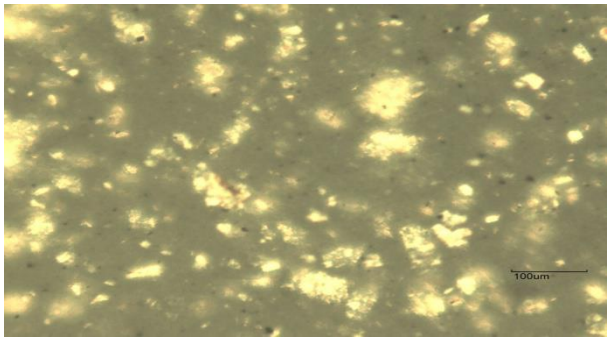

Fig. 5. *SEM of EVA + 5% cellulose loaded*

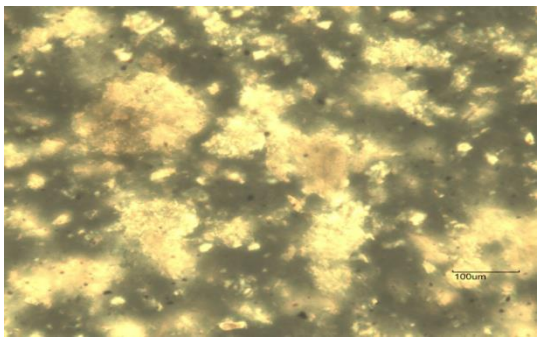

Fig. 6. *SEM of EVA + 10% cellulose loaded*

Fig. 4 shows the pure EVA system, it is not loaded with any substance. But in Fig.5, 5% cellulose is loaded to pure EVA system, it fills some of the porous structure of the system.10%cellulose is loaded to EVA in Fig.6 It has been found more particles in this system, it fills most of the porous sites.

Conclusion

Permeation of three aromatic solvent vapors viz. benzene, toluene, xylene through different samples of EVA-cellulose blend polymers has been studied with reference to the effect of blend ratio. The decrease in the permeability of aromas through these membranes with increase in the cellulose content has been attributed to the semicrystalline nature of cellulose. The morphological analysis of these membranes again confirmed the observed fact. Of the three aromatic vapors used, the trend is in the order: benzene> toluene > xylene. This is in accordance with their molecular size.

References

1. Y. M. Sun, C. H. Wu and A. Lin, *Polymer*, 47, 602, 2006.
2. S. Marain, Y. Hirata, C. Cahot, S. M. Groquet, M.R. Garda, H. Atmani, F. Ponlin-Epaillard, *Surface Coat. Technol.*, 201, 68, 2006.
3. K. Fialova, R. Petrychkovych, M. Shanma and P. Uchytil, *J. Membr.Sci.,* 275, 160 , 2006.
4. Briston, J.H., in The Wiley Encyclopedia of Packaging Technology, M.Bakker (Ed.), John Wiley and Sons, New York, 1986.
5. Ortego, J.D., Aminabhavi, T.M., Harlapur, S.F., Balundgi, R.H. J. Hazard.Mat., 42, 115, 1995.
6. B. K. Dutta, S. K Sridhar, *AIChE J*, *37 (4)*, 588, 1991.
7. R. C. Binning, R. J. Lee, J. F. Jennings, E. C. Martin, *Ind. Eng. Chem.*, *53*, 4, 1961.
8. R. W. Baker, N. Yashioka, J. M. Mohr, A. J. Khan, *J. Membr. Sci.*, *31*, 259, 1987.
9. V. Nitsche, K. Ohlrogge, K. Stürken, *Chem. Eng. Technol.*, *21 (12)*, 925, 1998.
10. K. Weh et al., *Chem. Eng. Technol.*, *21 (5)*, 408, 1998.
11. M. T. Uddin, *Chem. Eng. Technol.*, *30 (9)*, 1248, 2007.

ISBN 978-93-5279-420-1

12. J. Huang, R.J. Cranford, T. Matsuura, and C. Roy, J.Membr. Sci., 241, 187, 2004.
13. N. Morliere, J.P. Corriou, E. Favre, and D. Roizard, Desalination,144, 109, 2002.
14. S. Marais, E. Bureau, F. Gouanve, E.B. Salem, Y. Hirata, A.Andrio, C. Cabot, and H. Atmani, Polym. Test., 23, 475, 2004.
15. I. Blume, P.J.F. Schwering, M.H.V. Mulder, and C.A.Smolders, J. Membr. Sci., 61, 85, 1991.
16. A. Wolinska-Grabczyk, S. Smigusiewicz, and J. Muszynski,Polym. Bull., 40, 591, 1998.
17. L. Perrin, Q.T. Nguyen, R. Clement, and J. Neel, Polym.Int., 39, 251, 1996.
18. S. Anusree,1 A. Sujith,1 C.K. Radhakrishnan,1 G. Unnikrishnan2 Polymer engineering and Science, 199, 2008.

DEVELOPMENT AND ELECTROANALYTICAL SCREENING OF CHITOSAN/SiO_2 BASED ANTICORROSIVE NANOCOMPOSITE FILM ON MILD STEEL

Shamsheera K O* and Abraham Joseph

Department of Chemistry, University of Calicut, Calicut University PO, Kerala

**E-mail: shamsimanu@gmail.com*

Abstract: Chitosan based coatings considered as green alternative for the corrosion protection of mild steel mainly due to its barrier property and affinity towards metal. In this study Chitosan and Chitosan/SiO_2 nanocomposite film developed on mild steel surface via sol gel method and dip coating techniques. Films so formed were characterized by FTIR-ATR, X-ray diffraction (XRD), scanning electron microscopy (SEM), and energy dispersive X-ray fluorescence spectroscopy (EDX). The hydrophobicity of these surfaces is measured by contact angle studies. Corrosion protection behavior of these films for mild steel in 0.5 N HCl solutions was evaluated by potentiodynamic polarization (Tafel) and impedance studies (EIS). The result showed that Chitosan/SiO_2 film is superior in several respects to pure chitosan film particularly in its corrosion protection behavior, which can be correlated with its hydrophobic nature.

Introduction

Metals corrode, and this electrochemical process has a huge implication on their end-use and consequently, the economics of maintenance and repairs for industrial applications. The rate of metal corrosion is greatly influenced by substrate and surface chemistries as well

ISBN 978-93-5279-420-1

as some environmental influences, and by understanding these factors, adequate control methods can be employed to revert its degradation kinetics [1]. Chitosan (deacetylated chitin) obtained from the outer shell of crustaceans (crabs, lobsters, krills and shrimps). Chitosan primarily consists of β linked 2-amino-2-deoxy-β-D-glucopyranose units. Chitosan shows biocompatibility, low toxicity, biodegradability, osteoconductivity and antimicrobial properties. Modified chitosan are less susceptible to moisture and prevent the penetration of corrosive electrolyte species, providing good corrosion protection to the substrate [2,3]. In addition to its biodegradability and biocompatibility, this polymer can form various chemical bonds with transition metals and heavy metal components of composite materials and, thus, can enhance the stability of the nanoparticles [4]. Chitosan, a biowaste, can be used as an eco-friendly candidate for coating purposes because of its excellent film forming ability, low cost, biodegradability and non- toxic nature. Chitosan-silica hybrids were homogeneous transparent film-forming glassy materials that are compatible through a certain composition range [5].

Materials and Methods

Materials: The Chitosan (CS) with a degree of polymerisation 75-80% was obtained from Sigma Aldrich pvt.ltd (India).Tetra ethyl orthosilicate (Teos)(Otto), Acetic acid and all other reagents of Analar grade were used as such.

Methods of synthesis: SiO_2 nanoparticles were synthesized using Teos, acetic acid and water as per the procedure reported elsewhere [6]. Chitosan biopolymer (1gm) was dissolved in 1% acetic acid solution. The synthesized SiO_2 nanoparticles were dispersed in water and then magnetically stirred with the chitosan solution for about 8 hours. The Cs and Cs/SiO_2 films were made by drying 10 ml of the solution at 70^0C and neutralized using NaOH.

Preparation of chitosan coating on mild steel: Mild steel coupons were abraded with different grades of emery papers, degreased with acetone and finally washed with distilled water. Mild steel coupons were coated by the Cs and Cs/SiO_2 film by dip coating technique with a velocity of 15cm/sec. Then the coated substrates were dried in a fume hood for 12 hrs

Electrochemical measurements: EIS measurements and Tafel plots were carried out at room temperature in a three-electrode corrosion cell consisting of a saturated calomel reference electrode, a platinum counter electrode and chitosan coated steel coupons as the working electrode. 0.5 N HCl solution was used as the electrolyte. All measurements were carried out using Gill AC computer controlled electrochemical work station (ACM, U.K, model no: 1475)

Results and Discussion

FTIR-ATR: FTIR-ATR spectra of Cs and Cs/SiO_2 film are shown in Fig.1. Cs spectra show an intense and broad band between 3500 and 3150 cm^{-1}, associated with the axial stretching vibrations of the O-H and N-H bonds, a band at 2934cm^{-1}, corresponding to the symmetric or asymmetric C-H (of the pyranose ring) stretching vibration and bands centered at 1646 and 1548 cm^{-1}, assigned to the amide I and amide II vibrations, respectively, a band at 1057cm^{-1} corresponding to the C-O stretching vibration. All these bands are also present in the ATR spectra of Cs/SiO_2 film, but the intensity of the interaction between Si-O on silica and functional groups on chitosan decreases in the N-H region. Also the characteristic bands of

ISBN 978-93-5279-420-1

Chitosan (2934 cm^{-1}) and of silica (893 cm^{-1} and 647 cm^{-1}) retains in SiO_2–Chitosan nanocomposite film confirms the formation of the composite.

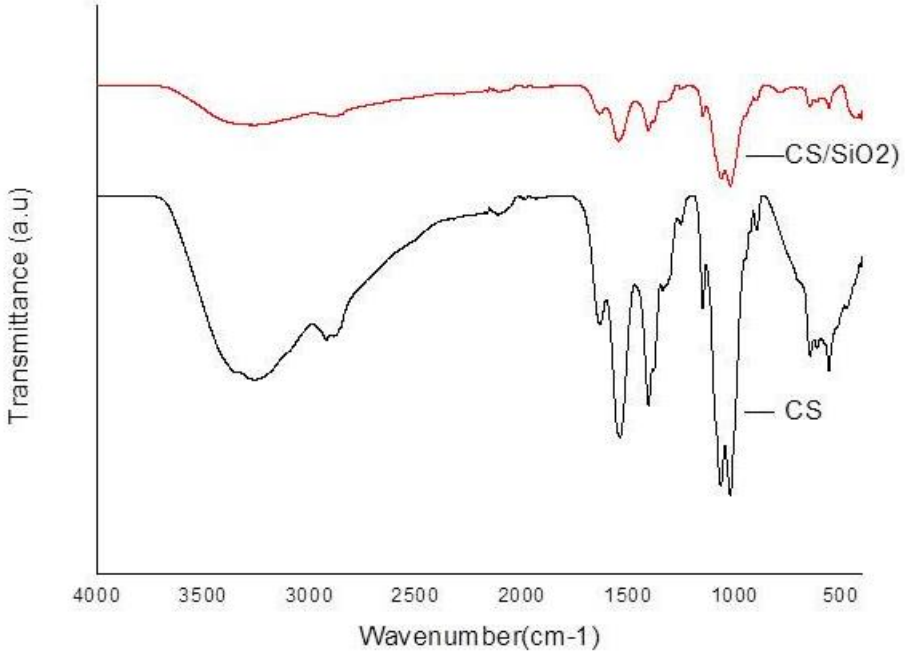

Fig.1. FTIR-ATR spectra of Cs and Cs/SiO_2 film

Surface wettability of the coated surface: In order to understand the water-film surface interaction, water contact angle of the Cs and Cs/SiO_2 film were measured which are shown in Fig.2. The highly hydrophilic chitosan possesses a contact angle of 89 which is due to the free –OH and –NH_2[7]. Upon loading SiO_2 to the chitosan matrix, water contact angle became 120^0, which indicates that the hydrophilic Cs film is modified to hydrophobic Cs/SiO_2 film.

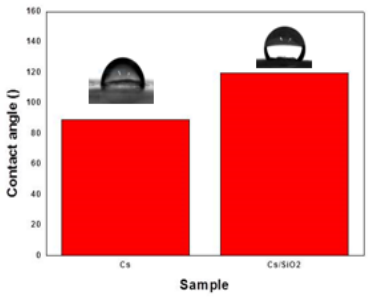

Fig 2. Water contact angles for Cs and Cs/SiO_2 film

SEM and EDX: Scanning microphotographs of the surfaces of pure Cs and Cs/SiO_2 composite film are shown in Fig.3a-c. Compared with the surface of pure CS membrane (Fig. 3b), the composite film possesses a network structure was attributed to the homogeneous dispersion of

ISBN 978-93-5279-420-1

SiO_2 nanoparticles within Cs (Fig. 3c) matrix. EDX spectrum (Fig.4) also proved the dispersion of SiO_2 into the Cs matrix.

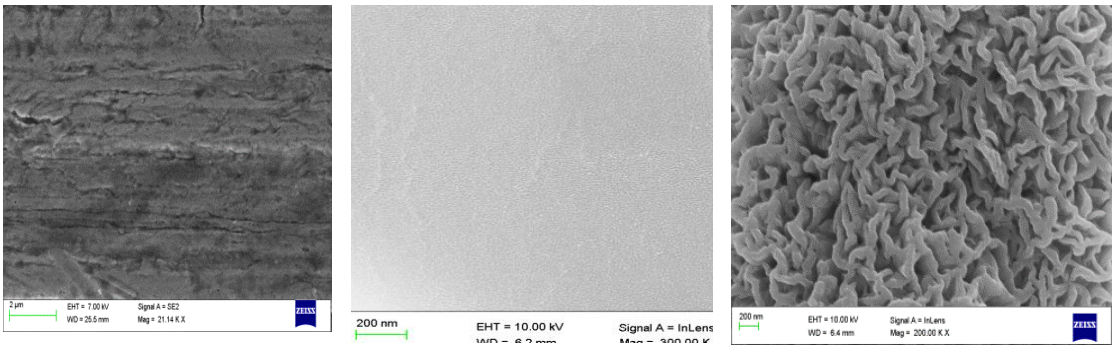

Fig.3. FESEM image of A) bare mild steel B) Cs C) Cs/SiO_2

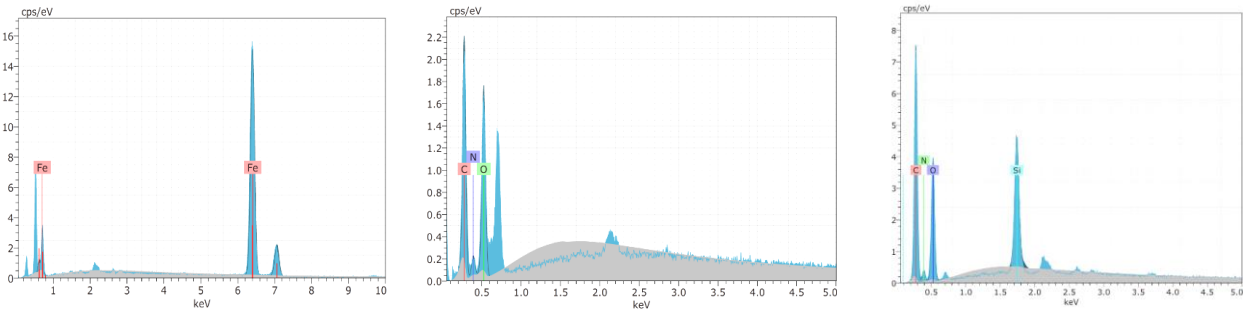

Fig 4. EDX spectra of A)bare mild steel B)Cs C) Cs/SiO_2

Potentiodynamic polarization studies

The tafel plots obtained from PDP studies shown in Fig.5 suggested that Cs/SiO_2 hydrophobic film has the lowest corrosion current and corrosion rate. The various electrochemical parameters obtained by Tafel extrapolation method are tabulated in Table.1.the inhibition efficiency can be calculated using the relation

$$IE = \frac{I_{corr} - I^*_{corr}}{I_{corr}} \qquad (1)$$

where I_{corr} and I^*_{corr} are the corrosion current densities of blank and coated mild steel.

ISBN 978-93-5279-420-1

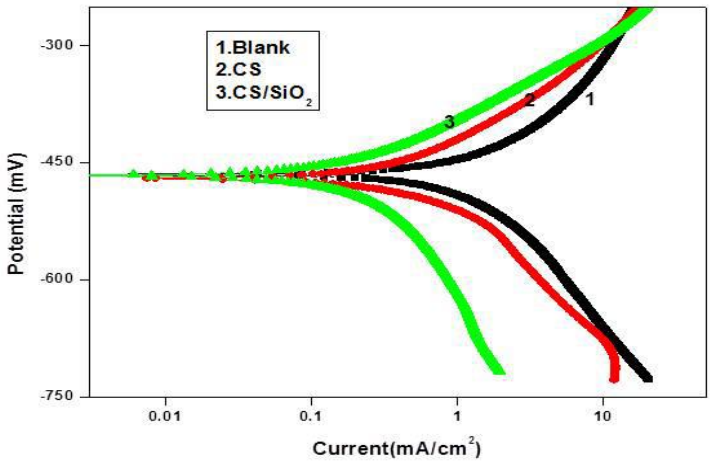

Fig. 5. Tafel plots for the mild steel, Cs and Cs/SiO_2

Table.1. **Different electrochemical parameters obtained by Tafel extrapolation in 0.5N HCl**

Sample name	$E_{corr}(mV)$	$I_{corr}(mA/cm^2)$	$\beta_a(mV/dec)$	$\beta_c(mV/dec)$	*IE %*
Blank	-462.5	1.2903	133.89	223.01	
CS	-469.8	0.4730	136.09	118.13	63.3
CS/SiO_2	-465.4	0.2588	113.3	244.69	80.0

Electrochemical impedance studies

Corrosion Inhibition efficiency was calculated from impedance measurements as

$$IE = \frac{R_{ct}^{*} - R_{ct}}{R_{ct}^{*}} \qquad (2)$$

where R_{Ct} and R_{Ct}^{*} represents the charge transfer resistance for the bare and coated mild steel samples. From the nyquist plot fig.6 and from table 2 the R_{ct} value of Cs/SiO_2 film is higher compared to pure Cs which confirms the better inhibition efficiency of the modified nanocomposite film.

ISBN 978-93-5279-420-1

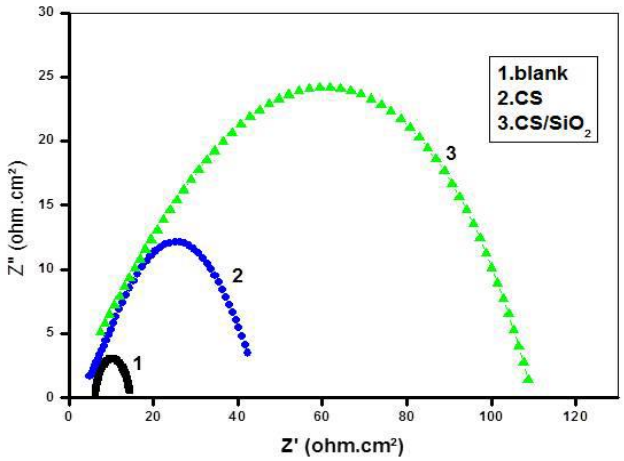

Fig.6. Nyquist plots for mild steel, Cs and Cs/SiO_2

Table 2. **Different electrochemical parameters obtained by EIS measurements in 0.5N HCl**

Sample name	*R_s(Ωcm²)*	*R_{ct}(Ωcm²)*	*Cdl(μF/cm²)*	*Corrosion Rate(mm/yr)*	*IE %*
Blank	6.25	8.41	737	35.94	
CS	4.16	40.99	438	7.37	79.5
CS/SiO_2	3.10	109.6	384	2.75	92.3

Conclusions

New Chitosan based anticorrosion film was developed with the addition of SiO_2 as filler via sol gel method. Electrochemical parameters obtained by Tafel polarization and impedance studies in 0.5N HCl showed that deposited hitosan/SiO_2 film significantly improved the corrosion resistance of mild steel. The corrosion protection performance by Chitosan/SiO_2 nanocomposite film could be due to its hydrophobic nature.

References

1. Saviour A. Umorena, Ubong M. Eduokb, Carbohydrate Polymers, 2016, 314-341.
2. Eram Sharmin, Sharif Ahmad and Fahmina Zafar, Renewable Resources in Corrosion Resistance.
3. Hui-Chia Yang, Wen-Hong Wang, Kuo-Shien Huang b, Min-Hsiung Hon, Carbohydrate Polymers, 2010, 176-179.
4. A. El. Shafei, A. Abou-Okeil, Carbohydrate Polymers, 2011, 920-925.
5. Retuert, J.; Nu~nez, A.; Martı´nez, F.; Yazdani-Pedram, Macro. Rapid Comm. 1997, 18, 163.
6. A. ELSAGH, E-Journal of Chemistry, 2012, 659-668.

ISBN 978-93-5279-420-1

7. Eman M. Fayyad, Kishor Kumar Sadasivuni, Deepalekshmi Ponnamma, Mariam Al Ali Al-Maadeed, Carbohydrate Polymers 151 (2016) 871–878.

SYNTHESIS AND CHARACTERIZATION OF COPPER AND ZINC COMPLEXES OF ACYLHYDRAZONE

Vineetha M C* and Asha P A

Department of Chemistry, Sree Kerala Varma College, Thrissur, Kerala

**E-mail:vineethamc85@gmail.com*

Abstract: Copper(II) and zinc(II) complexes have been synthesized by the reaction of copper acetate and zinc acetate with 3,5-dichloro-2-hydroxybenzaldehyde benzoylhydrazone and characterized by analytical and spectral studies**.**

Keywords: Cu^{II} complexes; Zn^{II} complexes, 3,5-dichloro-2-hydroxybenzaldehyde benzoylhydrazone.

Introduction

Coordination chemistry, the chemistry of metal complexes, is one of the most active areas of research in inorganic chemistry. The field of coordination chemistry has been explored. The importance of coordination complexes is increasing due to their complex structures and interesting magnetic, electronic and optical properties. Coordination complexes show diversity in structures depending on the metal ion, its coordination number and the denticity of the ligands used and therefore, the selection of ligand is crucial in determining the properties and structures of coordination compounds and their biological and medical applications.

Metal complexes of hydrazones have been found to have biological and therapeutic activity. Many hydrazone derivatives have been found to possess anti-inflammatory activities [1]. The biological results revealed that some of the hydrazones have prominent anti-convulsant activity. [2,3]. Recently Affan *et al*. have reported the cytotoxicity and anti-termitic property of thiophene-2-carboxaldehyde benzhydrazone and its tin complexes[4]. Metwally et al. (2006) synthesized a new series of hydrazones and evaluated. 6-Chloro-2-(4-methoxyphenyl) quinoline-4-carboxylicacid(4nitrobenzylidene)- hydrazide was found to be most potent against *Staphylococcus aureus, Escherichia coli and Candida albicans.* Hydrazone complexes show catalytic activity in various organic reactions [5]. Many Zn^{2+} fluorescent sensors have been reported, exhibiting high selectivity and sensitivity over other biologically essential metal ions in specific ranges of concentration [6,7].

Here we report the syntheses and spectral characterization of coppe and zinc complexes of 3,5-dichloro-2-hydroxy benzaldehyde benzoylhydrazone (H_2DHB). Structure of the hydrazone is shown in Fig. 1.

ISBN 978-93-5279-420-1

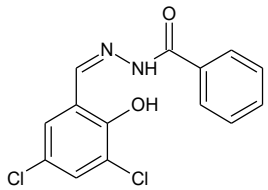

Fig. 1. Structure of the hydrazone

Experimental

Synthesis of copper complexes: To a solution of 3,5-dichloro-2-hydroxy benzaldehyde benzoic hydrazone, H_2DHB (1 mmol, 0.287 g) in methanol, $Cu(CH_3COO)_2 \cdot 4H2O$ (0.199 g, 1 mmol) was added. The brown solution was refluxed for 3 hours and green product was separated out was filtered, washed with methanol and dried in vacuo.

Synthesis of zinc complexes: Methanolic solution of nickel(II) acetate (0.219 g ,1 mmol) was added to a stirred mixture of H_2DHB(0.287 g, 1 mmol) in methanol. The resultant yellow solution was refluxed for 3 hours and product separated out was filtered, washed with methanol and dried in vacuum.

Results and Discussion

Copper and zinc complexes were characterized by elemental analysis, IR and electronic spectra. All the four complexes are coloured and soluble in DMF. The results of elemental analysis (Table 1) show that the complexes have the molecular formulas [Cu(DHB)H_2O] and [Zn(DHB)H_2O].

Table 1. ***Elemental analysis***

Compound	*Colour*	*Elemental Anal. Found (Calcd) %*		
		C	*N*	*H*
[Cu(DHB)H_2O]	Black	42.66 (43.26)	7.71(7.21)	3.19 (2.59)
[Zn(DHB)H_2O]	Shiny green	43.65 (43.05)	7.67(7.17)	3.00(2.58)

Infrared spectra: IR spectra in the range 4000-50 cm^{-1} were recorded for complexes and assignments were done in comparison with that of the respective free ligand**.** The selected IR bands of the hydrazone and complexes are represented in Table 2.

Table 2. ***IR spectral data of the hydrazones and their copper(II) and zinc(II) complexes***.

Compound	*ν(C=O)*	*ν(N–H)*	*ν(C=N)*	*ν(C=N)*	*ν(C–O)*	*ν(N–N)*	*ν(O–H)*
H_2DHB	1680	3065	1575	---	---	---	---
[Cu(DHB)H_2O]			1500	1600	1370	1131	3395
[Zn(DHB)H_2O]	----	----	1505	1595	1357	1143	3223

ISBN 978-93-5279-420-1

A comparison of the IR spectra of ligands and the metal complexes showed that significant variations have occurred in the characteristic frequencies upon complexation.

IR spectral analysis of the ligand (Fig. 2) confirms the presence of characteristic groups present in the compound. Strong bands due to the ν(N–H) and ν(C=O) modes at 3065 and 1680 cm^{-1} are observed in the spectrum which suggest that the hydrazone exists in the amido form in the solid state [8, 9]. A prominent band at 1575 cm^{-1} due to azomethine ν(C=N) linkage is observed in the spectrum indicating that condensation between ketone moiety of carbonyl compound and that of the hydrazide has taken place resulting into the formation of the desired ligand .

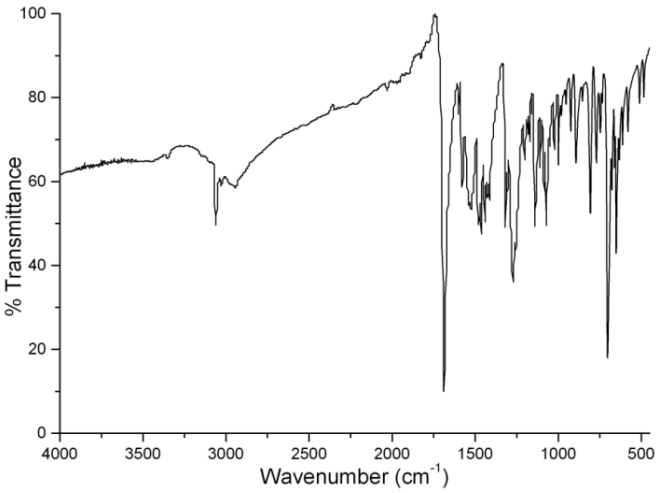

Fig. 2. IR spectrum of H_2DHB

A comparison of the IR spectra of ligand and copper complex shows that significant variations have occurred in the characteristic frequencies upon complexation. In this complex, it was found that the characteristic spectral bands for ν(N–H) and ν(C=O) stretches of the hydrazone appearing at 3065 cm-1 and 1680 cm^{-1} respectively disappear on complexation, which supports the coordination via enolate form instead of amido form, formed during tautomerization process [10, 11]. A new band appears at 1370 cm^{-1} due to the coordination of the ν(C–O) enolic mode [12]. The strong absorption band at 1575 cm^{-1} ascribed to the imine stretching frequency of the uncoordinated ligand, shifts towards lower frequency on complexation with the metal, suggesting coordination to the metal through imine nitrogen [13, 14]. On complexation a new band appeared at 1600 cm^{-1} due to ν(C=N) [15, 16].

ISBN 978-93-5279-420-1

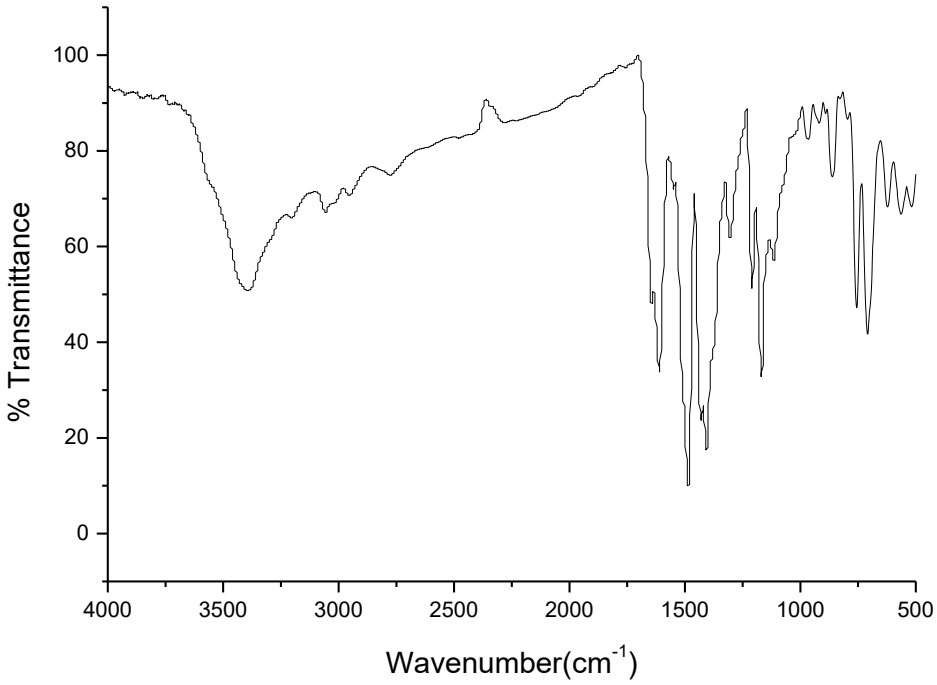

Fig. 3. IR spectrum of the copper complex

In the IR spectrum of zinc complex (Fig. 4), the bands at 3065 and 1680 cm^{-1} are absent, which indicate the coordination is via enolate form of the ligand. The azomethine band appears at 1505 cm^{-1}. On complexation a new band appeared at 1595 cm^{-1}. A band at 1357 cm^{-1} indicates the coordination of C–O group. ν(N–N) stretching appears at 1143 cm^{-1}. The IR spectrum exhibits a strong peak at 3223 cm^{-1}, which indicates the presence of coordinated water molecule.

ISBN 978-93-5279-420-1

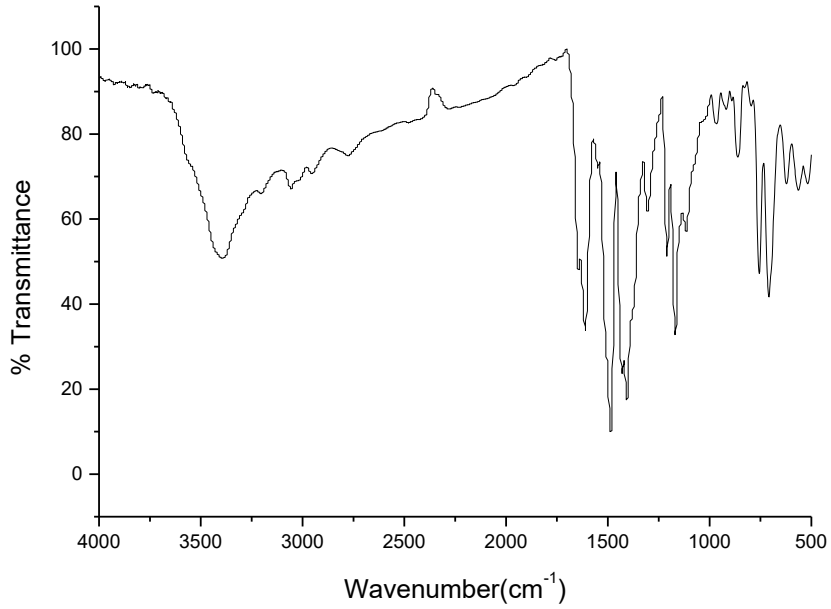

Fig. 4. IR spectrum of the zinc complex

Electronic spectra: The electronic spectra of prepared hydrazones were taken in DMF (Fig. 5). Important bands observed are listed in Table 3. Bands in the range 30070-33400 correspond to π-π* and n-π* transitions of the hydrazones.

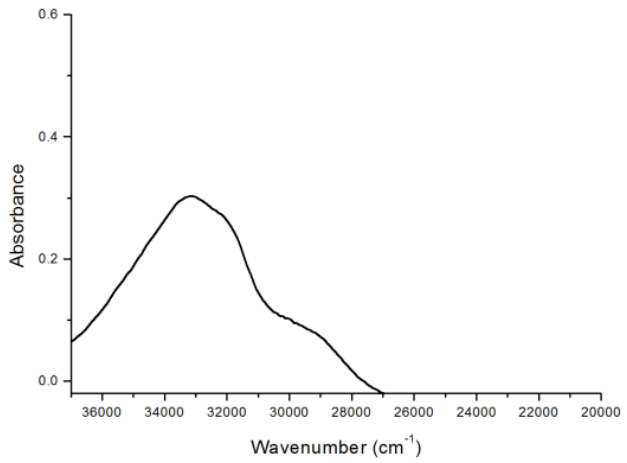

Fig. 5. Electronic spectrum of ligand

The electronic absorption bands of the complexes were recorded in DMF. The electronic transitions found in free ligands were slightly shifted on complexation. The presence of broad band in the complex in the range 14850 cm^{-1} can be assigned to d-d transition. The bands observed in the region 24540,24900 cm^{-1} are mainly due to the charge transfer transitions. The remaining bands correspond to the intraligand transitions (Fig. 6&7).

Table 3. ***Electronic spectral assignments (cm^{-1}) of Cu(II) and Zn(II) complexes***

ISBN 978-93-5279-420-1

Compound	*Intraligand transitions*	*LMCT/MLCT*	*d-d*
H_2DHB	33400, 32200, 30000		
[Cu(DHB)H_2O]	35500	24540	14850
[Zn(DHB)H_2O]	31500, 36600	24900	-----

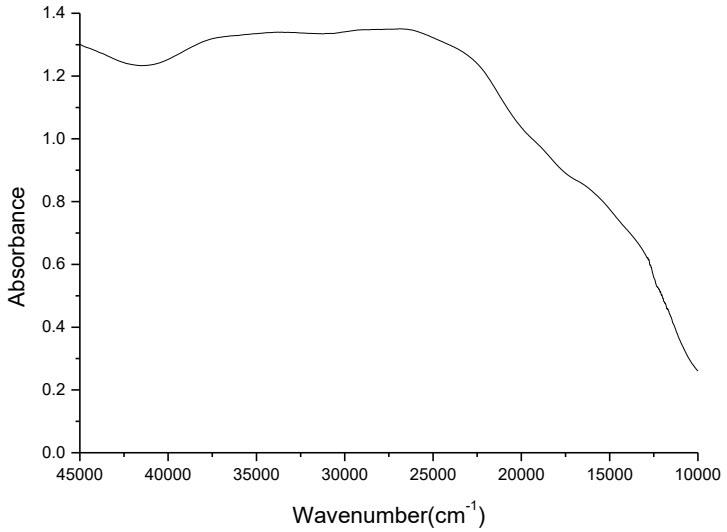

Fig. 6. Electronic spectrum of the copper complex

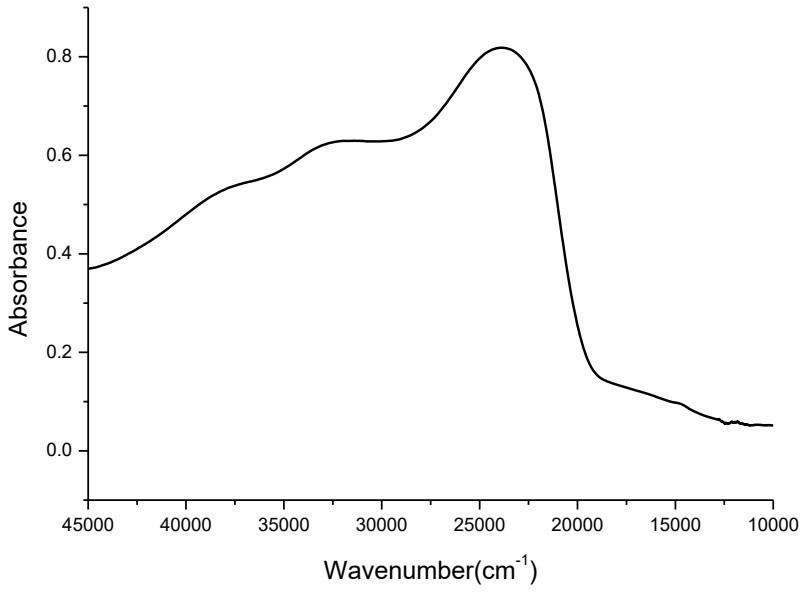

Fig. 7. Electronic spectrum of the zinc complex

Conclusions

ISBN 978-93-5279-420-1

The thesis deals with the synthesis and characterization of copper and zinc complexes of 3,5-dichloro-2-hydroxybenzaldehyde benzhydrazone. The thesis is divided into three chapters. First chapter includes introduction, tautomerism, coordination modes and importance of acylhydrazones. It also includes the scope of the work. Chapter 2 deals with preparation of ligand and its copper and zinc complexes. Also it contains different physicochemical techniques. The ligand acts as a tridentate ligand.

The elemental analyses clearly show that the complexes have the empirical formula [Cu(DHB)H_2O]and [Zn(DHB)H_2O] , where DHB stands for deprotonated ligand. These complexes are characterized by IR and UV-visible measurements.

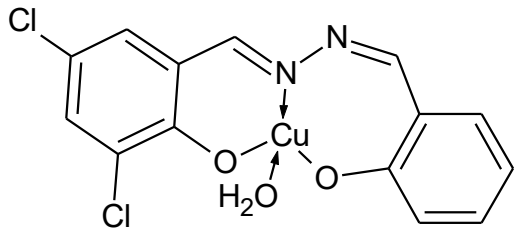

Proposed structure for the copper complex; [Cu(DHB)H_2O]

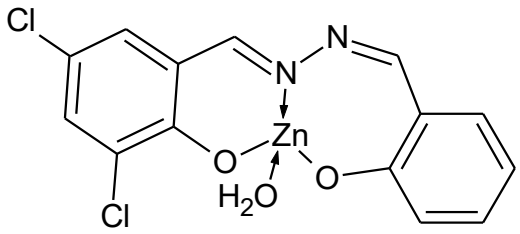

Proposed structure for the zinc complex; [Zn(DHB)H_2O]

References

1. A.R. Todeschini, A.L. Miranda, C.M. Silva, and S.C. Parrini, Eur. J. Med. Chem., 33.(1998) 189.
2. S. Rollas, and S. Gunizkucukguzel, "Biological Activities of Hydrazone Derivatives," Molecules, 12 (2007) 1910.
3. S.K. Sridhar, S.N. Pandeyta, J.P. Stables, and A. Ramesh, Eur. J. Pharm. Sci.,16, (2009) 129.
4. Md.A. Affin, S.W. Foo, I. Jusoh, S. Hanapi. And E.R.T. Tiekink, Inorg. Chim. Acta, vol. 362 (2009) 5031.
5. G.S. Vasilikiotis, Microchem. J.,13 (1968) 526.
6. C.J. Chang, E.M. Nolan, J. Jaworski, S.C. Burdette, M. Sheng, and S.J. Lippard, Chem. Biol., 11 (2004) 203.

ISBN 978-93-5279-420-1

7. A. Ajayaghosh, P. Carol, and S. Sreejith, J. Am. Chem. Soc. 127 (2005). 14962.
8. K. Nakamoto, Infrared and Raman spectra of Inorganic and Coordination Compounds, 5th ed., Wiley, New York, 1997.
9. N. Mathew, M. Kuriakose, E.B. Seena, and M.R.P. Kurup, Acta. Cryst. E,. 63 (2007)2190.
10. T. Ghosh, Trans. Met. Chem. 31 (2006) 560.
11. M.F. Iskander, T.E. Khalil, R. Werer, W. Haase, I. Svoboda, H. Fuess, Polyhedron 19 (2000) 949.
12. R.C. Maurya, S. Rajput, J. Mol. Struct. 833 (2007) 133.
13. P. Noblia, E.J. Baran, L. Otero, P. Draper, H. Cerecetto, M. Gonzalez, O.E. Piro, E.E Castellano, T. Inohara, Y. Adachi, H. Sakurai, D. Gambino, Eur. J. Inorg. Chem (2004) 322.
14. H. Yin, Acta Cryst. C 64 (2008) 324.
15. N.A. Mangalam, M.R.P. Kurup, Spectrochim. Acta Part A 71 (2009) 2040.
16. J. Chakraborty, S. Thakurta, G. Pilet, D. Luneau, S. Mitra, Polyhedron 28 (2009) 819.

ISBN 978-93-5279-420-1

CORROSION INHIBITION OF MILD STEEL IN SULPHURIC ACID SOLUTION BY THE EXTRACT OF *Lawsonia inermis*

Suhada K M

PG Department of Chemistry, KAHM Unity Women's College, Manjeri-676122, Kerala

E-mail: kmsuhada591989@gmail.com

Abstract: The corrosion behaviour of mild steel in H_2SO_4 solution in the absence and presence of ***Lawsonia inermis*** extract was investigated using weight loss measurement. It was found that, the inhibition efficiency of the extract depends on their concentration. The inhibitive action of this extract was discussed in terms of blocking the electrode surface by adsorption of the components through the active centres contained in their structure.

Introduction

Corrosion is a natural process, defined as the deterioration of a material that results from a chemical or electrochemical reaction with its environment, *ie*. , it converts a refined metal to a more chemically stable form, such as its oxide, hydroxide or sulphide. It is a gradual destruction of materials (usually metals), by chemical and other electrochemical reaction with their environment [1].

Many structural alloys corrode merely from exposure to moisture in air, but the process can be strongly affected by exposure to certain substances. Corrosion can be concentrated locally to form a pit or crack, or it can extent across a wide area more or less uniformly corroding the surface. Because corrosion is a diffusion-controlled process, it occurs on exposed surfaces [2].

Due to corrosion there are indirect costs associated with plant shut down, lower efficiency of equipments, contamination and over design, parts and labour to replace corroded equipments are often minor compared to the loss of production while the plant is nonoperational. Thus leaks in a pipelines and tanks result n loss of costly products and this leaks can also pose a serious environmental problems. Soluble corrosion products can contaminate a system and decontamination is costly. In the absence of adequate corrosion rate information over design is required to ensure reasonable service life. This leads to wastage of resources and for moving parts, greater power requirements.

Iron and its alloys exhibit high electrical and thermal conductivity, high formability, machinability and strength. Because of these favourable properties they are extensively used in a industrial fields.

The first step in effective corrosion control, however, is to have a thorough knowledge about the type of corrosion, the mechanism involved, how and why they occur. In virtually all situations, metal corrosion can be managed, slowed or even stopped by using the proper

ISBN 978-93-5279-420-1

techniques. Corrosion prevention can take a number of forms depending on the circumstances of the metal being corroded [3].

Corrosion inhibitors are either organic or inorganic chemicals that are added in small amounts (parts per million) to corrosive environment in order to delay or decrease the corrosion process of the substance to be protected. Due to the fact that equipment constructed with materials resistant to corrosion is very expensive, it is common to use corrosion inhibitors as a practical, economical and a simple alternative. The effectiveness of a corrosion inhibitor depends on fluid composition, quality of water and flow regime [4].

The term "green inhibitors" or "eco-friendly inhibitor" refers to the substances that have biocompatibility in nature. The inhibitors like plant extracts presumably possess biocompatibility due to their biological origin. Similar to the general classification of inhibitors, 'green inhibitors' can also be grouped into two categories, namely organic green inhibitors and inorganic green inhibitors [5].

Lawsonia inermis belonging to family *Lyrthaceae*, is a medium sized herb with many branches. The leaves, barks, roots and fruits are useful parts of henna plant. Henna has anti-bacterial, anti-fungal, aromatic and cooling properties. Lawsone is the active constituent of henna leaves, which is the main colouring constituent of henna obtained by degradation of hennosides A, B and C. Apart from having medicinal properties, water extracts of henna leaves powder were evaluated as corrosion inhibitors for steel and commercial aluminium in saline, acidic and alkaline medium.

Lawsonia inermis leaf have the components, gallic acid, 2-Hydroxy-1,4-naphthoquinone etc., which contains aromatic rings and high electron density. All this may make *Lawsonia inermis* leaf extract a good corrosion inhibitor.

Experimental

Inhibitor: *Lawsonia inermis* (henna) leaf extract.

Preparation: *Lawsonia inermis*'s leaves were dried under shade for several days. After the complete dehydration of leaves, it was crushed into very fine powder. A mixture of 10g Lawsonia inermis (henna) and 100ml ethanol was taken in a round bottomed flask and was refluxed at 100ºC for about 2-3 hours and filtered. The obtained filtrate was concentrated to 50 ml using a water bath. Varying the concentration of the extract, it was subjected to further corrosion studies.

Medium for corrosion: The medium for the study was 1N. H_2SO_4 prepared from reagent grade Sulphuric acid from E. Merk and distilled water.All the tests were done at room temperature and normal atmospheric pressure.

Results and Discussion

Weight loss and corrosion rate: The weight loss experiments were carried out under total immersion conditions in test solutions maintained at room temperature. Iron specimens (mild steel) of required dimensions are initially rubbed with different grades of emery papers. The experiments were carried out in 100 ml beaker containing the solutions. The metal coupons with freshly prepared surfaces were then fully immersed in a corrodent. 1N H_2SO_4 and 0.5 N

ISBN 978-93-5279-420-1

H_2SO_4 inhibitor for 24 hr, 48 hr and 72 hr. All solutions were opened to air. After the exposure period, the specimens were removed , washed initially under running tap water to remove the loosely adhering corrosion products. Then is dried and weighed. From the weight loss each experiment, corrosion rate was calculated in millimetre per year (mm yr^{-1}). The mean corrosion rate (CR) and inhibition efficiency (IE) were calculated from the following equation,

$$CR = \frac{87.6 \times W_i}{D\ A\ T} \text{ in mm/yr} \quad \text{or} \quad CR = \frac{534X\ W_i}{D\ A\ T} \text{ in miles/yr}$$

Where, CR= Corrosion rate, Wi = Weight loss in milligram, D = Density of the metal in g/cm^3 (iron = 7.86), A = Area of metal coupon, T = Time in hours.

The inhibition efficiency values are calculated as follows

$$IE = \frac{W_b - W_i}{W_b} \times 100$$

Wb = Weight loss in blank; Wi = Weight loss in presence of inhibitor.

The result indicated that the introduction of *Lawsonia inermis* leaf extract into the corrosive medium causes a significant reduction in the corrosion of iron. The corrosion inhibition efficiency increased with a corresponding increase in the concentration of the inhibitor. This may have resulted due to the sufficient adsorption and wider coverage by the inhibitor molecule. The calculated values of corrosion rate of mild steel in the corrodent medium were reduced on addition of different concentrations of the inhibitor. It has also been observed that the weight loss increases as the time of exposure increased. It was noted that the Corrosion Rate increases with increase in acid concentration. Results are given in the Tables 1-6.

Table 1. ***Corrosion rate and inhibition efficiency of mild steel in 1N H_2SO_4 at different concentration of Lawsonia inermis leaf extract for 24 hours***

Concentration of the inhibitor (ml)	*Weight of metal before immersion (g)*	*Weight of metal after immersion (g)*	*Weight loss (g)*	*Inhibition efficiency (%)*	*Corrosion rate*
Blank	3.378	2.447	0.931		0.731
1	2.457	2.345	0.112	87.97	0.0880
2	3.424	3.371	0.053	94.31	0.0416
3	3.648	3.596	0.052	94.41	0.0408
5	3.592	3.532	0.060	93.55	0.0471

ISBN 978-93-5279-420-1

Table 2. ***Weight loss of mild steel in different concentrations of H_2SO_4 for 24 hours***

Concentration of acid (N)	*Weight of metal before immersion (g)*	*Weight of metal after immersion (g)*	*Weight loss (g)*	*Corrosion rate*
0.5N	3.522	2.929	0.593	0.4659
1N	3.378	2.447	0.931	0.731

Table 3. ***Corrosion rate and inhibition efficiency of mild steel in 1N H_2SO_4 at different concentrations of Lawsonia inermis leaf extract for 48 hours***

Concentration of the inhibitor (ml)	*Weight of metal before immersion (g)*	*Weight of metal after immersion (g)*	*Weight loss (g)*	*Inhibition efficiency (%)*	*Corrosion rate*
Blank	2.507	0.449	2.058		0.8085
1	3.468	2.852	0.616	70.07	0.2420
2	2.152	1.875	0.277	86.54	0.1088
3	3.441	3.087	0.354	82.80	0.1390
5	3.279	3.236	0.043	97.91	0.0168

Table 4. ***Weight loss of mild steel in different concentrations of H_2SO_4 for 48 hours***

Concentration of acid (N)	*Weight of metal before immersion (g)*	*Weight of metal after immersion (g)*	*Weight loss (g)*	*Corrosion rate*
0.5N	3.554	2.439	1.115	0.438
1N	2.507	0.449	2.058	0.808

Table 5. ***Corrosion rate and inhibition efficiency of mild steel in 1N H_2SO_4 at different concentrations of Lawsonia inermis leaf extract for 72 hours***

Concentration of the inhibitor (ml)	*Weight of Metal before immersion (g)*	*Weight of Metal after immersion (g)*	*Weight loss (g)*	*Inhibition efficiency (%)*	*Corrosion rate*
Blank	2.429	0.253	2.176		0.569
1	3.516	2.685	0.831	61.81	0.2176

ISBN 978-93-5279-420-1

2	2.331	2.160	0.171	92.14	0.0448
3	3.570	3.451	0.119	94.53	0.0312
4	3.358	3.304	0.054	97.52	0.0141

Table 6. ***Weight loss of mild steel in different concentrations of H_2SO_4 for 72 hours***

Concentration of acid (N)	*Weight of metal before immersion (g)*	*Weight of Metal after immersion(g)*	*Weightloss (g)*	*Corrosion rate*
0.5N	2.920	1.810	1.110	0.290
1 N	2.429	0.253	2.176	0.569

Conclusions

The following observations are drawn from the present project on co-ordination ability and corrosion inhibition measurements of *Lawsonia inermis* leaf extract derivatives. *Lawsonia inermis* leaf extract is acting as a ligand with Oxygen as the coordinating atom. The results of experimental investigations of the studies *Lawsonia inermis* leaf extract show that, It reduces the corrosion rate of mild steel in acid medium remarkably. The corrosion rate of mild steel reduces remarkably as the concentration of inhibitor increases. Inhibition efficiency of the studied inhibitor decreases with increasing the concentration of the corrodent, H_2SO_4. The study at different exposure time gives the result that the corrosion inhibition efficiency of the inhibitor decreases as exposure time increases.

References

1. Mars G Fontana, Corrosion Engineering, 3rd Edn., Mc Graw Hill Book Company, 1987.
2. Inemesit A, International Journal of Corrosion 2013, 301689.
3. D.A.Jones, “Principles and Prevention of Corrosion”, Prentice – Hall Inc., New Jersey, (1996), 9.5.
4. V.S.Sastri, “Corrosion Inhibitors: Principles and Applications”, John Wiley & Sons, West Sussex, (1998), P.25.
5. Krishnaveni etal. Acta Metallurgia Sinica vo.26 No.3, pp 321-27 2013.

ISBN 978-93-5279-420-1

CHARACTERISATION STUDIES ON POLYMORPHISM OF COMMERCIAL ASPIRIN TABLETS

Bijudas K* and Bashpa P

Department of Chemistry, N. S. S. College, Manjeri, Malappuram (Dt), Kerala, 676122

**E-mail: bijudask@gmail.com*

Abstract: Aspirin shows polymorphism and two polymorphic forms of aspirin were characterized. These forms are named as Form I and Form II. Various commercial aspirin tablets were collected, powdered and after proper clean up procedure, their melting points were determined to identify its polymorphic form. This was further confirmed by infra red spectral analysis. It was found that all the commercial drug samples under study belong to the polymorphic form II.

Key words: Aspirin; Polymorphism; melting point; infrared spectrum.

Introduction

Aspirin, also known as acetylsalicylic acid (ASA), is a medication used to treat pain, fever, and inflammation. Aspirin is one of the most widely used medications globally with an estimated 40,000 tonnes (50 to 120 billion pills) being consumed each year. It is on the World Health Organization's list of essential medicines, the most effective and safe medicines needed in a health system.

The synthesis of aspirin is an esterification reaction. Salicylic acid is treated with acetic anhydride, an acid derivative, causing a chemical reaction that turns salicylic acid's hydroxyl group into an ester group (R-OH → R-OCOCH$_3$). This process yields aspirin and acetic acid, which is considered as a byproduct of this reaction. Small amounts of sulfuric acid (and occasionally phosphoric acid) are almost always used as a catalyst.

ISBN 978-93-5279-420-1

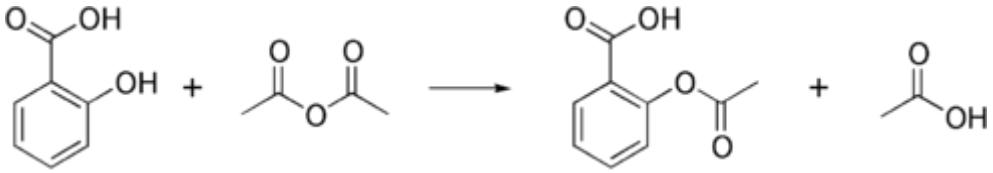

Aspirin shows polymorphism and two polymorphic forms of aspirin were characterized. These forms are named as Form I and Form II. Polymorph I was prepared by slow crystallization at room temperature from a saturated solution of commercial aspirin (U.S.P.) in 95 percent ethanol. The melting point was 143 ^{0}C to 144 ^{0}C, a value which is in agreement with the monoclinic crystal structure. Polymorph II was prepared by slow crystallization from a saturated solution of commercial aspirin (U.S.P.) in n-hexane at room temperature and melted at 123 to 125 ^{0}C. Both forms meet the U.S.P. specifications. X-ray diffraction (powder method) with nickel-filtered copper radiation and infrared spectra (Nujol mull) were used to characterize the two crystalline forms. Differences in x-ray diffraction patterns and in absorption spectra indicated different arrangements of aspirin molecules in the crystal lattice of each forms. There are lots of reports on the studies of polymorphism shown by aspirin tablets[1-8].

The extensive use of aspirin, the polymorphism shown by it and commercial preparation of these drugs by various pharmaceutical companies prompted us to carry out this work.

Experimental

Commercial aspirin tablets have been collected from various medical shops in and around Manjeri and listed below.

1. Ecosprin 75 (USV Limited, Bangalore)
2. Aspirin (Unicure India Limited, Noida)
3. Loprin 75 (Unichem Laboratories Limited, Mumbai)
4. ASA 50 (Cadila Healthcare Limited, Ahmedabad)

The collected drug samples were finely powdered and proper clean up procedure was carried out as in literature [9-10]. The dried samples were recrystallised and the melting point was determined by using a digital melting point apparatus. The obtained results were compared with the authentic values reported in literature.

The infra red spectrum of drug samples was recorded by Jasco FT-IR double beam spectrophotometer. The obtained infra red spectrum was analysed and peaks due to various functional groups were identified. Moreover the obtained spectrum was compared with the reported one in the literature.

Results and Discussion

The polymorphic study of commercial aspirin tablets was carried out by determining its melting point. The melting point determination is done in triplicate and all results are tabulated in Table 1.

ISBN 978-93-5279-420-1

Table 1. ***Melting points of various commercial aspirin samples***

Sl. No.	*Trade name*	*Manufactured by*	*Melting point (^0C)*
1.	**Ecosprin 75**	USV Limited, Bangalore	122± 2
2.	**Aspirin**	Unicure India Limited, Noida	125± 2
3.	**Loprin 75**	(Unichem Laboratories Limited, Mumbai)	123± 2
4.	**ASA**	Cadila Healthcare Limited, Ahmedabad	122± 2

All the aspirin tablets under investigation have melting point in the range 122-125 ^{0}C. This shows that all drug molecules belong to polymorphic form II.

The IR spectrum was recorded from KBr pellets using Jasco FT-IR 4100 spectrophotometer (Japan) and is shown in Fig. 1.

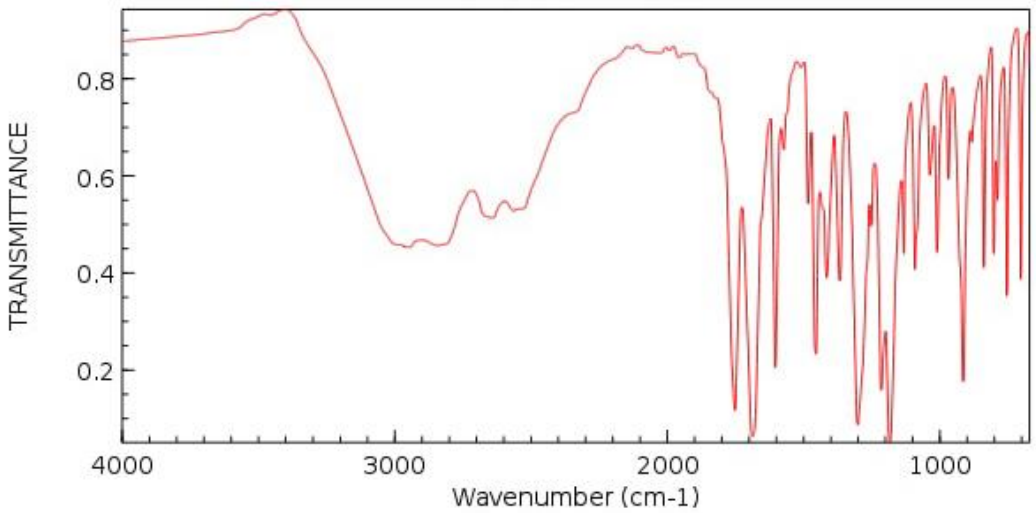

Fig. 1. IR spectrum of aspirin (ASA)

The IR spectrum gives the following information. It has three functional groups. A benzene ring (aromatic group), a carboxylic acid (COOH) group and an ester (R-C=O--O-R) group. In the IR spectrum a very broad peak at 3100 to 3200 cm^{-1} proves the presence of COOH group. A sharp peak at 3050 cm^{-1} indicates the presence of C-H stretching and a medium C=C peak at 1600 cm^{-1}. The peak at 1740 cm^{-1} shows the presence of C=O group stretching. Presence of all these peaks leads to the conclusion that the analyte is aspirin which was further proved on comparison the IR spectrum available in literature[11-12].

All the aspirin tablets under investigation have melting point in the range 122-125^0 C. This shows that all drug molecules belong to polymorphic form II. This can be further proved by various advanced analytical techniques like XRD, SEM, TEM etc.

ISBN 978-93-5279-420-1

Conclusions

Aspirin is the common analgesic and antipyretic drug used today. Various commercial aspirin drug samples were collected and their polymorphic form is determined by melting point determination. The results obtained clearly confirm that all the aspirin drugs under study belong to Form II polymorph. These drug samples were further analysed by infra red spectral analysis and can further be done by advanced techniques like NMR, XRD, SEM, TEM etc.

References

1. Llinas A, Goodman M J. *Drug Discovery Today,* 13, **2008**, 5&6.
2. Bond A D, Boese R, Desiraju G R. *Angewante Chemie Int. Edn*., 46, **2007**, 618.
3. Li T. *J. Pharm. Sci.,* 96, (**2007**) 755.
4. Bond A D, Solanko K A, Parons S, Redder S, Boese R. *Cryst. Engg. Commn*., 13, **2011**, 399.
5. Summers M P, Carless J E, Enever R P. *J. Pharm. Pharmacology,* 22(8), **1970**, 615.
6. Reilly A M, Tkatchenko A. *Phys. Rev. Lett.,* 113, **2014**, 55701.
7. Mulley B A, Rye R M, Shaw P. *J. Pharm. Pharmacology,* 23(11), **1971**, 902.
8. Upadhay P, Dantuluri A K, Kumar L, Bansal A K. *J. Pharm. Sci.*, 101(5), **2012,** 1843.
9. Perrin D D. Armarego WL, Perrin DR. *Purification of Organic Compounds*, Oxford, Pergamon Press, **1966.**
10. Vogel A I. *Text book of practical organic chemistry*, Longman, London, **1967.**
11. Vishweshwar P, McMahon J A, Oliviera M, Peterson M L, Zavorotkao M J. *J. Amer. Chem. Soc.,* 127(48), **2005,** 16802.
12. Bauer D J, Haussuhl E, Winkler B, Arbeck D. *Cryst. Growth Des.* 10(7), **2010**, 3132.

ISBN 978-93-5279-420-1

AUTOMATED IDENTIFICATION OF MEDICINAL PLANT LEAVES

Afsal K[1*], Sainul Abideen[2] and Haris Ummath[3]

[1]*Department of Computer Science, Malabar College of Advanced Studies, Vengara, Malappuram (DT), Kerala*

[2]*Department of Computer Science, Farook College, Calicut (DT), Kerala*

[3]*Department of Computer Science, KAHM Unity Women's College, Manjeri, Malappuram (DT), Kerala*

[*]*E-mail: afsalafsal@gmail.com*

Abstract: Identify or recognize a medical plant from a set of plants is a kind of task which needs high professionalism and expertise. Here we conduct a study and investigation about the various possibilities of automated identification of medicinal plants. Detecting or recognising the plant by the image of the leaf is actually a challenging task. We study and evaluate the present techniques used for plant identification. We also discuss relevant issues such as data collection, evaluation, benchmarking, etc. After analysing present methods we conclude with promising directions for the future.

Keywords- Leaf Identification; Pattern Recognition; Automated medicinal plant identification.

Introduction

ISBN 978-93-5279-420-1

Medicines are the second most essential requisite after food for mankind. For medicines, medicinal plants are the important sources of raw drugs. According to WHO report, over 80% of the world population relies on traditional medicine largely on plants based for their primary health care needs.

Identifying a medicinal plant and its medicinal value by looking at its leaves is actually a challenging task, which requires some specialised knowledge. Most of the people may be unfamiliar with the medicinal plants and hence they cannot identify most of the medicinal plants even if some of these plants are present in their near by localities. To manually recognise a medicinal plant from a set of plants, some may need a good amount and knowledge and experience.

An efficient automated system for medical plant identification will be very much useful for recognising the presence of medicinal plants. This may be very much helpful for botanical researchers, medical field, and even for those who study about plant taxonomy. This may even lead to the identification of new species of plants because any non- professionals can also start identify and classify the plants by taking the images of leaves, which in turn gives a wide reach.

Review of Literature

Leaf image recognition methods have recently received a good importance among the researchers of pattern recognition and computer vision. There are several methods proposed and many of them having high accuracy in the testing environment. But it is still have scope for more research and innovation as its having huge demand and most of the methods are not working accurately in the real world scenarios.

A. Geometric Features

Many of them are making use of the geometrical measurements. A major line of such work includes those measuring geometric features. For instance, Wu et al. [1] used aspect ratio, rectangularity and narrow factor as features, and employed Neural Network as the classifier. They achieved up to 90.3% recognition rate on a 10-species dataset. Pahalawatta et al. [2] used a different set of features – stem-to- blade ratio and compactness. A common downfall of these approaches is that the geometric features are difficult to be accurately extracted under imperfect measurements, and weighting between them is also problematic. Therefore, they cannot differentiate a large number of species.

B. Shape Description

Another line of work makes use of shape descriptors. Soderkvist [3] combined Curvature Scale Space, Fourier descriptor and Hu's moments in building a tree-structured classification system, and tested on the Swedish dataset including 15 species. Very recently, several researchers realized the unsuitability of using shape-matching for leaf image recognition, and proposed to use curvature histograms [4] and linear subspaces [5]. However, these methods either needed special treatment of leaf petiole or could not achieve good results.

C. Combination of Visual features

Several efforts have also been found using flowers [6] for plant recognition. Their method combined many visual features together, and was able to classify 102 categories with a recognition rate up to 72.8%.

ISBN 978-93-5279-420-1

Computer-Aided Plant Species Identification Technique (CAPSI) [7] method is proposed for fruit tree recognition using the chain code method. Based on the image matching technique of leaf shape, It identifies different biometric features like width factor, diameter, major axis, minor axis, area, perimeter and aspect ratio of the leaf image are extracted.

D. Statistical Parameters

Recognition by using statistical parameter [8] in leaf images, methodology achieved 93.75% accuracy. The three major phases are pre-processing, feature extraction and classification. Pre-processing highlights the relevant features as well as to reduce unwanted noise from the input image, which reduces the chance of getting optimal feature values. In feature extraction phase, different morphologic features such as mean, standard deviation, convex hull ratio, iso-perimetric quotient, eccentricity and entropy are extracted from the pre-processed leaf image.

Vijay Satti et.al [9] describes how features are extracted after pre-processing. The procedure involved are pre-processing, RGB to Gray scale and then Gray scale to binary followed by smoothing and filtering. Finally the colour shape and geometric features are extracted. The paper deals with the disease detection in paddy leaves by the approach of histogram processing mechanism. The original disease free leaf is stored in the database and whenever a disease affected leaf image is given as input to the system, it predicts the amount of disease infected in the leaf by analyzing the histogram.

Ji-Xiang Du et.al [10] proposed a new classification method called Move Median Centres (MMC) hyper sphere classifier. From the experimental results of this paper, the methodology save both storage space and reduces the classification time. From the above review of literature it is very clear that no effective methods were proposed for Ayurvedic plant species recognition and hence this proposed system addresses the Ayurvedic plant recognition

E. Other Methods

Abdul Kadir et.al [11] proposed a method to identify the plants and various features like texture, vein, shape and colour of the leaves are extracted. The vein feature is extracted using the morphological opening operation and probabilistic neural network is used for classification. The paper limits in achieving reliability with respect to color feature.

Principal Component Analysis Algorithms (PCA) and Gray Level Co-occurrence Matrix (GLCM) given 78 percentage accuracy in texture feature extraction in leafs, by the study conducted by Abdolvahab Ehsanirad et.al [12]

Another methodology proposed by A.J. Pérezet.al [13] used the colour and shape feature of leaf . It deals with different shape features like ratio of the major axis length squared to the area, first invariant central moment, major axis length, ratio of the perimeter squared to the area, minor axis relation, distance to the crop row are used to discriminate soil and weeds. K-Nearest Neighbor (KNN), bayes rule and heuristic approaches are used in classifying the leaf image. An accuracy of 89.7% is acquired from the proposed method.

Another interesting innovation in the field is identification of leafs using contour in leaves.[14] both leaf teeth and global structure of leaf is calculated in this method. The leaf is identified using hierarchical method in classification.

Kue-Bum Lee et.al [15] proposed a Methodology to extract the features of the leaf vein. This work is carried out by finding the contour of the leaf. Firstly by converting the colour

ISBN 978-93-5279-420-1

image into a gray scale and then to binary image and hence outline of the leaf is extracted. To extract the veins of the leaf, opening operation is done on the grayscale image and the difference in the final image and gray scale image is obtained to get the features extracted.

Sandeep Kumar E[16] proposed a system with devised methodology which gives the identification of medicinal plants based on its edge features. The colour image is converted to its gray scale equivalent image. From this gray scale image edge histogram is calculated. Canny edge detection algorithm is implemented in this work. The process includes the stages of Image acquisition, feature extraction and comparing the image with those images that are previously stored on the database and the area of leaf is determined by taking one Rupee coin's area as the reference, which is comparatively effective since the photograph taken may vary from person to person. This work is limited to detect only the mature leaves since the tender leaves changes slightly when it became mature.

Conclusions

We should develop a digital database of images of leaves to promote the researchers in the process of automated identification of plant leaves are as follows. It actually includes collection of digital images of plant leaves. Then we should focus on developing good algorithms to detect the leaf and its boundary from the image, which includes preprocessing. This preprocessing will eliminate the noise in the images. The Feature extraction needs to be performed. Researchers need to design and development methods for feature extraction based on neuro-fuzzy pattern recognition methods. A digital database of medicinal plant leaves will be very much helpful for the researchers for future use.

References

1. S. Wu, F. Bao, E.Y. Xu, Y.X. Wang, Y.F. Chang, Q.L. Xiang, A leaf recognition algorithm for plant classification using probabilistic neural network, IEEE Int. Symp. Signal Process. Inf. Technol. (2007) 11–16.
2. K.K. Pahalawatta, Plant Species Biometric Using Feature Hierarchies, Master thesis, University of Canterbury, 2008.
3. O.J. Soderkvist, Computer Vision Classification of Leaves From Swedish Trees, Master Thesis, Linkoping University, 2001.
4. N. Kumar, P.N. Belhumeur, A. Biswas, D.W. Jacobs, W.J. Kress, I. Lopez, J.V. B. Soares, Leafsnap: a computer vision system for automatic plant species identification, Eur. Conf. Comput. Vis. (2012) 502–516.
5. R. Hu, W. Jia, H. Ling, D. Huang, Multiscale distance matrix for fast plant leaf recognition, IEEE Trans. Image Process. 21 (11) (2012) 4667–4672.
6. M.E. Nilsback, A. Zisserman, Automated flower classification over a large number of classes, IEEE Conf. Comput. Vis. Pattern Recognit. (2008) 722–729.
7. Vijayashree, T. and Gopal, A., 2015. Classification of Tulsi Leaves Based on Texture Analysis.

ISBN 978-93-5279-420-1

8. Ayurvedic Plant Species Recognition using Statistical Parameters on Leaf Images. Pushpa BR, Anand C and Mithun Nambiar P. Department of Computer Science Amrita Vishwa Vidyapeetham, Mysuru Campus Amrita University, India.
9. Satti, V., Satya, A. and Sharma, S., 2013. An automatic leaf recognition system for plant identification using machine vision technology. International Journal of Engineering Science a nd Technology, 5(4), p.874.
10. Du, J.X., Wang, X.F. and Zhang, G.J., 2007. Leaf shape based plant species recognition. Applied mathematics and computation, 185(2), pp.883-893.
11. Kadir, A., Nugroho, L.E., Susanto, A. and Santosa, P.I., 2013. Leaf classification using shape, color, and texture features. arXiv preprint arXiv:1401.4447.
12. Ehsanirad, A. and Sharath Kumar, Y.H., 2010. Leaf recognition for plant classification using GLCM and PCA methods. Oriental Journal of Computer Science and Technology, 3(1), pp.31-36.
13. Perez, A.J., Lopez, F., Benlloch, J.V. and Christensen, S., 2000. Colour and shape analysis techniques for weed detection in cereal fields. Computers and electronics i n agriculture, 25(3), pp.197-212.
14. Im, C., Nishida, H. and Kunii, T.L., 1998, November. A Hierarchical Method of Recognizing Plant Species by Leaf Shapes. In MVA (pp. 158-161).
15. Lee, K.B. and Hong, K.S., 2013. An implementation of leaf recognition system using leaf vein and shape. International Journal of Bio-Science and Bio-Technology, 5(2), pp.57-66.
16. Kumar, S., 2012. E, "Leaf Color, Area and Edge features based approach for Identification of Indian Medicinal Plants". International Journal of Computer Science and Engineering, 3(3), pp.436- 442.

AN UNUSUAL SPECTRAL FEATURE OF CATIONIC NEAR INFRA-RED ABSORBING SQUARAINE DYES

M C Basheer

PG & Research Department of Chemistry, Pocker Sahib Memorial Orphanage College, Tirurangadi, Malappuram 676 306, Kerala

E-mail: basheermc80@gmail.com

Abstract: Two novel cationic squaraine dyes **CATSQ2** and **CATSQ3** have been synthesized and their spectral features in different solvents were investigated. These compounds show unusual spectral behavior in which they show sharp absorption around 800 nm regions in dichloromethane and chloroform whereas in acetonitrile and in protic solvents like methanol, ethanol n-butanol and isopropanol they show a broad and blue shifted absorption band. These compounds show dual fluorescence in non-protic solvents like acetonitrile, dichloromethane and chloroform where they show two emission maxima around 820 nm and 660 nm regions. In protic solvents, a fluorescence maximum around 660 nm region only observed. It has been noted that solvent polarity doesn't significantly influence quantum yield of fluorescence (Φ_f) of these compounds.

 ISBN 978-93-5279-420-1

Introduction

Squaraine dyes have attracted much attention because of their unusual electronic structures as well as their potential application in photogeneration materials in electrophotographic photoreceptors,[1] optoelectronic media,[2] and organic solar cells,[3] on account of their special properties such as photoconductivity and sharp and intense absorption in the visible or near-infrared (NIR) regions.[4] Commonly, squaraine dyes are 1, 3- or 1, 2-disubstituted squaric acid derivatives.[5] The use of squaraine dyes as molecular probes in biological applications has also attracted attention in recent years, due to the strong absorption and emission of these dyes in the near infrared (NIR) region.

Although a number of such dyes possessing strong absorption at wavelength greater than 600 nm regions are known, those possessing absorption in the region, 780-840 is limited. Recently, Nakazumi *et al*. [6] have reported the formation of a cationic squaraine dye (**CATSQ1**) which have an absorption maximum around in addition to the symmetrical dye bis- (3-methyl benzothiazole-2-ylidine) squaraine during the reaction of N-ethyl-2-methyl benzothiazolium iodide with squaric acid. This dye is found to be an extended □- electron system, whose two squaric acid substituents are stabilized by the formation of intramolecular H-bond which leads to an effective delocalization of □-electrons over the polymethine sub unit. These dyes exist in acid-base equilibrium in aqueous and other protic solvents. The pKa of this equilibrium in water-acetonitrile mixture was estimated as 4.9.[7] The absorption spectrum of the cationic squaraine dye in a water:acetonitrile mixture (4:1) was found to be highly sensitive to the presence of trace amounts of transition and lanthanide metal cations. On complexation with these metal cations, a new absorption band characteristic of the metal ion used is formed. The potential application of these type of cationic squaraine dyes for sensing trace amounts of transition metal ions like Hg^2, Pb^{2+}, Mn^{2+} and Zn^{2+} in aqueous solutions have been reported.[8] In the present study, I have been successful in synthesizing a new variety of cationic squaraine dyes (**CATSQ2** and **CATSQ3**) by the reaction of 1, 3-substituted symmetrical squaraine dyes with the semi squaric acid derivative, 1-(*p*-N, N-dioctyl aniline)-2-hydroxy-3, 4-dione in the presence of *p*-toluene sulphonic acid and sodium tetraphenyl borate. Moreover, we report the dual luminescence properties of **CATSQ2** and **CATSQ3,** in very low polar solvents like acetonitrile, dichloromethane and chloroform. Second emission of these dyes is attributed to the second excited state S_2 to the S_0 state.

Experimental

Materials

Bis-(3-methylbenzothiazole-2-ylidine)squaraine and bis-(3-methyl benzoselenazole-2-ylidine)squaraine were synthesized according to the very versatile procedure reported by Sprenger *et al*.[8] Squaric acid, 2-methylbenzothiazole and 2-methylbenzoselenazole were purchased from Aldrich and used as such without further purification. Other chemicals and reagents obtained from local chemical suppliers were used after purification. The cationic squaraine dyes **CATSQ2** and **CATSQ3** were synthesized according to the following procedure.

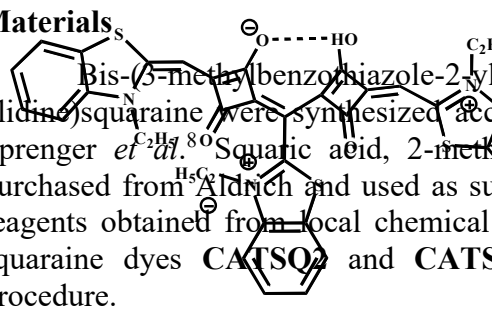

CATSQ1

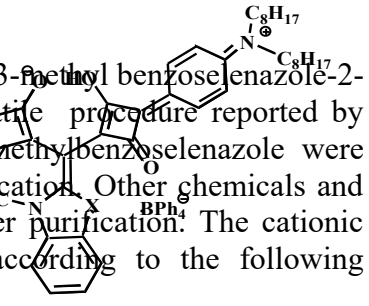

CATSQ2 X =Se
CATSQ3 X =S

ISBN 978-93-5279-420-1

Synthesis of CATSQ2

1-(*p*-N, N-dioctylaniline)-2-hydroxycyclobutene-3, 4-dione, (165 mg, 0.4 mmol) and *p*-toluene sulphonic acid (mol) were added to a mixture (1:2) of toluene and *n*- butanol (30 mL) and the solution was refluxed for 60 min at 110 ^{0}C. After cooling to room temperature, bis (3-methylbenzoselenazole-2-ylidine) squaraine (200 mg, 0.4 mmol) was added to the reaction mixture and further refluxed for 20 h at 110 ^{0}C, accompanied by azeotropic distillation of water using Dien-Stark condenser. The reaction mixture was cooled to room temperature and sodium tetraphenylborate (137 mg, 0.40 mmol) was added and the solution was stirred at 60°C for 3 h. This mixture was then concentrated to 1 mL by removing the solvent under reduced pressure. To this concentrated solution, excess hexane (20 mL) was added to precipitate out the product. The crude product was filtered and purified by column chromatography using neutral alumina as the stationary phase and a mixture (3:97) of methanol and chloroform as eluent to give 18 mg (3.6%) of the pure product. mp 230°C (decomp.).

IR ν_{max} (neat): 3394, 2360, 1605, 1268, 834 cm^{-1}. ^{1}H NMR (300 MHz, MeOD), ™ 0.88-1.1 (m, 6H, CH_3), 0.9-1.3 (m, 24H, CH_2), 3.1-3.9 (m, 10H, NCH_2, NCH_3), 6.1-8.1(m, 33H, aromatic) Anal. Calcd for $C_{48}H_{54}N_3O_4Se_2$: C,64.42; H, 6.08; N,4.7; Found: C,64.07; H, 6.43; N,4.46.

Synthesis of CATSQ3

The cationic squaraine dye **CATSQ3** is prepared in a similar manner to that of **CATSQ2**. Reaction of 1-(*p*-N, N-dioctylaniline)-2-hydroxycyclobutene-3, 4-dione, (217 mg, 0.52 mmol) and bis (3-methylbenzothiazole-2-ylidine) squaraine (200 mg, 0.52 mmol) after purification using column chromatography over neutral alumina as the stationary phase and a mixture (3:97) of methanol and chloroform as the eluent gave 50 mg (8.5%) of pure product, mp 175°C (decomp.).

IR ν_{max} (neat): 3415, 1590, 1263, 781 cm^{-1}; ^{1}H NMR (300 MHz, MeOD) ™ 0.88-1.1 (m, 6H, CH_3), 0.9-1.3 (m, 24H, CH_2), 3.1-3.9 (m, 10H, NCH_2, NCH_3), 6.1-8.1(m, 33H, aromatic). Anal. Calcd for $C_{48}H_{54}N_3O_4S_2$: C, 71.97; H, 6.79; N, 5.25; S, 8.01. Found: C, 71.59; H, 6.49; N, 5.42; S, 8.31. MW calcd for $C_{48}H_{54}N_3O_4S_2$ (M+H): 800.3556. Found: 800.3582 (High-resolution mass spectrometry, FAB).

General Techniques

All new compounds unambiguously characterized on the basis of analytical results and spectral data. All melting points are uncorrected and were determined on a Mel-Temp II melting point apparatus. ^{1}H NMR spectra were recorded on Bruker 300 MHz NMR spectrometer. IR spectra were recorded on a Nicolet Impact 400D Infrared Spectrophotometer. Mass spectra were measured on a Shimadzu 2401 or 3101PC Spectrophotometer. Elemental analyses were done using a Perkin-Elmer series II 2400 CHN Analyzer. Absorption spectra were recorded on a Shimadzu UV-3101 PC UV-Vis-NIR Scanning Spectrophotometer. Fluorescence spectra were recorded on SPECTRACQ spectrofluorimeter and corrected using the program supplied by the manufacturer. The fluorescence quantum yields were determined by the relative method using optically dilute solutions with Nile blue A perchlorate (Φ_f=0. 23 in ethanol) [9] and IR-125 (Φ_f =0.13 in DMSO) [10] as standards. Fluorescence lifetimes were measured using a Tsunami Spectra Physics Single Photon Counting System using LED as exciting source and decay data is further analyzed using IBH software library, which includes an iterative shift of the fitted function as a part of chi-squared goodness of the fit criterion.

ISBN 978-93-5279-420-1

Results and Discussion

Absorption and emission properties of **CATSQ2** and **CATSQ3** are summarized in Table 1. Fig. 1 shows absorption spectra of **CATSQ2** in different solvents. **CATSQ2** and **CATSQ3** show two or more than two absorption maxima in all solvents. Both the compounds show very sharp absorption at around 800-nm region in non-protic solvents like chloroform and dichloromethane. Whereas in acetonitrile and protic solvents like methanol, butanol and isopropanol absorption is extraordinarily blue shifted and broadened.

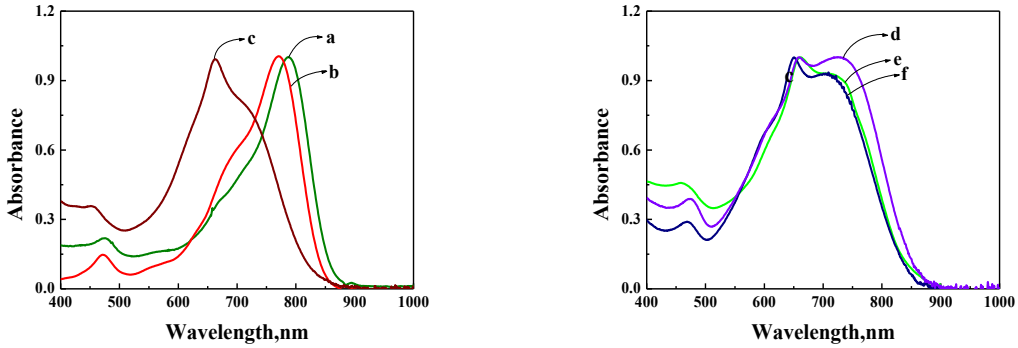

Fig 1. Absorption spectra of **CATSQ2** in a) Chloroform b) Dichloromethane c) Acetonitrile d) Isopropanol e) Butanol f) Methanol.

Table 1. ***Absorption and fluorescence data of CATSQ2 & CATSQ3 in different solvents***

Solvents	*CATSQ2*			*CATSQ3*		
	Abs. max ⌊max, nm	*Em. max ⌊max, nm*	*√f x 10²*	*Abs. max ⌊max, nm*	*Em. max ⌊max, nm*	*√f x 10²*
Chloroform	786	662 823	5 1	792	673 833	1.2 12
Dichloromethane	771	654 824	3 16	773	672 824	1.9 14.6
n-Butanol	660	667	1.8	656	663	3.8
Isopropanol	658	666	1.7	656	663	2.6
Acetonitrile	662	675 821	2 9	662	671 819	0.8 1.5
Methanol	650	662	1.2	650	653	1

It can be seen that both the dyes (**CATSQ2** and **CATSQ3)** show dual luminescence in less polar solvents like acetonitrile, chloroform and dichloromethane, in which they fluoresce around two distinct peaks around 820 nm and 660 nm regions, which is not reported hitherto.

ISBN 978-93-5279-420-1

They show only single hypsochromic fluorescence around 660-nm region in protic solvents like methanol, isopropanol and butanol as depicted in Fig. 2.

It is noted that solvent polarity doesn't significantly influence Φ_f of these compounds. (Table1). Slight increase in Φ_f of **CATSQ 2** in butanol among protic solvents and for dichloromethane among non-protic solvents was observed. **CATSQ 3** shows same changes akin to **CATSQ 2**.

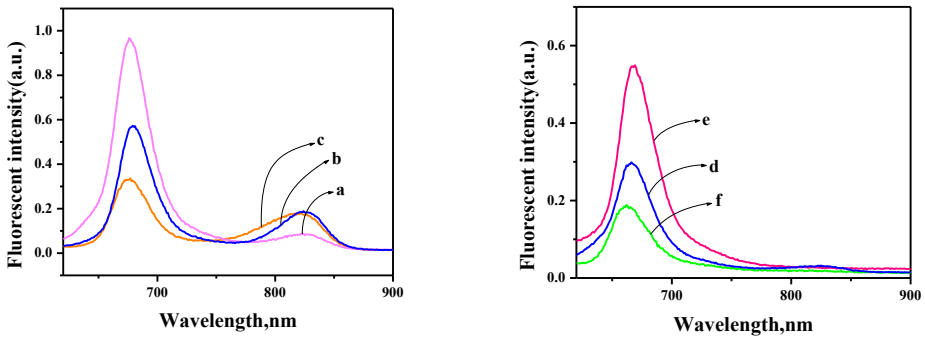

Fig. 2. Emission spectra of **CATSQ2** in a) Chloroform b) Dichloromethane c) Acetonitrile d) Isopropanol e) butanol f) Methanol.

One of the proposed reasons for unusual absorption changes in different solvents is due to the existence of two different conformations of the dyes, a fully conjugated planar state and a half conjugated twisted form in which one of the fluorophore is twisted out of the plane (Fig. 3). In non-polar solvents like chloroform and dichloromethane these dyes exist in fully delocalized planar state (Fig. 3a) due to the intramolecular hydrogen bonding between two squarate moieties as reported by Nakazumi[6]. So conjugation extends through out the molecule, correspondingly longer wavelength absorption maxima observed. In protic solvents like methanol, butanol and isopropanol, due to intermolecular hydrogen bonding, the intramolecular hydrogen bonding between squarate moieties break and a twisted structure is favored (Fig. 3b). In this confuguration there is lesser conjugation throughout the molecule compared to the other planar confuguration since the conjugation is extended only through two benzoselenazole moieties and hence a blue shifted absorption is observed.

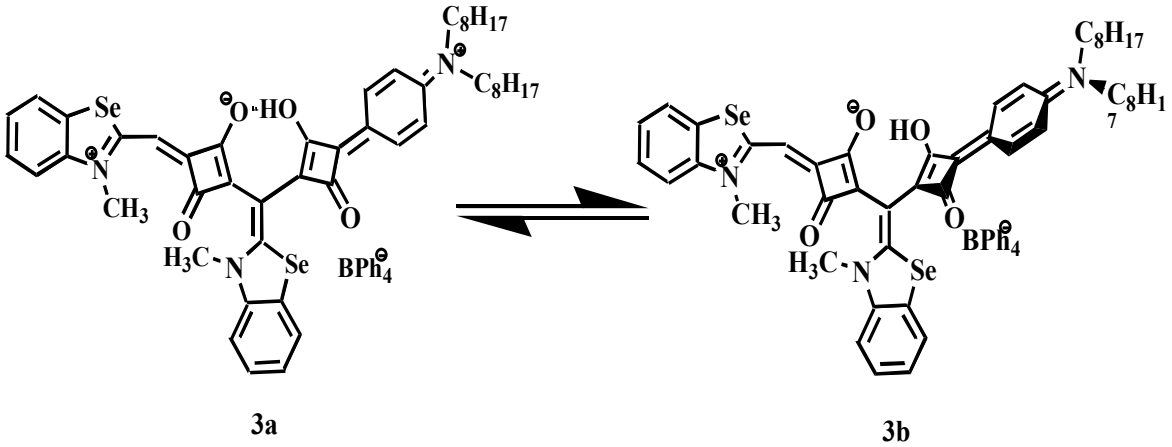

ISBN 978-93-5279-420-1

Fig 3. Conformation changes of **CATSQ2** in a) non-protic solvents b) protic solvents

Fig. 4 depicts changes in absorption and emission properties in different ratio of chloroform/methanol. It was found that as the ratio of methanol to chloroform increases, longer wavelength absorption hypsochromically shifted. This spectral shift suggests that planarity of the compound disturbed as the ratio of hydrogen bonding solvent increases. Also dual emission observed in chloroform disappeared slowly and fluorescence at shorter wavelength region only observed. This suggests that **CATSQ2** exhibits two conformations planar, fully conjugated or longer wavelength emitting species and twisted, half-conjugated or short wavelength emitting species at the same tame in non-protic solvents. Equilibrium of these two conformations is shifted more towards non-planar twisted state as the amount of hydrogen bonding solvent increases and only twisted conformation is possible in protic solvents.

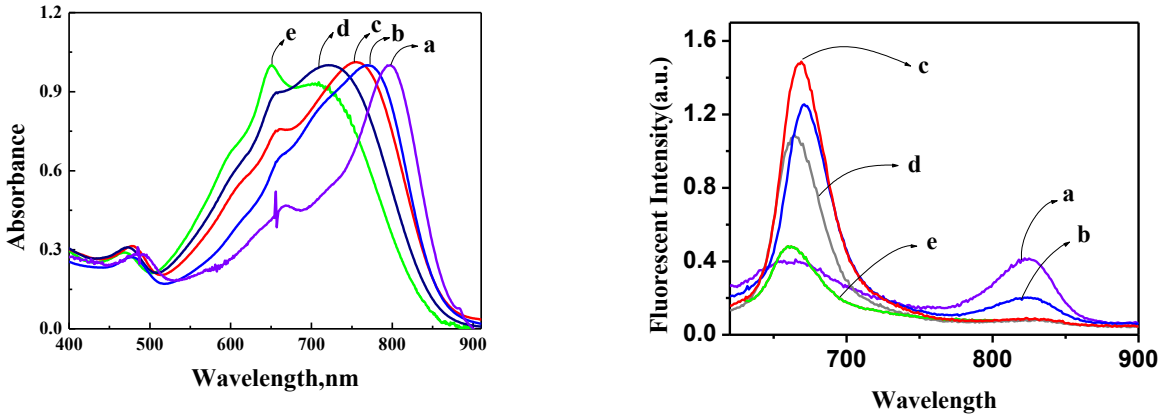

Fig. 4. Absorption and emission changes of **CATSQ2** in a) $CHCl_3$ b) 3:1 $CHCl_3$ /MeOH c) 1:1 $CHCl_3$ /MeOH d) 1:3 $CHCl_3$ /MeOH e) MeOH.

Fig. 5 shows temperature effects of **CATSQ2** on fluorescence properties. The fluorescence spectra of **CATSQ2** in acetonitrile at room temperature show two pronounced emission maxima at 821 nm and 675 nm. These both maxima decreased intensity by increasing temperature from 100^0K to 145^0K. The intensity of shorter wavelength emission maximum get decreased more than longer wavelength emission. By cooling, both emission maxima increased. Relative increase is more for shorter wavelength maximum. Same observation akin to **CATSQ2** underwent in the case of **CATSQ3** also. Equilibrium of above two conformation of the compound changes from one state to another upon heating or cooling. Effects of temperature on fluorescence properties of **CATSQ3** in protic solvent (butanol) have been carried out. Compound shows one prominent emission at room temperature. These emissions at 665 nm get decreased upon heating from 98^0K to 148^0K. The intensity of emission at 665 nm gets increased upon cooling from 148^0K to 88^0K.

ISBN 978-93-5279-420-1

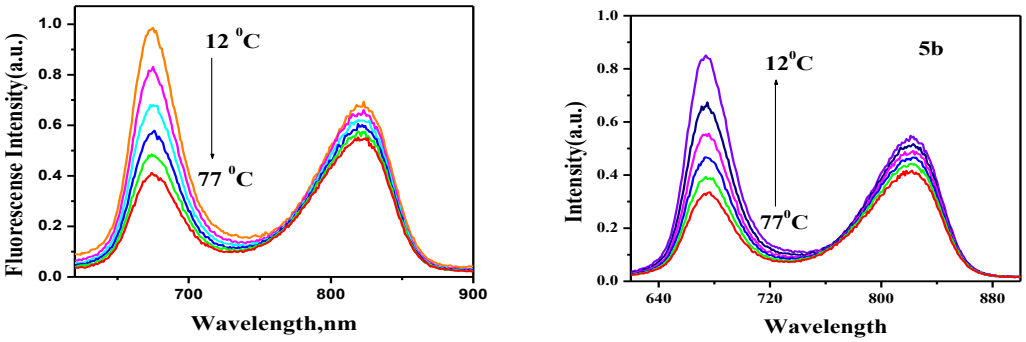

Fig. 5. Temperature effect on **CATSQ2** a) heating cycle b) cooling cycle in acetonitrile

Fig. 6 shows effect of addition of trifluoroacetic acid TFA on **CATSQ2** in acetonitrile. **CATSQ2** possesses two peaks centered at 666 nm and 456 nm in acetonitrile. On addition of 57.5 mM amount TFA into solution the peak centered at 666 nm decreases and peak centered at 456 nm shifted to 572 nm by a clear isosbestic point 529 nm. Changes in fluorescence upon TFA addition in the same solvent also observed. The peak centered at 821 nm decreases and concomitant appearing of new band at 610 nm increases by a clear isoemissive point 746 nm. Protonation studies demonstrated that dual fluorescence is not due to the protonated species of the compound, since protonated species is emitting in different region. Protonation studies in dichloromethane were also carried out. It possesses two peaks in absorption spectra centered at 765 nm and 470 nm. The peak at 765 nm decreases on adding 120 mM TFA and a new blue shifted maximum centered at 541 nm observed by a clear isosbestic point at 591 nm and corresponding fluorescence changes also observed. The fluorescence emission maximum at 825 nm decreases and broad blue shifted maximum at 558 nm increases and new emission maximum at 606 nm is observed. Protonation studies of **CATSQ3** in acetonitrile were carried out. In acetonitrile, absorption band at 662 nm decreases along with the formation of new band at 530 nm upon addition of 29.3-mM trifluoroacetic acid (TFA). Correspondingly fluorescence at 820 nm decreases and a new broad blue shifted peak centered at 596 nm increases. Finally a new fluorescence maximum at 551 nm observed.

The molecular modeling calculation of **CATSQ2** was carried out using Titan software. The equilibrium geometry was estimated using AMI calculation. The energy-minimized conformation obtained through molecular modeling calculation is shown in Fig. 7. Calculation suggests that the whole molecule is not planar due to steric hindrance. Two benzothiazole are in the same plane. Calculation also supports intramolecular H-bonding makes the aniline nucleophiles to come to the same plane of the benzothiazole. This also augments evidence for different conformational changes.

ISBN 978-93-5279-420-1

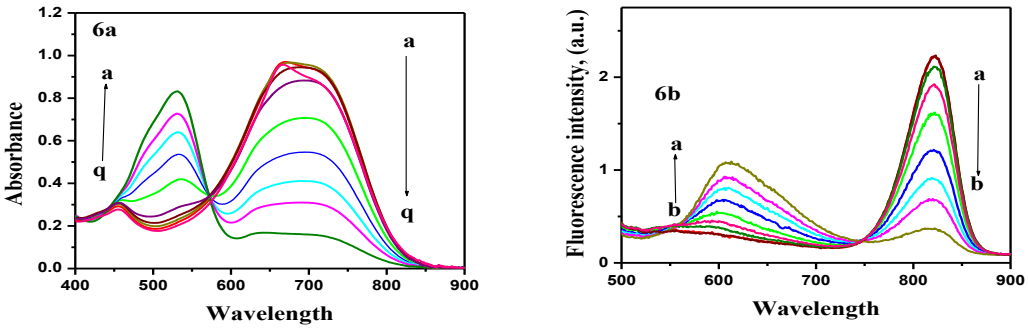

Fig. 6. Effect of addition of 57.5 mM **TFA** in a) absorption and b) emission spectra on 18.4µM **CATSQ2** in acetonitrile

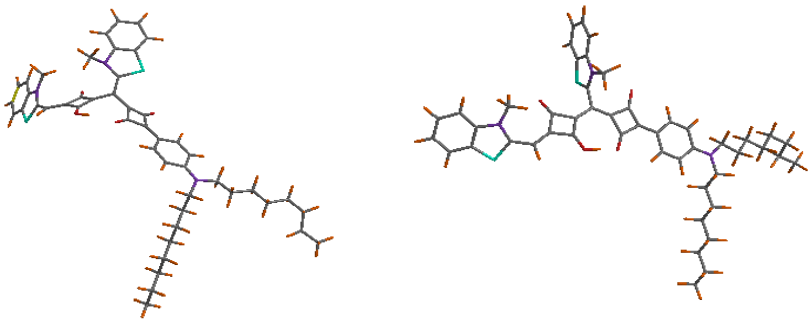

7a **7b**

Fig. 7. Minimum energy configuration of **CATSQ3** obtained using molecular mechanics calculation b) with and a) without intramolecular H-bonding

Conclusions

The photophysical properties of two novel classes of unsymmetrical cationic squaraine dyes **CATSQ2** and **CATSQ3** have been investigated. Both the dyes show two or more than two absorptions in all solvents and dual fluorescence in non-protic solvents like acetonitrile, dichloromethane and chloroform. While only one prominent blue-shifted fluorescence observed in protic solvents like methanol, n-butanol and isopropanol. Stoke's shift in absorption and fluorescence of these two dyes is sensitive to the polarity of the solvent. As the polarity of solvent increases, dramatic hypsochromic shift observed. This different spectral behavior of these two dyes **CATSQ 2** and **CATSQ 3** is due to existence of two states due to molecular constraints by bulky group present in the molecule. One state of molecule is planar, fully conjugated due to intramolecular hydrogen bonding between two squarate moieties. Another state is non-planar, twisted or half conjugated due to breaking of intramolecular hydrogen bonding between two squarate moieties, hence one of the fluorophore became out of plane. These both states are in equilibrium in non-protic solvents, while only twisted state of molecule can be seen in protic solvents. So we can induce dual fluorescence in squaraine dyes by introducing bulky groups with molecular constraints into a molecule. Further examinations of these classes of dye underway in our laboratory.

Acknowledgment

ISBN 978-93-5279-420-1

The National Institute of Science and Technology (NIIST), Trivandrum & Council of Scientific and Industrial Research, Government of India, gratefully acknowledged for financial support.

References

1. Tam, A. C., *Appl. Phys. Lett*. **1980**, *37*, 978; Law, K. Y.; Bailey, F. C. ; *J. Imaging Sci.* **1987**, *31*, 172.
2. Gravesteijn, D. J.; Steenbergen, C.; Vander Veen, J.; *Proc. SPIE Int. Soc. Opt. Eng*. **1988**, *420*, 327; Jipson, V. P.; Jones, C. R.; *J. vac. Sci. Technol*. **1981**, *18*, 105
3. Meritt, V. Y.; Hovel, H. J. *Appl. Phys. Lett*. **1976**, *29*, 414. Loutfy, R. O.; Hasiao, C. K.; Kazmaier, P. M. *Photogr. Sci. Eng*., **1983**, *27*, 5
4. For reviews on near-infrared absorption spectra of squarylium dyes, see: Fabian, J.; Nakazumi, H.; Matsuoka, M. *Chem. rev*. **1992**, *92*, 1197. Nakazumi, H. *J. Soc. Dyes Colour*. **1998**, *104*, 121. Emmelius, M.; Pawlowski, g.; Vollmann, H. *Angew. Chem. Int. Ed. Eng.* **1989**, *28*, 1445.
5. Zeigenbein, W.; Sprenger, H. E.; *Angew. Chem. Int. Ed. Engl.* **1966**, *5*, 893.; *ibid*. **1967**, *79*, 581 and **1967**, *78*, 937; Treibs, A.; Jacob, K. *Justus Leibigs. Ann. Chem*. **1968**, *712*, 123; Schmidt, A. *Synthesis*, **1980**, 961; Law, K. Y.; Bailey, E. C. *Can. J. Chem*. **1986**, *64*, 2267.
6. Nakazumi, H.; Natsukawa, K.; Nakai, K.; Isagawa, K. *Angew. Chem. Int. Ed. Engl.* **1994**, *33*, 1001.
7. Thomas, K. G.; Thomas, K. J.; Das S.; George, M.V. *Chem.Commun*. **1997**, 597.
8. Sprenger, H. E.; Ziegebien, W. *Angew Chem. Int.Ed. Engl.* **1967**, *6*, 553.
9. J. M. Yarborough, *Appl. Phys. Lett*., **1974**, *24/12*, 629.
10. Soper, S. A.; Mattingly, Q. L. *J. Am. chem. Soc***. 1994**, *116*, 3744.
11. Lakowicz, J. R. *Principles of Fluorescence Spectroscopy*; Plenum Press: New York, 1983 p.8.

GREEN COMPOSITES FROM NITRILE BUTADIENE RUBBER AND CASSAVA STARCH

P Divia and C Rajesh*

Research and Post Graduate Department of Chemistry, MES Keveeyam College Valanchery, Malappuram Dist, Pin-676552, Kerala

**E-mail: rajeshvlcy@rediffmail.com*

Abstract: Filler reinforced rubber composites are of immense importance both in the industrial field and in the area of research and development. Particulate filling has been used extensively in rubber industry to improve various properties because it is effective yet inexpensive. The properties like tensile strength, elasticity, ductility, impact strength, abrasion resistance etc. of rubber can be improved by the incorporation of particulate fillers. Acrylonitrile butadiene rubber (NBR) is a special purpose synthetic rubber having exceptional resistance to most of the oils and solvents, which makes it one of the apt candidates in industry for making oil hoses.

 ISBN 978-93-5279-420-1

The nutritive reserves of cassava is made up of starch, which is one of the most important products synthesized by plants that is consumed as food and used in industrial processes. The present work deals with the development and characterization of green composites of NBR containing different loading of cassava starch. The properties of NBR have been found to improve upon the incorporation of cassava starch. The studies show that with increase in the loading of cassava starch in NBR, the tensile strength increases progressively up to 25 phr. The tensile modulus value is increased with the amount of filler loading. The tensile strength decreased after the soil burial for one month due the biodegradability of cassava starch and palm oil which was used as plasticizer. The swelling characteristics of NBR/Cassava starch composites have been studied which indicated improved solvent resistivity of the composite.

Keywords: Composites, NBR, starch.

Introduction

Polymer composites are heterogeneous structural materials which are made up of a polymeric matrix containing reinforcing agents and are often better suited for specific applications than any of the original components. They have a premier role among engineering materials with the advantages such as light weight, corrosion resistance, high fatigue strength and faster assembly. Growing environmental and social concern and the high rate of depletion of petroleum resources have forced the search for new composites and green materials, compatible with the environment. In the context of eco–friendly materials, recyclability of the material is one of the major problems. Recyclability of the composites will lead to cost effective products as well as a remedy for the increased amount of waste materials. Green composites can replace all hazardous and waste producing counterparts. Life cycle analysis should be done for all newly synthesized materials and thus the biodegradability can be measured. This will help us to develop eco–friendly and acceptable materials.

In recent years bio-based polymer composites have been the subject of many scientific and research projects, as well as many commercial programs [1-3]. Biodegradable polymers are designed so that degradation happens by the enzymatic action of living micro-organisms such as bacteria or fungi to produce carbon dioxide, water and nontoxic biomass [4]. Polymer blends and composites with natural polymers as one of the components have been developed by many researchers [5, 6].

Starch, obtained from renewable resources, has many advantages, such as low cost, abundant supply, and environmental amity, and it is widely used in food, paper-making, fine chemicals, packing material industry, etc. Ways to find out its other potential applications on a big scale have attracted much interest. To reduce dependence on synthetic polymers made from oil, much effort has been made on developing starch based biocomposites [7-13]. Chin-San [14] studied improving polylactide/starch biocomposite by grafting polylactide with acrylic acid characterization and biodegradability assessment. Mohammad *et. al* [15] studied essential work of fracture of low-filled poly (methyl methacrylate)/starch composites. Thermo gravimetric analysis showed that the thermal stability increased as the starch content increased in the composites. The biodegradability of the PMMA/starch composites was studied with a soil burial test. The degradability was measured in terms of mechanical strength, which increased as the starch content increased.

 ISBN 978-93-5279-420-1

Shogren et. al.[16] studied biodegradation of starch/polylacticacid /poly (hydroxyester ether) composite in soil. Rates of weight loss increased in the order pure PLA < starch/PLA < starch/PHEE/ PLA and increased with increasing starch and PHEE contents. Some formulations containing PHEE and lower starch levels had higher tensile strength after initial exposure to soil than those without PHEE.

Soykeabkaew and Supaphol [17] studied preparation and characterization of jute- and flax-reinforced starch-based composite foams (SCFs). Both the flexural strength and the flexural modulus of elasticity appeared to be markedly improved with addition by weight of the fibers. The improvement in the mechanical properties of SCFs was attributable to the strong interaction between fibers and the starch matrix. Srithongkham et.al.[18] investigated starch/cellulose bio composites prepared by compression molding. It was found that starch bio composites made from cassava starch and glycerol provided good results on shape stability with relatively high modulus and tensile strength. Adding cellulose nanofibers increased tensile strength and modulus of bio composites. More recently, in the patent literature [19-21], starch has been creatively used as filler in tyre compounds in order to lower the rolling resistance and reduce the use of carbon black made from natural gas or oil resource. With anticipated low cost, light weight and good comprehensive performance, starch/rubber composites will be applied not only in rubber tyres, but also in other kinds of rubber products.

The present work deals with the preparation and characterization of composite materials of acrylonitrile butadiene rubber (NBR) with cassava starch. The effect of starch on mechanical properties, biodegradability and swelling characteristics of NBR composites has been studied. The aim of developing composite materials by reinforcing polymers with suitable fillers is to achieve commercially viable products having unique properties at lower cost.

Experimental

NBR used in the present work was of commercial grade and obtained from Apar Industries, Mumbai, India. It is reported to contain 35% acrylonitrile. 40% activated Dicumyl Peroxide (DCP) used as vulcanizing agent and cassava starch were of commercial grade. Palm oil used as the plasticizer for the present work was manufactured by M/s. Parrisons Liberty, Kozhikode, Kerala.

The formulations of the mixes used in the present work are given in Table 1. A, B, C and D, E and F represent mixes containing NBR and cassava starch with dicumyl peroxide as vulcanizing agent. Mix A is the gum sample. B, C, D,E and F are mixes containing 5, 10, 15, 20 and 25 phr of starch respectively.

Table 1. ***Formulation of NBR composites (phr*)***

*Components (phr)**	*Mix*					
	A	*B*	*C*	*D*	*E*	*F*
NBR	100	100	100	100	100	100
DCP**	0.5	0.5	0.5	0.5	0.5	0.5
Palm oil	1.25	1.25	1.25	1.25	1.25	1.25
Cassava starch	0	5	10	15	20	25

ISBN 978-93-5279-420-1

* phr: parts per hundred rubber. ** DCP: Dicumyl Peroxide

The composites were prepared by using a laboratory two roll mixing mill. Initially NBR was masticated on the mill for 2 minutes followed by the addition of the ingredients. The nip gap, mill roll speed ratio and the number of passes were kept the same for all the mixes. The samples were milled for sufficient time to disperse the filler in the matrix. The cure characteristics of the mixes were measured by using a Goettfert elastograph rheometer. Vulcanisation of the mixes was done at 160°C using a hydraulic press having electrically heated platens to their respective cure times as obtained from the rheographs. The sheets were kept for 24 hours. Tensile properties of different mixes were examined using an Instron Universal Testing Machine (Model 4411; Instron Ltd. Buckinghamshire, U.K) at crosshead speed of 500mm/ min. The tensile tests were conducted according to the ASTM D 412-06A test procedures using dumb bell – shaped test pieces. The hardness (Shore A) of samples was measured by using Durometer (Modex India Pvt. Mumbai, India) according to ASTM 2240 – 86. Surface morphology of fracture surfaces of tensile bars of feather fiber reinforced NBR and NR composites were imaged using Hitachi SU – 6600 Scanning Electron Microscope.

Diffusion and sorption of organic solvents through the composite has been studied by conventional equilibrium swelling technique. Swelling coefficient [22] is index showing the extent to which the sample swells. The reinforced composites were swollen in the suitable solvent at room temperature and the swelling coefficient was evaluated by the equation.

$$\text{Swelling coefficient} = \frac{W_2 - W_1}{W_1} \times \frac{1}{\rho_s}$$

Where W_1 is the initial weight of the sample, W_2 is the final or swollen weight of the sample and ρs is the density of the solvent used. The direct involvement of micro-organisms in rubber can be studied by a method known soil burial test. Effect of soil burial on the rubber was primarily followed by quantitatively observing the change in their mechanical properties.

Results and Discussion

Mechanical properties

Table 2 shows the mechanical properties of NBR/Cassava starch composite with different amount of starch.

Table 2. ***Mechanical properties of composites***

Mechanical Properties	*Filler loading (phr)*				
	0	*10*	*15*	*20*	*25*
Tensile Strength	2.73	2.84	2.87	4.14	4.15
Elongation at Break	585.21	661.62	664.86	724.47	754.6
Modulus at 100%	0.63	0.67	0.68	0.69	0.87

It can be seen from the table that as amount of the cassava starch increase the tensile strength increases. Tensile values are increased due to the interaction between NBR and

ISBN 978-93-5279-420-1

cassava starch. Tensile values reach an optimum value at 25 phr of starch in the composite. The elongation at the break (Eb) is the strain on the sample when it breaks. From the result in Table 1, it clear that as the loading of cassava starch increases the elongation at break increases. Modulus values of mixes increase with increase the amount of cassava starch and attain an optimum value at filler loading 25 Phr. The modulus is increased due to the increasing interaction between the NBR matrix and the reinforcing filler.

Biodegradability

Mechanical properties of the composite before and after ageing under soil burial were compared. Table 2 shows that the mechanical properties of composite before and after ageing under the soil burial test.

Table 3. ***Mechanical properties of NBR/Cassava starch composite before and after ageing under soil burial test.***

Mechanical Properties						
	Before Ageing			*After Ageing*		
Filler loading	*Tensile Strength*	*Elongation at Break*	*Modulus at 100%*	*Tensile strength*	*Elongation at Break*	*Modulus at 100%*
0	2.73	585.21	0.63	2.08	516.88	0.50
10	2.84	661.62	0.67	2.35	637.70	0.59
15	2.87	664.86	0.67	2.56	643.33	0.62
20	4.14	724.47	0.69	3.80	711.89	0.62
25	4.15	754.47	0.87	3.89	722.92	0.74

From the table it can be seen that, tensile strengths of composite are decreased after the soil burial test when it is compared to the tensile values of mixes before ageing. The decrease in tensile values is due to the degradability of cassava starch and the palm oil. The Elongation at break value is decreased after the ageing under the soil burial, due to decrease in elasticity of composite by the biodegradability of cassava starch and palm oil. It can also be seen from the table that the modulus values of composites at 100% elongation are decreased after one month under the soil burial test due to the biodegradability of reinforcing filler and the plasticizer palm oil.

Fig. 1 shows the percentage decrease in mechanical properties of the composites after soil burial test.

ISBN 978-93-5279-420-1

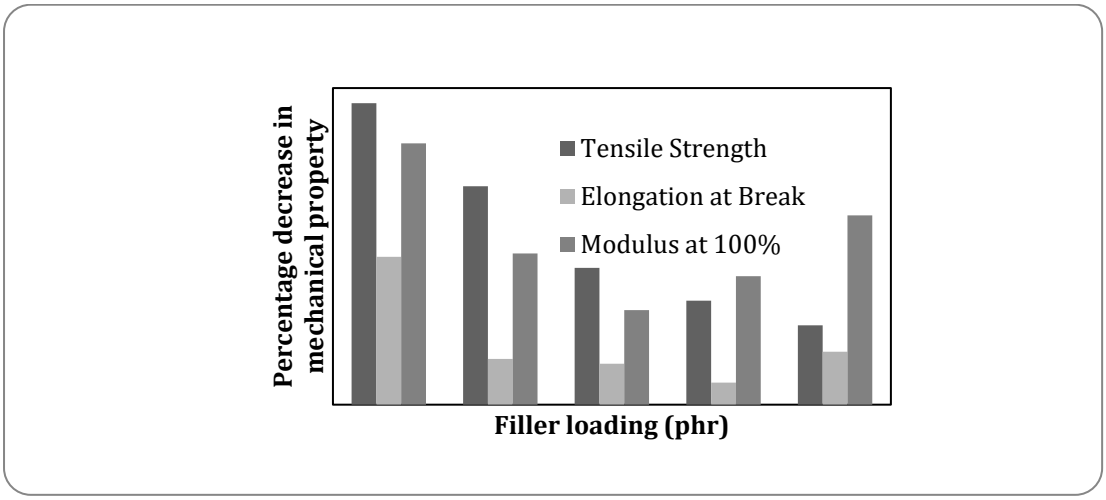

Fig. 1. Percentage decrease in mechanical properties after soil burial test

The graph clearly shows that the gum sample has maximum degradation than other mixes. It can be seen that at higher filler loadings the decrease in modulus values are more than that at lower loadings.

Swelling Characteristics

Table 4 shows the swelling coefficient values of NBR/starch composites in N,N-dimethyl formamide (DMF). From the Table, it is clear that the swelling coefficients of composite are comparatively lower than that of the gum compound when DMF is used as the solvent which indicates improved resistance to swelling on adding starch. It can be seen that composite containing 25 phr loading of starch has the highest resistance to swelling.

Table 4. ***Swelling Coefficient of NBR/Cassava starch mixes in DMF***

Filler loading (phr)	*Swelling Coefficient*
0	2.8752
5	1.1261
16	1.482
15	2.2865
20	1.9372
25	0.9338

Surface Morphology of the Composites

The SEM photograph of NBR/Cassava starch composite with 25 phr filler loading (mix F) is shown in the Fig. 2(a) and 2(b). The figure shows the particles have globular like structures. The black particles in the photographs represent NBR rubber and the other particles seen in white are the cassava starch and the chemical DCP etc. The figure also shows the interaction between the NBR matrix and the reinforcing filler cassava starch.

ISBN 978-93-5279-420-1

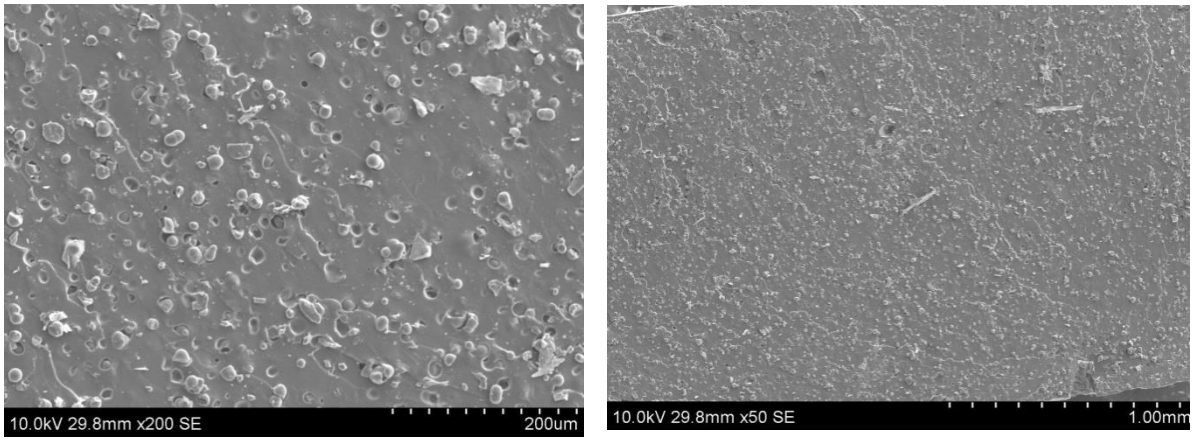

Fig. 2(a) and (b). SEM Photograph of MIX F in different magnifications

Conclusions

From the studies on NBR/cassava starch composites, it has been found that with increase in the loading of cassava starch in NBR, the tensile strength increases progressively up to 25 Phr loading. Tensile values increased due to the increase in interaction between NBR matrix and the filler. The tensile values decreased after the soil burial test for one month due the biodegradability of cassava starch and palm oil. The solvent resistivity has been found to be increased with the filler loading. The SEM result of composites shows that the mechanical properties of NBR/Cassava starch composite is higher due to its miscibility.

References

1. Maurizio A, Aleksandra B, Maria E E, Gennaro G and Anita G, *Materials*, 2 (2009) 911-925.
2. Adeosun S O, Lawal G. I., Balogun S A. and Akpan EI, *Journal of Minerals & Materials Characterization & Engineering*, 11 (2012) 483-514.
3. Zhihong Y, Mrinal B and Utpal RV, *Polymer*, 37 (1996) 2137–2150.
4. Tharanathan RN , *Trends Food Sci. Technol*, 14 (2003) 71.
5. Alain B and Sylvie P, *Appl. Sci. Manuf*. 4 (2008) 1444–1454.
6. Tae I M and Hiroshi I, *Polymer* 21 (1980) 309–316.
7. You-Ping W, Qing Q , Gui-Hua L and Li-Qun Z, *Carbohydrate Polymers*, 65 (2006) 109–113.
8. Lu Y., Weng L and Cao X., Macromolecular *Bioscience*, 5 (2005), 1101.
9. Vaidya UR , Bhattacharya M and Zhang D, *Polymer*, 36 (1995),1179.
10. Pallay J, Kelemen P, Berghmans H and Dommelen DV, *Macromol. Mater. Eng*. 275 (2000), 18.
11. Romha´ny G, Jo´zsef KK and Cziga´ny T, *Macromol. Mater. Eng*, 288(2003), 699.

ISBN 978-93-5279-420-1

12. Rouilly A, Rigal L and Gilbert RG, *Polymer*,45 (2004), 7813.
13. Ha SK and Broecker HC, *Macromol. Mater. Eng*, 288 (2003), 569.
14. Chin-San Wu, *Macromol. Biosci.* (2004), 352-363.
15. Mohammad Ali S, Unnikrishnan G and Joseph M A, *Inc. J. Polym. Sci.* (2013).
16. Shogren R L, Doane W M, Garlotta D, LawtonJ W and Willet J L, *Polymer Degradation and Stability* (2013), 405-411.
17. Nattakan Soykeabkaew, *Carbohydrate Polymers* (2004), 53-63.
18. Srithongkham S, Lalita V H and Chularat K, *J. Materials Sci. and Engineer.,*(2012), 213-222.
19. USP 6273163 (2001), The Goodyear Tire & Rubber Company, invs.: Materne, T.F.E., Corvasce F. G. Chemistry Abstract, 135, 305039r.
20. USP 6391945 (2002). The Goodyear Tire & Rubber Company, invs.:Sandstrom P. H. Chemistry Abstracts, 134, 164327y.
21. USP 6548578 (2003). Bridgstone/Firestone North American Tire, LLC, invs.:Pawlikowsk J. F. Chemistry Abstracts, 137, 186870j.
22. Smith TL*, J. Polym. Eng. Sci*., (1977) 129.
23. Tonukari NJ, *Electro. J. Biotech. ,* **1** (2004).

ISBN 978-93-5279-420-1

SYNTHESIS OF SOPHOROLIPIDS USING ORGANICALLY SYNTHESIZED CARBOXYLIC ACID AND THEIR APPLICATION IN SYNTHESIS OF SILVER NANOPARTICLES

Shabana K[1*] and B L V Prasad[2]

[1]*PG Department of Chemistry, KAHM Unity Women's College, Manjeri-676122, Kerala*

[2]*Physical & Material Chemistry Division, National Chemical Laboratory, Pune, Maharashtra*

[*]*E-mail: shabshabana@gmail.com*

Abstract: Sophorolipids as a body care products, therapeutic agents for cancer and immune disorders, oil recovery agents etc. In this study C14-COOH-SL prepared and checked its efficiency as a capping and reducing agent for silver nanoparticles. We found that this new sophorolipid is indeed capable of reducing Ag ions in to silver nanoparticles. Metal nanoparticles are known to be very important for many important applications. Preparing them and capping them with active molecules like SLs can enhance their utility and open new avenues for research and applications.

Introduction

Sophorolipids (SL) formerly named sophorosides is found and excreted into the culture medium by Candida or related yeast species and is a good surfactants. They were first described by Tulloch AP and found to be composed of a disaccharide moiety linked to one hydroxyl group of one ω or (ω -1)-hydroxy fatty acid (saturated or monounsaturated). The sugar (sophorose or 2-O-glucopyranosyl--D-glucopyranose) may further show mono- or diacetylation at the 6' and 6" positions. The nature of the hydroxy fatty acid is characteristic, with the hydroxyl group being located on the n or n-1 carbon atom. In general, fatty acids of carbon chain length of 16, 17 or 18 are used and subjected to modification to lead to different SLs by the composition of the growth medium. Sophorosides with unsaturated C18 fatty acids have been recognized in Candida bogoriensis. Sophorolipids exhibit surfactant activity because of their amphiphilic structure. Among the sophorolipid producers, Candida bombicola is the most studied species because it produces sophorolipid molecule in large quantities. Products yields up to 300 g of sophoroses per liter of culture medium have been reached. The composition of the hydroxylated fatty acid varies depending on the culture conditions. Furthermore, lactonization frequently occurs between the carboxyl group and the 4" OH group of the sophorose. Sophorolipids are used as bacteriocides in the formulation of skin and body-care products (deodorant, anti-acne ingredient, from Soliance) but these emerging biosurfactants may have many other application potentials such as use as a capping agent for providing stability to nanoparticles. Hydroxy fatty acids may be released from sophorolipids and lactonized into macrocyclic esters; they are used in the perfume and fragrance industry.

Materials and Methods

Chemicals used: ***Synthesis of sophorolipids*** [Malt extracts (Hi-media chemicals), Glucose extracts (Hi-media chemicals), Yeast extracts (Hi-media chemicals), Peptone (Hi-media

ISBN 978-93-5279-420-1

chemicals), Ethyl acetate, Sodium sulphate, Precursors: Oleic acid (Aldrich chemicals)], Pure culture of yeast; ***Synthesis of SL-Ag*** [Silver nitrate, Sophorolipids, Sodium borohydride, Potassium hydroxide].

Methods: ***MGYP broth (Composition of 100ml MGYP broth)*** Maltose extract: 0.3 g, Glucose extract: 2 g, Yeast extract: 0.3 g, Peptone: 0.5g, Millipore water: 100 ml

Organism: The fungal culture, Candida bombicola was used for the sophorolipid synthesis.

Synthesis of sophorolipids : Two to three weeks old culture of Candida bombicola grown on MGYP slant was used for the pre-inoculum preparation. Colonies were transferred to 20ml MGYP broth in a test tube and kept at room temp for 18 hrs, 2ml of this culture were added to each of 100 ml and 20 0ml MGYP broth in 500ml and 1000ml conical flask respectively and kept it on rotary shaker for 2 days. The biomass of culture grown for 2 days were separated by centrifugation at 5000 rpm for 10 minute at 20°C and these cells were redispersed in 100ml of 10% glucose solution and 10^{-3}M precursor (oleic acid, C14-1-OH, C12-1-OH) were added in each flask and kept on rotary shaker for 24hrs (All precursors are dissolved in 1ml ethanol). After 1day, 10^{-2}M of precursors in ethanol was again added to the respective flask and kept on rotary shaker for 3-4 days followed by addition of 50ml of 10% glucose in each flask and kept on shaker for 8-10 days till complete conversion of precursor to sophorolipid occurred.

Separation of sophorolipid: Sophorolipid formed was taken out and was collected in a test tube. Remaining sophorolipid along with biomass was collected as a pellet by centrifugation at 5000 rpm for 10 minute and supernatant was discarded. The pellet was redispersed in 100ml of 10% glucose and with 10^{-2}M respective precursor and kept on rotary shaker for 10-15 days until the formation of sophorolipid. The sophorolipid formed was then extracted by mixing with equal volume of ethyl acetate in a separating funnel, organic layer was dried over anhydrous sodium sulphate and the excess solvent was removed using rotary evaporation. A yellowish brown, honey like viscous liquid was obtained. This is the sophorolipid. The yield for a flask of 250ml of sophorolipid was approximately 1.045g. A minimum of three batches were required to make sufficient amount of sophorolipid enough for further analysis.

Synthesis of silver nanoparticles: The set of experiment performed are given in Table 1.

Table 1. ***Effect of capping and reducing agents on the formation of silver nanoparticles***

Sl. No.	*Capping agent*	*Substrate*	*Reducing agent*	*Result*	*Time taken for reduction*
1	C14-COOH (10^{-4}M)	$AgNO_3$ (10^{-4}M)	Nil	No colour	Nil
2	C14-COOH (10^{-4}M)	$AgNO_3$ (10^{-4}M)	NaBH4	Yellow	Instantaneous
3	C14-COOH (10^{-4}M)	$AgNO_3$ (10^{-4}M)	KOH	Yellow	After 10 minutes
4	C14-COOH-SL (10^{-4}M)	$AgNO_3$ (10^{-4}M)	Nil	No colour	Nil
5	C14-COOH-SL (10^{-4}M)	$AgNO_3$ (10^{-4}M)	$NaBH_4$	Yellow	Instantaneous
6	C14-COOH-SL (10^{-4}M)	$AgNO_3$ (10^{-4}M)	KOH	Yellow	After 5 hrs

ISBN 978-93-5279-420-1

Results and Discussion

1. ***UV-VISIBLE Analysis of Silver (Ag) nanoparticles and Sophorolipid capped Silver nanoparticles***

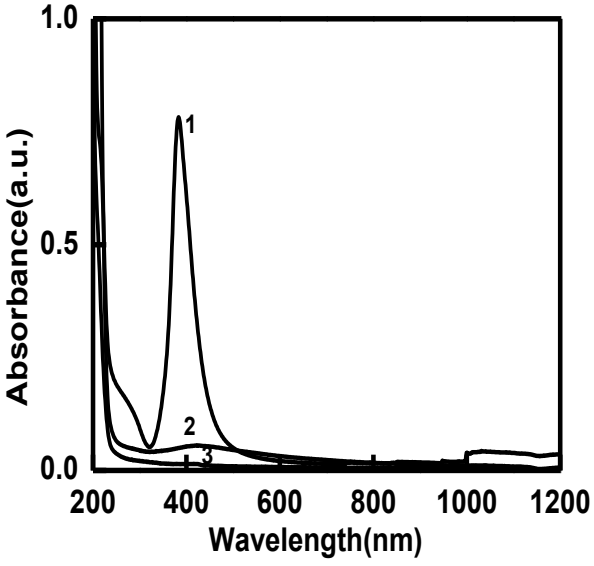

Fig. 1. UV-VISIBLE spectrum of Ag nanoparticle synthesized using C14-COOH of concentration 10^{-4}M with $NaBH_4$ (curve 1) and KOH (curve 2)

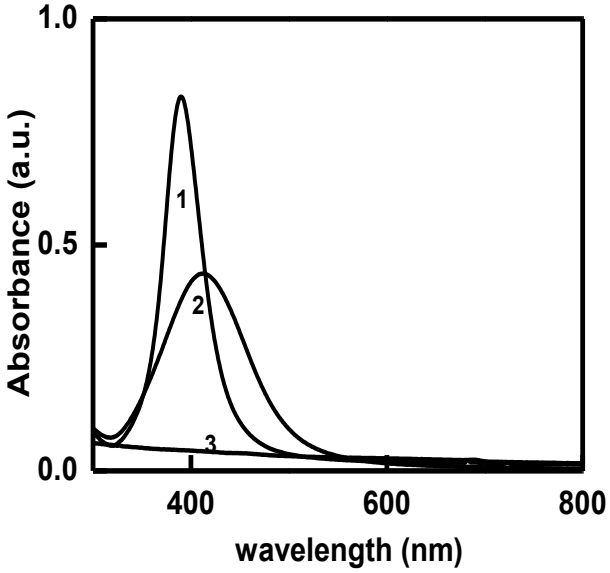

Fig. 2. UV-VISIBLE spectrum of Ag nanoparticles synthesized using C14-COOH-SL of concentration of 10^{-4}M with $NaBH_4$ (curve 1) and KOH (curve 2)

In Fig. 1,Curve 1 represent the silver nanoparticles synthesized using C14-COOH (10^{-4}M) as capping agent and $NaBH_4$ as reducing agent (C14-COOH+$AgNO_3$+$NaBH_4$), curve 2 represent the silver nanoparticles synthesized using C14-COOH (10^{-4}M) in presence of KOH (C14-COOH+$AgNO_3$+KOH) and curve 3 corresponds to C14-COOH (10^{-4}M) and $AgNO_3$ without any reducing agent (C14-COOH+$AgNO_3$). Curve 1 shows sharp peak at 380nm, which indicate the formation of Ag nanoparticles. Curve 2 shows peak positioned at 438nm, which indicate the formation of Ag nanoparticles and which also indicate the reduction can also occur with C14-COOH in presence of KOH. Curve 3 shows monotonous increase and no peak is observed, which implies that, when Ag^+ ions are exposed to C14-COOH alone there is no reduction.

In Fig. 2, curve 1corresponds to Ag nanoparticles synthesized using C14-COOH-SL (10^{-4}M) and $AgNO_3$ in presence of $NaBH_4$ (C14-COOH-SL+$AgNO_3$+$NaBH_4$), curve 2 represent the silver nanoparticles synthesized using C14-COOH-SL (10^{-4}M) and $AgNO_3$ in presence of KOH (C14-COOH-SL+$AgNO_3$+KOH) and curve 3 corresponds to C14-COOH-SL (10^{-4}M) and $AgNO_3$ in absence of reducing agent (C14-COOH-SL +$AgNO_3$). Curve 1 shows sharp peak at 390 nm, which indicate the formation of Ag nanoparticles. Curve 2 shows peak centered at 412nm, which indicate the formation of Ag nanoparticles and which also

ISBN 978-93-5279-420-1

indicate that the reduction can also occur with KOH. Curve 3 shows monotonous increase and no peak is observed, which implies that in absence of reducing agent no formation of silver nanoparticles take place.

2. *TEM Analysis*

The TEM images (Fig. 3) for sophorolipid capped Ag nanoparticles of a concentration of 10^{-4}M show that the particles were observed to be irregular in shape, polydisperse in nature and well separated from each other having an average particle size of 25nm.

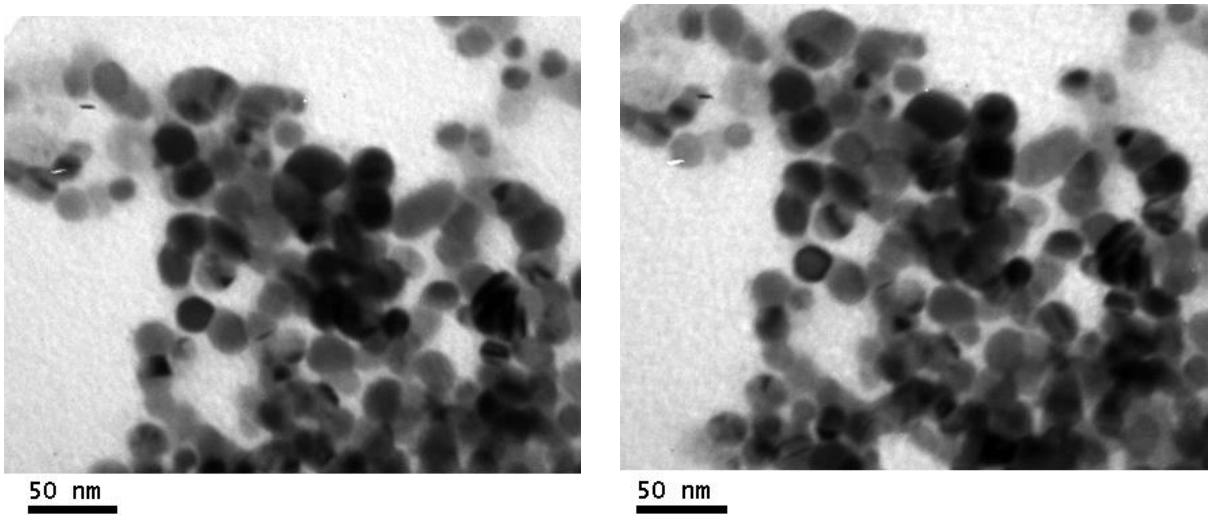

Fig. 3. TEM images of Ag nanoparticle synthesized using C14-COOH-SL with $NaBH_4$.

Conclusions

In this study, we have described the synthesis of C14-COOH-SL and its application as a capping and reducing agent on silver nanoparticles. It is characterized by using UV-VISIBLE Spectra. The TEM images indicate the presence of spherical, polydisperse silver nanoparticles capped with sophorolipids with average particle size of 25nm.

References

1. http://www.Nanoscience.com/education/overview.html.
2. www.nanotec.org.uk/
3. www.en.wikipedia.org/wiki/Nanotechnology.
4. New methods for the synthesis of magnetic nanoparticles- Thesis by Tanushree Bala University of Pune.
5. www.crnano.org/whatis.htm
6. Sophorolipid production by candida bombicola: Medium composition and culture methods- Journal of Bioscience and Bioengineering 88,No.5,488-494.1999.
7. Phadtare Sumant, Parekh Parag, Shah sachin, Tambe Amruta, Joshi Rohini, Sainkar S.R, Prabhune Asmita, and Sastry Murali Biotechnol. Prog. (2003) 19, 1659-1663.

ISBN 978-93-5279-420-1

8. Http: // en. Wikipedia. Org /wiki /UV/VIS _spectroscopy.
9. Http: //en.wikipedia. Org/wiki/Top-down- and-Bottom-up-design.
10. Http: // nobelprize. Org/ educational –games/physics/microscopes/ tem/ind ex.html.
11. Cavelaro David A., Cooper David G; Biotechnology; (2003); 103; 31-41.

STUDY OF THE IMPACT OF MUNICIPAL SOLID WASTE DUMPING ON SOME SOIL PARAMETERS NEARER TO VETTEKODE SOLID WASTE LANDFILL SITE IN MANJERI MUNICIPALITY

Deepa K

PG Department of Chemistry, KAHM Unity Women's College, Manjeri-676122, Kerala

E-mail: deepakarat@yahoo.com

Abstract: Dumping of solid wastes on land is a common waste disposal method and practiced almost by all the cities around the globe. Precipitation that infiltrates through the municipal solid waste leach the constituents from the decomposed waste mass and while moving down cause the subsurface soil to be contaminated by organic and inorganic solutes. In the present study an attempt has been made to evaluate the impact of municipal soild waste on the properties of soil at a landfill site of Manjeri Municipality at Vettekode. We have studied and made a comparison in properties of soil from dump site and non dump site area. The physical and chemical parameters such as pH, electrical conductivity, total organic matter, moisture content, available nitrogen, phosphorus, potassium in the soil samples were studied using various analytical techniques. The findings show that pH values are slightly higher in the polluted area than in the control. The electrical conductivity values are found to be very high for soil samples from polluted area when compared to control soil. Other parameters such as organic matter, total nitrogen, available potassium and available phosphorus are also found to be higher in the polluted area than the control.

Introduction

Solid waste land filling is the most common method of solid waste disposal. The landfill site at Vettekode is an open dumpsite, because the open dumpsites are low operating costs and lack of expertise and equipment provided no systems for leachate collections [1]. Open dumps are unsightly, unsanitary, and generally smelly. They attract scavenging animals, rats, insects, pigs and other pests. Surface water percolating through the trash can dissolve out or leach harmful chemicals that are then carried away from the dumpsites in surface or subsurface runoff [2, 3]. The Municipal Solid Waste (MSW) includes commercial and residential waste generated in municipal areas, in either solid or semi-solid form, excluding industrial hazardous waste, but including treated biomedical waste. The dumping of MSW without proper segregation adds to the complexity of the issue. The most commonly adopted method to manage solid waste in developing countries is to dispose in open dumps which causes serious environmental problems including health hazards [4]. Dumping of solid waste on land is a common waste disposal method, and practiced almost by all the cities around the

 ISBN 978-93-5279-420-1

globe. In the last 200 years, world population has increased six times, and the urban population has multiplied 100 times [5]. Population growth and industrial revolution contribute to enormous amount of solid waste generation.

The solid waste dumping plant existed in Vettekode of Manjeri municipality has a capacity of two tonnes per day and run successfully by Socio economic unit foundation and was closed down three years back on account of public protest. This study involves the soil quality analysis in the Vettekode solid waste dumpsite nearer area. The aim of the study is to understand how the soil gets polluted due to the dumping of solid waste. The ten samples were selected for analysis Samples 1-4 were taken from dumpsite area and samples 5-10 were taken from less polluted areas.

The Municipal Solid Waste dumping plant at vettekode

Experimental

Sampling

For routine soil testing the field is divided to proportions according to variations. Separate samples are collected from different portions .These samples are mixed thoroughly and spread on a clean sheet of paper and divided into a 4 equal parts . Two opposite quarters are rejected and samples from the other two are mixed and the procedure is repeated till the desired quantity of the samples is obtained (1-2 kg). The final sample must be dried before collecting care has to be taken in to avoid contamination. The bag or the box must be properly labelled and taken to laboratory for analysis.

Laboratory Determinations

The soil pH was measured using a pH meter in 1:2.5 soil to water ratio. The electrical conductivity (EC) is used to measure the ability of an aqueous solution to carry an electric

ISBN 978-93-5279-420-1

current. The EC was determined using a conductivity cell containing a platinized electrode.For the determination of percentage organic matter the sample is made into fine powder by sieving. Take 10g of each ten soil samples. After pouring it in the separated crucible weight-out the ten samples. Then they are heated in a muffle furnace to 600^0C and again weighed. Total organic matter is calculated from the difference between the two weights. Total Moisture content is determined by heating a known weight of the soil sample to constant weight in an electric oven at 70^0c and finding the loss in weight. A known weight of the soil sample is oxidized using $K_2Cr_2O_7$ followed by the determination of nitrogen present in the soil sample by using digital balanced cell colorimeter. Potassium present in the soil is extracted with neutral ammonium acetate of 1M. This is considered as plant available K in the soil and it is estimated with the help of flame photometer. The readily soluble Phosphorus is extracted by combination with HCl and NH_4F phosphate in the extract is determined calorimetrically with ammonium molybdate and ascorbic acid as reducing agent

Results and Discussion

Experimental results obtained on effect of municipal solid waste Lechate on the characteristics of soil on both contaminated and uncontaminated soil were presented in Table 1. The pH of all the 10 samples lies in the acidic range, (i.e., <7). We can conclude that, pH value of uncontaminated soils is higher than the contaminated soils. The pH of the soil samples taken from dumping site signifies that it is slightly acidic in nature compared to uncontaminated soil which may be due to the presence of the solid waste [6]. The electrical conductivity of samples taken from less polluted areas have the value less than one and the samples taken from dumpsite have value greater than one [7]. The highest and lowest value of electrical conductivity is 0.183 and 1.839. All samples except sample 6, which is taken from a less polluted area, has a moisture content greater than five (5.8337) . The total organic matter present in the soil is higher for samples taken from dumpsite. The nitrogen availability in the soil is greater than one for highly polluted soil samples and that of samples from less polluted areas is less than one. The phosphorus present in soil for sample 6 and 9 is less and sample 10 is moderate (15.7), that of other samples are much high (32). The potassium present in the soil for all samples is greater than 200 and samples taken from dumpsite have value around 450. The results are consolidated in the in Fig. 1.

Table 1. ***Soil Parameters estimated in contaminated and uncontaminated soils***

Samples	*p^H*	*EC (ds/m)*	*Moisture (%)*	*Organic Matter (%)*	*Nitrogen (N in Kg/Ha)*	*Phosphorus (P in Kg/Ha)*	*Potassium (K in Kg/Ha)*
Sample 1	5.09	1.040	2.8808	22.3584	1.25	32	448
Sample 2	6.4	1.350	2.6950	28.2302	1.25	32	448
Sample 3	5.4	0.194	2.4976	23.0736	0.63	32	296
Sample 4	6.4	1.839	2.1002	16.6119	1.25	32	448

ISBN 978-93-5279-420-1

Sample 5	5.8	0.278	3.8093	11.1443	0.66	32	448
Sample 6	6.1	0.459	5.83377	16.4313	0.26	5.8	264
Sample 7	5.0	0.183	2.8037	11.5409	0.48	32	448
Sample 8	5.6	0.326	1.6519	11.1410	0.95	32	448
Sample 9	5.1	0.231	0.9869	10.8682	0.96	1.3	340
Sample 10	4.8	0.253	2.7884	20.3651	0.78	15.7	305

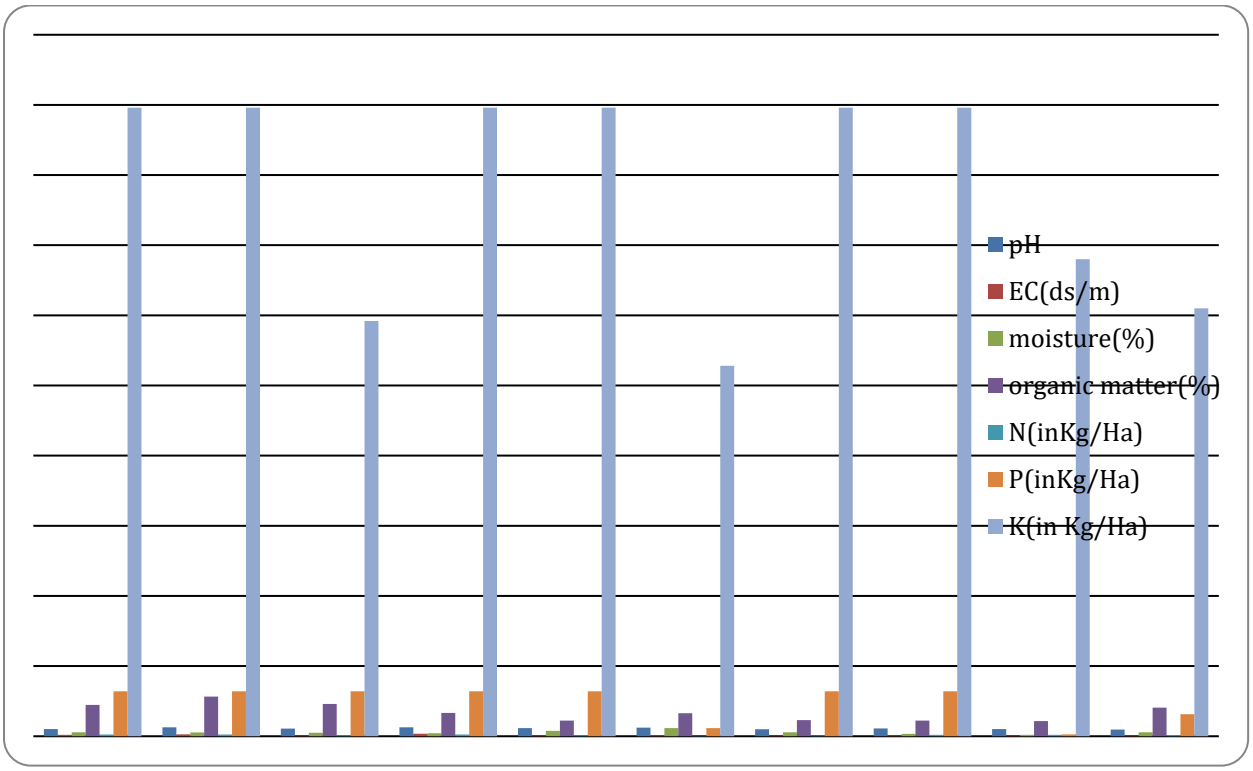

Fig. 1. Consolidated result of soil parametrs

Conclusions

The present investigation gives an insight into the probable impact of municipal solid waste on soil properties in comparison to control soil. It is apparent from experimental results that physicochemical properties of soil differ for municipal solid waste treated soil collected from different locations of dumpsite. The presence of large amount of ionic substances and soluble salts may have resulted in increased value of electrical conductivity in municipal solid waste treated soil in comparison to control samples. The samples from dumpsite show high organic content than samples from outside buffer zone [8, 9]. The values of NPK measurement also show a higher value for samples from dumpsite. After analysing data obtained from

ISBN 978-93-5279-420-1

studies of various parameters we should bear in mind that wastes should be sorted and wastes should be treated if possible [10]. When it comes to dumping of wastes a properly designed and engineered landfill should be constructed.

References

1. A Asadi Huat BBK, H Moayedi, Shariatmadari N, Parsaie A (2011), Changes of hydraulic conductivity of silty clayey sand soil under the effects of municipal solid waste leachate. International Journal of the Physical Sciences, 6(12): 2869-2874.
2. A.J. Hernandez, M.J.Adarve, A. Gil, J. Pastor (1999), Soil Salivation from Landfill Leachates: Effects on the Macronutrient Content and Plant Growth of Four Grassland Species. Chemosphere, 38(7): 1693-1711.
3. M. Maftoun, F. Moshiri (2008). Growth, Mineral Nutrition and Selected Soil Properties of Lowland Rice, as Affected by Soil Application of Organic Wastes and Phosphorus, J. Agric. Sci. Technol., 10: 481-492.
4. E. Panahpour, A. Gholami, A.H. Davami (2011). Influence of Garbage Leachate on Soil Reaction, Salinity and Soil Organic Matter in East of Isfahan, World Academy of Science, Engineering and Technology, 171-176.
5. O. Schwarz-Herion, A. Omran, and H.P. Rapp, (2008), "A Case Study on Successful Municipal Solid Waste Management in Industrialized Countries by the Example of Karls ruhe City, Germany", Journal of Engineering Annals, of the Faculty of Engineering Hunedoara. 6(3) pp. 266-273.
6. A.A. Ibitoye, KO Ipinmoroti and IA Amoo (2005), Effects of municipal refuse dump on the Pysico-chemical Properties of soil and water, Nig. J. Soil Sci. 15(2):122-128.
7. U Goswami, HP Sarma (2008), Study of the impact of municipal solid waste dumping on soil quality in Guwahati city, Poll. Res., 27(2), 2008, 327-330.
8. N. Raman and D.Sathiya Narayanan (2008), Impact of solid waste effect on groundwater and soil quality nearer to Pallavaram solid waste landfill site in Chennai, Rasayan J. Chem. Vol.1, No.4, 828-836.
9. M.S. Barjinder Bhalla, M.K. Saini, Jha (2012), Characterization of Leachate from Municipal Solid Waste (MSW) Landfilling Sites of Ludhiana, India: A Comparative Study International Journal of Engineering Research and Applications (IJERA), pp. 732-745.
10. B. Calli, B. Mertoglu, B. Inanc (2005) Landfill leachate management in Istanbul: applications and alternatives, Chemosphere 59:819–829.

ISBN 978-93-5279-420-1

GREEN SYNTHESIS OF COPPER AND SILVER NANOPARTICLES USING EUCALYPTUS LEAF EXTRACT

Mohammed Ziyad P A*, Reji Thomas, Rafeeque P, Varsha P, Gopika K, Hafsa Mol P P, Haleema Busthana K and Shahansha Mohammed M

PG and Research Department of Chemistry, Farook College, Kozhikode (DT), Kerala

**E-mail: mhdzyd@gmail.com*

Abstract: Nanoparticles of copper and silver are prepared using Eucalyptus leaf extract from copper sulphate, and silver nitrate. It is observed that Eucalyptus leaf extract is more effective in copper nano particle synthesis. Small amounts of silver nano particle are obtained by the reduction of silver nitrate solution. On the other hand, zinc sulphate solution did not yielded any zinc nano particle. The morphological studies of the synthesized nano particles revealed that copper nano particles are having cubic morphology.

Keywords: Eucalyptus leaf extract, nano particle, cubic morphology.

Introduction

Nanoscale particles of nanostructures[1], including nanoparticles, nanorods, nanowires, nanotube and most recently the graphenes[2] have been drawing much attraction and recognized as the technology for the future due to optical and electronic properties of these structures. Nanoparticle systems have also shown self-healing[3] properties.

Among the metal nanoparticles, copper nanoparticlesare potentially attractive due to their good catalytic[4], optical, electrical, and thermal properties. Sub-10-nm[5]copper nanoparticles can be used as a low-cost replacement for silver and gold nanoinks that are used in inkjet printing of conductive patterns.Silver nanoparticles have unique optical electrical and thermal properties and are being incooperated in to products that range from photovoltaic'sto biological and chemical sensors.

ISBN 978-93-5279-420-1

Synthesis of well-dispersed copper nanoparticles was earlier achieved by reduction using $NaBH_4$. Instead of copper oxide produced in aqueous solution, metallic copper particles are formed in w/o microemulsions because of the high local copper concentration in water pools of the microemulsions[6]. Silver nanocubes were obtained by reducing silver nitrate with ethylene glycol in the presence of poly (vinyl pyrrolidone) (PVP)[7]. The presence of PVP and its molar ratio (in terms of repeating unit) relative to silver nitrate both played important roles in determining the geometric shape and size of the product.

The present report discusses the synthesis and characterization of cubic copper and silver nanoparticles using Eucalyptus leave extract as a reduction medium.

Experimental

Preparation of Eucalyptus Leaf Extract: Eucalyptus leaves were collected from Farook College, washed well, and dried in shade. 50g of leaves were cut in to small pieces and washed with distilled water. It is taken in a 400 ml beaker; 200ml of distilled water was added and boiled for 40 minutes when the colour of the extract was brown. The extract obtained was stored in refrigerator.

Preparation of Copper, Silver, and Zinc nanoparticles: 10 ml of Eucalyptus leaf extract was added to 50ml of 0.01 molar aqueous copper sulphate silver nitrate and zinc sulphate solutions separately. The colour of salt solution changes to pale yellow. The solutions were then stirred for homogenous mixing.

UV spectra of the prepared particles were taken using Cary50 instrument from 200 nm to 800 nm with a data interval of 5 nm. SEM images were obtained from Hitachi SU6600 Variable Pressure Field Emission Scanning Electron Microscope (FESEM) with an accelerating potential of 5 KV with a magnification of 15000.

Results and Discussion

Ultra-violet spectrum of the prepared nano particle system is given in Fig. 1-3. It is seen from the spectra that copper sulphate solution forms copper nano particles in large amounts as evident from the intensity of Surface Plasmon Resonance peak at 540 nm[7].

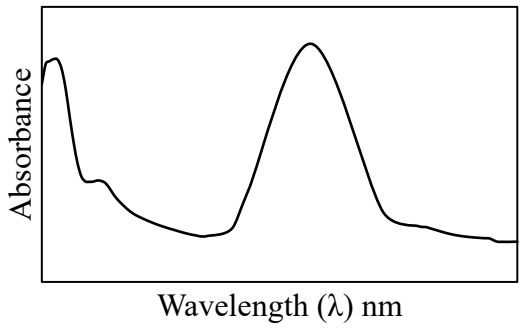

Fig. 1. UV Spectra of copper nanoparticles

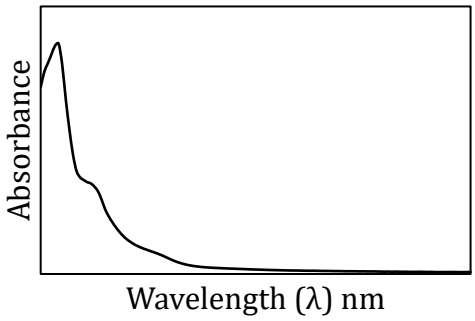

Fig. 2. UV spectra of silver nanoparticles

ISBN 978-93-5279-420-1

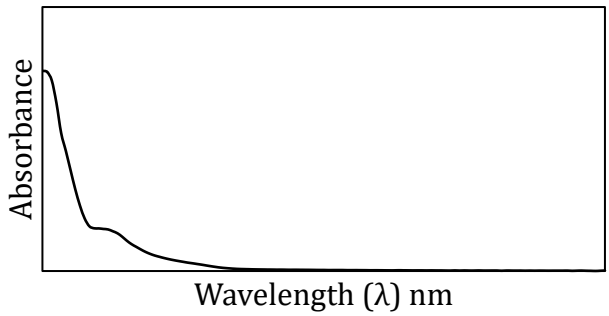

Fig. 3. UV spectra of zinc nanoparticles

Silver system shows a small peak in the area of 380 nm owing to the further aerial oxidation to silver oxide particles. Zinc system, on the other hand, does not show any Surface Plasmon Resonance peaks, and hence does not get reduced to form zinc nano particles.

The SEM image of copper nano particles show that the particles are agglomerating in nature. The morphology of the particles is more or less cubic. The SEM image of silver particle shows fewer amounts of dispersed particles. There is no regular morphology for the particles.

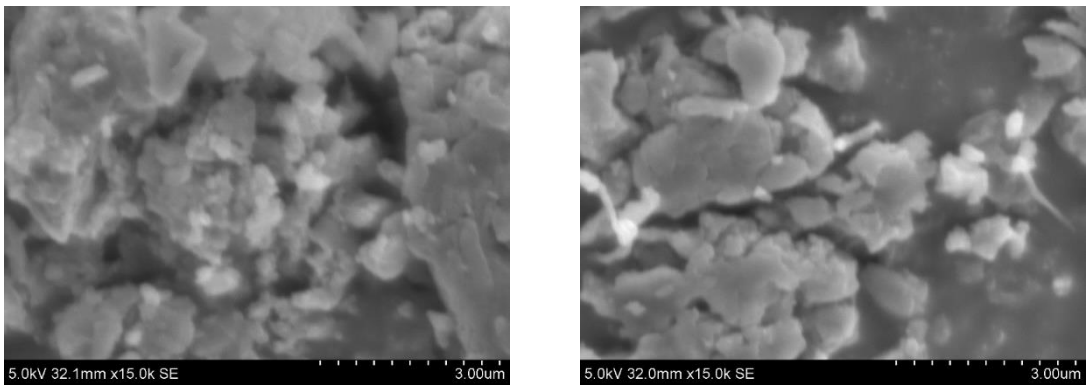

Fig. 4. SEM image of copper and silver nano particles

Conclusions

Eucalyptus leaf extract were prepared and used to prepare nano particles from copper sulphate, silver nitrate and zinc sulphate solutions. It was found that Eucalyptus leaf extract were more effective in copper nano particle synthesis. Small amounts of silver nano particle were only obtained by the reduction of silver nitrate solution. On the other hand, zinc sulphate solution did not yielded any zinc nano particle. The morphological studies of the synthesized nano particles revealed that copper nano particles were having cubic morphology.

ISBN 978-93-5279-420-1

References

1. George M. Whitesides, John P. Mathias and Christopher T. Seto, *Science*, **1999**, *254*, 1312-1319.
2. Dan Li, and Richard B. Kaner*Science*, **2008**, *320*, 1170-1171.
3. Shuai Chen, Fu Tang, Liangzhen Tang, and Lidong Li, *ACS Appl. Mater. Interfaces*, **2017**, *9*, 20895–20903.
4. N. Arul Dhas, C. Paul Raj, and A. Gedanken, *Chem. Mater.*, 1998, *10*, 1446–1452.
5. Yuki Hokita, Mai Kanzaki, Tomonori Sugiyama, Ryuichi Arakawa, and Hideya Kawasaki,*ACS Appl. Mater. Interfaces*, **2015**, *7*, 19382–19389.
6. Limin Qi, Jiming Ma, andJulinShen, *J. Colloid Inter. Sci*. **1997**, *186*, 498–500.
7. Yugang Sun, and Younan Xia, *Science*, **2002**, *298*, 2176-2179.

ISBN 978-93-5279-420-1

- *Prathibha Scholarships for Students opting Science learning*
- *Kerala Shastra Puraskaram for eminent scientists*
- *Kerala Science Literature Award*

FINANCIAL GRANT FOR RESEARCH PROJECTS

- *Science Research Scheme*
- *Engineering & Technology Programme*
- *Ecology & Environment Programme*
- *Individual and collaborative projects in Engineering & Environment areas*
- *Intensive programmes for Innovators of Rural Technology and Biotechnology*
- *SARD Scheme focusing activity specific areas*
- *Technology Development and Adaptation Programme*

PROMOTIONAL PROGRAMMES

- *Kerala Science Congress*
- *Back to Lab Programme for Women*
- *Vocational skill oriented reinstated training*
- *Tech Fest, Green Corps, Eco Clubs*
- *Sasthraposhini & Sasthra Bhodhini*
- *SPYTIS Project for School and College Students*
- *Patent Information Centre*
- *Scientific Management Training*
- *Rural innovators Meet*

POPULARISATION PROGRAMMES

- *Science Popularization Programmes*
- *Support for Seminar, Symposia and Workshop*

National Science Day, National Technology Day, World Environmental Day, Ozone Day etc.

ISBN 978-93-5279-420-1